UNIVERSIDAD DE CHILE
FACULTAD DE CIENCIAS FÍSICAS Y MATEMÁTICAS
DEPARTAMENTO DE ASTRONOMÍA

THE DRY MERGER RATE AND MERGER RELIC FRACTION IN THE COMA CLUSTER CORE

TESIS PARA OPTAR AL GRADO DE MAGISTER EN CIENCIAS, MENCION ASTRONOMÍA

JUAN PABLO CORDERO GARAYAR

PROFESOR GUÍA:
LUIS EDUARDO CAMPUSANO BROWN

MIEMBROS DE LA COMISIÓN:
GUILLERMO BLANC MENDIBERRI
ROBERTO DE PROPRIS
RICARDO MUÑOZ VIDAL

SANTIAGO DE CHILE
2016

RESUMEN DE LA MEMORIA PARA OPTAR
AL TÍTULO DE MAGISTER EN CIENCIAS, MENCION ASTRONOMÍA
POR: JUAN PABLO CORDERO GARAYAR
FECHA: 2016
PROF. GUÍA: SR. LUIS EDUARDO CAMPUSANO BROWN

THE DRY MERGER RATE AND MERGER RELIC FRACTION IN THE COMA CLUSTER CORE

TASA DE INTERACCIONES Y FRACCION DE GALAXIAS CON EVIDENCIA DE INTERACCIONES RECIENTES EN LA REGION CENTRAL DEL CUMULO DE COMA

Mediante la inspección de un conjunto espectroscopicamente completo de 70 galaxias de secuencia roja del cumulo de Coma, de las cuales un alto porcentaje ($\sim 75\,\%$) se encuentran ubicadas a una distancia inferior a $0{,}2R_{200}$ ($\sim$ 0,5 Mpc) del centro del cúmulo, estudiamos el nivel de actividad de interacciones galácticas entre galaxias con bajo contenido de gas, utilizando datos del *Coma Treasury Survey* obtenidos con el Telescopio Espacial Hubble. La estimación de la actividad de interacciones se realiza a partir de la fracción de galaxias involucradas en pares. Identificamos 5 pares y un sistema triple, para un total de 13 galaxias, basados en los limites de distancia proyectada y diferencia en velocidad radial. De estos sistemas, ninguno muestra signos de interacción reciente por lo que ninguno es identificado como una colisión de galaxias en curso. Este resultado nos permite establecer un limite superior para la taza de interacciones de galaxias de bajo contenido en gas de un 1,5 % por Gyr, lo que se condice con las bajas tazas de interacción esperadas para los cúmulos en su estado evolutivo actual. Una inspección detallada de las imágenes de todas las galaxias de secuencia roja en nuestro conjunto revela que solo una galaxia muestra signos identificados a un limite en brillo superficial de 26,5 mag/arcosegundo^2, indicadores de una interacción recientemente producida, lo que implica una fracción de galaxias perturbadas recientemente menor a un 2 %.

Para Oscar

Agradecimientos

Agradezco el inmenso apoyo de mi familia, quienes han estado en todos los momentos de mi vida y me han dado todo de sí para hacerme quien soy. Los amo! ♡
Agradezco a mis hermanos putativos, Mauri, Manuel, Negro, Giani, Ñaño, Piwi y sobre todo a Oscar que siempre nos acompaña, por los infinitos momentos que hemos vivido juntos y por todos los que vendrán. Salud!
Agradezco a mis colegas y amigos de Calán, Seba, Pelao, Grecco, Mati, Jorge, Juan, Carlos, Blake, Gus, Valentin, Paula, Mari, Coni, Mati, Sudeep, José, Pepe, Marcelo, Julian, Felipe, Ricardo, Thomas, Nina, Amber, Alessandro, Armin y Lipsum por todos los panoramas y pelambres que le dieron condimento a mi pasada en Calán y me demostraron que la mejor parte del trabajo es cuando no se trabaja.
Agradezco a mi profesor guía Luis Campusano, a Roberto De Propris y a Chris Haines, quienes me dieron la oportunidad de trabajar junto a ellos e hicieron posible este trabajo de tesis.
Agradezco a los miembros de la comisión, Guillermo Blanc, Cesar Fuentes y Ricardo Muñoz por sus comentarios y acotaciones que fueron sumamente imrpotantes para la calidad de este trabajo. Además les agradezco a ellos junto a todos los integrantes del cuerpo docente y funcionarios de Cerro Calan por hacer posible el funcionamiento del departamento.
Finalmente agradezco el apoyo otorgado por el Anillo CONICYT de Cosmología ACT-1122 y el apoyo financiero otorgado por CONICYT y su Programa de Capital Humano Avanzado a traves de las Becas de Magíster Nacional, folio 22141888.

Contents

List of Tables

List of Figures

Chapter 1

Introduction

1.1. Background

The formation and evolution of galaxies is an intricate process that occurs in an expanding universe, and where different phenomena mix. Cold mode (Brooks et al., 2009; Dekel et al., 2009) hot mode gas accretion(Faucher-Giguère et al., 2011; van de Voort et al., 2011), secular processes (Kormendy & Kennicutt, 2004; Jogee et al., 2005) and major/minor mergers (Springel et al., 2005; Khochfar & Silk, 2009) are among the most important in this picture. These events do not occur in isolation and are, in some cases, strongly dependant on the environment surrounding the galaxy. The environment is usually defined in terms of the galaxy density per unit volume, where three main categories exist: the *field* which is usually a few galaxies per Mpc^3, *groups* which considers small bounded systems with density on the order of a few tens of galaxies per Mpc^3 and *clusters* which varies from a few hundred to even thousands of galaxies per Mpc^3.

Galaxy mergers are believed to be one of the main processes by which galaxies evolve over time, given the strong implications on several measurable properties. They play a fundamental role on the current paradigm of the hierarchical evolution of galaxies, on which massive present-day systems come from repeated mergers of smaller, less massive progenitors. The details of each merger are unique, given the infinite variety of physical and dynamical conditions that can lead to a galaxy-galaxy collision, although some common consequences result from such events. Galaxy mergers contribute directly to the stellar mass growth, trigger star formation, induce nuclear activity and lead on certain cases to a complete transformation in morphology. Also, merging is believed to be the main mechanism by which elliptical galaxies form (Toomre & Toomre, 1972; Toomre , 1977), and some observational evidence can be found on local ongoing mergers (Schweizer, 1996, 1982).

The frequency at which mergers occur, and its connection with the environment and the epoch of the universe are key aspects of galaxy evolution. Work by De Propris et al. (2007) and Muzzin et al. (2008) suggests that a large fraction of the mass inside clusters assembled at redshift $z \gtrsim 1$, leaving these structures in passive evolution since then. This picture seems to be enforced by the fact that scaling relations such as the Fundamental Plane show little

scatter, contrary to what would be expected in the scenario of mergers inducing star formation, and dissipative processes affecting the central velocity dispersion. Dry mergers, between gas-poor quiescent galaxies, may offer an escape to the apparent contradiction between these observations and the expected high importance of mergers in galaxy evolution, as they are believed no to affect the scaling relations (Fernández Lorenzo et al., 2011; van de Sande et al., 2014). The high fraction of elliptical and lenticular galaxies in high density environments makes clusters and massive groups particularly interesting since a large member fraction of these structures correspond to red early type galaxies and S0, which have low gas contents and thus can be involved in dry mergers.

In the hierarchical agglomeration of mass in the Universe, dark matter distributes into filamentary structures as it evolves with galaxy clusters, which are the densest structures in the Universe, residing at the intersections of these filaments. They started forming at $z \sim 2$, probably from the merging of galaxy groups, that are smaller structures. The evolution of clusters depends strongly on the capacity to accrete mass from the surroundings (via galaxy/group infalling), but also on the internal processes that shapes the dynamics of its members and their physical properties. Given that clusters are defined as large overdensities in space, it is natural to consider them as likely location for mergers to happen. A very crude estimation of the number of encounters can be made assuming galaxies as spherical systems, very much like the definition of an ideal gas. A typical number of encounters can be estimated to be:

$$N \approx n\sigma v t$$

where n is the number density of galaxies, σ is the cross section for interactions, v is the typical encounter velocity, and t can be any time-scale considered (for example, the age of the cluster). If $\sigma = \pi R_p^2$, where R_p is the impact parameter, and for the sake of using only observable quantities, we take v to be $\sqrt{2}\sigma_v$, then the number of encounters for a cluster like Coma is:

$$N \approx 4 \left(\frac{n}{250\mathrm{Mpc}^{-3}}\right) \left(\frac{R_p}{20\ \mathrm{kpc}}\right)^2 \left(\frac{\sigma_v}{1000\mathrm{km\ s}^{-1}}\right) \left(\frac{t}{10\ \mathrm{Gyr}}\right)$$

While a galaxy is expected to be involved in several close encounters during its life in a cluster, these encounters will be in general fast given the high velocity dispersion observed in clusters, as a consequence of virial relaxation. It has been shown that when the encounters between particle systems have a typical velocity v_∞ higher than a critical velocity v_f, dynamical friction by which stars suffer a gradual deceleration while passing trough multiple close encounters with other stars, causes only small perturbations on their position with respect to their system's centers and on their velocities (Aarseth & Fall, 1980; Binney & Tremaine, 1987). Moreover, in the case of very fast encounters ($V \gg \sigma$) between spheroidal systems the relative positions of the stars with respect to the centers of their systems appear to remain almost unchanged. In this scenario, the approximation of neglecting the binding forces, also called the impulse approximation, reproduces with remarkably accuracy various numerical experiments (Aguilar & White, 1985). Under this scenario, intra-cluster encounters not only do not seem to perturb the parent galaxies dramatically, but also are not believed to lead to mergers on which the pair members coalesce to form a single galaxy.

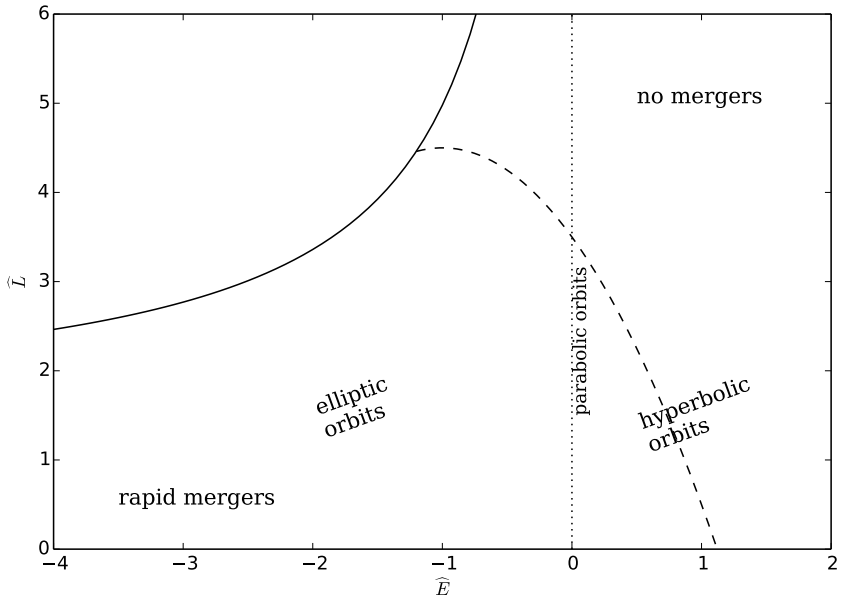

Figure 1.1 Adapted from figure 7-9 of Binney & Tremaine, the figure shows the $\hat{E} - \hat{L}$ plane and the different orbits for a given point on the plane. Orbits are only possible below and to the right of the full curve formed by circular orbits. In principle all elliptic orbits with $\hat{E} < 0$ will eventually lead to a merger but the time to merging increases rapidly towards the upper right. For typical galactic parameters, orbits below and to the left of the dashed line evolve to a mergers in about a Hubble time.

1.2. Physics of a merger

As mentioned, the relative velocity at which the encounter of two galaxies occurs has a strong incidence on the fate of the system. While no collisions between stars are expected, their interaction with the gravitational potential of the host and perturber galaxy does have an impact on the final orbital paratemers of the star.

Basic N-body simulations suggest that even when not merging, two colliding systems exchange energy in a way that their original projected trajectories are lost, since the kinetic energy associated with the relative motion diminishes during the encounter because the internal energies of the galaxies (associated with the internal motion of stars and/or gas) increases. While this disruption can lead to changes in the internal behaviour of galaxies (by triggering star formation), the most notable observation is that orbits can decay from parabolic to closed, eventually leading to a merger. Whether this occurs in a large or short time-scale depends on the initial parameters of the encounter; in particular, of the encounter velocity, v_∞ , and the ratio of the masses, q.

1.2.1. Criteria for merging

While in the high velocity regime and high mass ratios the impulse approximation and the dynamical friction approximations are valid to explain the perturbations suffered during collisions, they are no longer valid in the case of bodies of comparable masses colliding at low speed. In order to determine some more precise conditions for the merger, it is common to assume the case of two colliding spheroidal galaxies of equal mass, characterized by an effective mass radius r_h and a mean square velocity $\langle v^2 \rangle$. The system is also characterized by an orbital energy $E_{\rm orb}$ and an angular momentum, per unit mass L. We can define two dimensionless parameters over which we study the feasibility of a merger.

$$\hat{E} \equiv \frac{E_{\rm orb}}{\frac{1}{2}\langle v^2 \rangle}, \text{ and } \hat{L} \equiv \frac{L}{r_h \langle v^2 \rangle^{1/2}}$$

For every value of $\hat{E}$ there is a limit for $\hat{L}$ given by the angular momentum of a circular orbit, where it is maximum. Therefore, there are forbidden points in the $(\hat{E}, \hat{L})$ plane towards on the upper left quadrant. The smaller the energy for a circular orbit, the smaller the radius of the orbit is, so the angular momentum of the circular orbit must decrease. (See figure 1.1). Since we have mentioned that orbits can decay because of the transformation of orbital energy into internal energy we consider that any orbit with $\hat{E} < 0$ will eventually merge, but we differentiate those who will within a Hubble time from those whose decay will take longer, which happens at high values of $\hat{L}$.

A maximum value for the orbital energy, $\hat{E}_{\rm max}$, that leads to a merger is obtained when no angular momentum is present on the system which is the case of a head on collision, while for each value of $0 < \hat{E} < \hat{E}_{\rm max}$ there is a value $\hat{L}_{\rm max}$ that leads to a rapid merger.

1.2.2. Structure of ongoing mergers and merger remnants

During or after the merging of two systems, characteristic features are expected to appear on the stellar distribution of galaxies, mainly as a result of gravitational interaction. Also, the internal dynamics of the stellar component are expected to show different behaviour depending on the initial parameters of the merger, such as the relative velocity vector and the impact parameter. For instance, numerical simulations of head-on encounters ($\hat{L} = 0$) of spherical non-rotating galaxies have shown that the remains are usually prolate ellipsoids where the longest axes coincide with the initial direction of the parent galaxies. On the other hand, elliptical orbitals can lead to oblate rotating systems with flattening caused partly by rotation, and partly by differences in the velocity dispersion measured parallel and perpendicular to the plane. Similar simulations can be done in order to study the characteristics remnants after collisions of rotating systems, but in either case the dynamics are not observable directly and cannot be related to the global morphology of the remnant.

In this section we describe the observable structures than can arise from an on-going merger or a merger remnant, and that we expect to observe in the morphological inspection

Figure 1.2 Three example galaxies showing different features that can be considered to be a consequence of an ongoing or recent interaction. Left panel shows the galaxy pair NGC 5574/76, with a prominent tidal tail emerging from NGC 5574. Center panel shows an intricate system of shells and possibly some tidal tails in NGC 474. Right panel shows galaxy UGC 09519, where a blue star forming ring can be observed around the central old bulge of the early type galaxy.

done to the red sequence galaxies. Figure 1.2 show some examples of the different features expected to be observed as a consequence of recent or ongoing mergers, such as rings, shells and tidal tails.

Tidal tails and streams

In the case of systems characterized by rotation such as S0 or spirals, an encounter can be characterized by the relative alignment of the internal rotation of the approaching galaxies, and its orientation with respect to the angular momentum of the orbit. Numerical simulations performed by Toomre & Toomre (1972) showed that the two different scenarios of a pro-grade encounter and a retrograde encounter lead to completely different structure formation during the process. In the prograde encounter, when the the stellar component rotates in the same direction as the passing perturber, at a certain radius, the stellar component is in resonance being continuously pulled either inward or outward, depending on the initial position in relation to the disturbing mass. These stars are then pushed away from their host galaxies forming a large, thin and distinctly curved structure called **tidal tail**.

Bridges and stellar **streams** and **brigdes** share some observational properties since both appear as gas and stellar structures related to close encounters of galaxies. Bridges are often referred as structures that connect two interacting galaxies, and are believed to form in fairly high velocity encounters where the two galaxies interpenetrate or have very small impact parameters Condon et al. (1993). Stellar streams appear as elongated structures and while the most recent literature focuses on the accretion of dwarf satellite galaxies by the Milky Way and local spirals when considering the term “stream”, they are also believed to occur in major mergers (Bournaud et al., 2008). Their formation is believed to be a consequence of the collision system behaving as a two body problem on which particles located at the Lagrange points L1 and L2 tend to escape radially. Those escaping towards higher radius will have a smaller angular velocity than the ones escaping inwards, leading to the formation of trailing and leading stellar streams.

Shells

Shells can be described as sudden drops and increases in the surface brightness superimposed on the steady outward decrease in the galaxy surface brightness. They sometimes appear as concentric ripples or arcs at high radius, not encircling the entire galaxy, but often covering up to 90 degrees. They seem to be three-dimensional structures opposed to stellar streams, and on occasions certain symmetry can be observed as they appear on both ends of the semi-major axis of elongated ellipticals. Quinn (1984) proposed that shells form when a giant elliptical galaxy and a smaller companion collide, causing the stars from the disk to oscillate around the center of the potential of the larger elliptical. This oscillation causes groups of star to apparently accumulate on the return point since their velocity is smaller. This explains several observed properties such as the colors observed in the shells resembling those of disk stars, the apparent symmetry on the larger axis of the elliptical and the shells not encircling the whole galaxy. Also, they are relatively short-lived (At most a 1-2 free-fall times, or around 1-2 Gyr) (Hernquist & Quinn, 1988; Barnes, 1988, 1992) which suggests that in case of being observed, they were produced as a result of recent interaction. Shells have been also observed in simulations of major mergers (Cooper et al., 2011) which suggests that collisions between red sequence galaxies could also cause remnants to show these structures.

Ring galaxies and collision rings

Ring galaxies are very particular galaxies showing a prominent ring enclosing one ore sometimes two small bright patches of light. Their are believed to be the result of a head-on collision between a flat rotating system and a perturber that goes trough its center. The total gain in speed of the star in the rotating disk is only on the radial direction, so after the first pass of the perturber the stars in the outer disk are moving towards the center of the galaxy, until the centrifugal force of the rotating system stops them from going inside, but the ones towards the central part of the disk will move to higher radius in a non oscillating way, causing them to catch up with the ones moving harmonically. This creates a ring of stars and a void in the central part of the disk leaving the galaxy with its characteristic shape.

1.3. Measuring the incidence of galaxy mergers on mass growth

Two main strategies have been extensively used in the literature in order to quantify the frequency of galaxy mergers.

1.3.1. Pair and merger fractions

The first one is to search for galaxy pairs in order to estimate the *pair fraction*, which is defined as the fraction of galaxies involved in a pair from a definite sample of N galaxies

$$F = \frac{N_p}{N}$$

While this quantity is not indicative of the actual fraction of galaxies that will merge, it gives certain flexibility on the assumptions to be made for pairs to be considered true mergers. Pairs are usually defined as galaxies that lie close to each other on the sky, which is a minimum condition for them to be considered mergers. Typical values for the separation limits are on the order of tens of kpc. When line-of-sight velocity information is available, galaxies in pairs are required to have low velocities with respect to each other, typically a few hundred km s^{-1}. This increases the possibility that the galaxies are physically close and that they may encounter with low relative velocity. This method is particularly useful in large surveys where spectroscopic completeness is an issue and no morphological evaluation can be done in the low resolution regime (i.e.: high redshift). When high resolution and depth is achieved, the addition of a third criteria can be added: that the pair members already show evidence of ongoing interaction. From this definition, the *merger fraction* and *merger rate* can be obtained. Their respective definitions are

$$\mathcal{F} = \frac{N_m}{N} \qquad ; \qquad \mathcal{R} = \frac{\mathcal{F}}{\langle T_{\texttt{merge}} \rangle}$$

where N_m is the number of galaxies from a total sample of N that are considered part of an on-going or future merger. The parameter $\langle T_{\texttt{merge}} \rangle$ is the merger time-scale, and provides an estimation of the time during which a merger is observable. Different definitions for the merger timescale are present in the literature, ranging from values derived from dynamical friction simulations to some other, more simplistic, based on orbital parameters.

1.3.2. Post-merger galaxies

We define as post-mergers those galaxies showing features that deviate from a smooth, symmetric light distribution and whose features cannot be explained due to the presence of a companion, or as result of the internal expected structure like spiral arms or bars, so they are considered to have undergone a recent event of merging. Galaxies having suffered a recent merger event are identified by studying the light distribution of its stellar component. While this method usually requires the intervention of a trained human eye, several 'objective' approaches can be taken in order to introduce the use of automatic tools. The CAS system (Conselice, 2003), for instance, measures three structural parameters of the 2D intensity map of a galaxy: Concentration (C), Asymmetry (A), and Smoothness (S) which can be calibrated in order to identify possible merger relic candidates. The search for merger relics rely strongly on the quality of the data used: both high resolution and fairly deep observations are required in order to correctly identify perturbed galaxies. Depending on the assumptions made for the visibility of these structures, the recent merger history of these galaxies can be studied.

1.4. Merging in clusters or "pre-processed"?

The main question that arises from the previous section refers to the origin of early type galaxies in clusters, as they may be a result of past galaxy-galaxy interactions. The case of central dominant galaxies, which are giant super massive ellipticals (CDs) typically found on cluster centres is of particular interest. Numerous CD galaxies have been found to show multiple structures in their cores, which could be indicative of merger events in the past (van Dokkum et al., 2001; Yamada et al., 2002; Gu et al., 2013). Current theories consider galaxy infall being the main responsible for the evolution of early type galaxies (ETGs), as the accretion of galaxies and galaxy groups into a cluster induces the system out of equilibrium, allowing low velocity encounters to occur, and therefore mergers (Haines et al., 2015).

In recent observations of 4 local massive clusters at $z \sim 0{,}1$ (A119, A389, A2670, A3330) Sheen et al. (2012) identified features in $\sim 25\,\%$ of the Red Sequence cluster galaxies, a result particularly surprising for such dense environments. They suggested that these faint features could be residuals of mergers that took place several Gyr ago, prior to the accretion of their galaxies into the clusters themselves. Yi et al. (2013) performed hydrodynamical simulations of major merging galaxies indicative that post-merger signatures could remain detectable within a cluster for 3-4 Gyr.

1.5. This work

This work focuses on the search for interacting red sequence galaxy pairs in the Coma cluster and it is intended to act as a template for future studies of similar characteristics, at low and high-z, given the increasing imaging capabilities of future facilities such as the James Webb space telescope. Making use of the high resolution achievable at low redshift plus the extensive spectroscopic information available, a spectroscopically and photometric complete sample of red sequence galaxies can be built in the desired mass/luminosity ranges.

The cluster was imaged using the Hubble Space Telescope (From now on, HST) using the Advance Camera for Surveys (ACS) for the Coma Treasury Survey (Carter et al., 2008), aimed at imaging the central 'core' region of the cluster and the a south-west infall region in the outskirts. Coma is an excellent prototype of a local massive rich cluster, with more than 500 confirmed members and with an estimated population of over 1000 galaxies.

The motivation of this work is to provide an accurate measurement of the evolutionary state of the cluster members, to be compared with theoretical expectations and with similar studies performed both at low and intermediate redshift. This information can lead to a better understanding of the impact of environment in the mass evolution of galaxies, and the role that infalling galaxies into clusters plays in the evolution of ETGs.

1.5.1. Aims

- Provide a systematic method for estimating an accurate merger rate for clusters in the local universe, considering not only phase space proximity, but also making use of high resolution imaging and spectroscopic completeness.
- Determine the merger rate and post merger fractions for the Coma cluster, and compare them with the ones found in the literature for low z clusters.
- Present the advantages of adopting this method for similar studies at intermediate redshift ($z \sim 0{,}8 - 1{,}6$) where only pair counts have been used so far to estimate the frequency of mergers.

1.5.2. Outline

In chapter 2, a detailed description of the cluster is given, highlighting its relevant properties as well as those of its constituent members. In chapter 3, the Coma Treasury Survey and its data products are described, as well as the preliminary data treatment in order to build the final sample of galaxies that will be subjected to the pair search. Chapter 4 describes the pair selection process, including the visual inspection, modeling process and asymmetry calculations. Also, after models, residuals and original images have been inspected and asymmetry parameters are considered, a statistical calculation regarding the pair likelihood for the final sample is presented. In chapter 5, the merger rate and post merger fraction are presented for the final pair sample Finally, a summary of the main results and their implications is given, along with ideas for future work.

Chapter 2

Previous work and a description of the Coma cluster

The question whether galaxies do merge or collide with each other has been long answered by observations of famous examples in the near universe, such as the Antennae, and numerous studies carried out at high redshift. A completely different question is if these events are rare or if, on the other hand, they dominate over other processes to drive galaxy evolution. Toomre (1977) suggested that elliptical galaxies could be the result of collisions and mergers between disk galaxies based on the extrapolated merger fraction and fraction of elliptical galaxies in the local Universe, and in the fact that mergers could be responsible of the large velocity dispersion caused by violent relaxation that is observed in ellipticals. Averaged over all environments, spirals and irregulars account for a large $\sim$ 70 % of all galaxies, but a clear trend is observed with respect to this percentage, decreasing dramatically towards high density environments such as clusters where elliptical and S0 galaxies dominate. Dressler (1980) showed that there is a tight correlation between the density of the environment and the dominant morphology of galaxies populating those environments, being clusters composed mostly of elliptical and S0 and the field having a large fraction of spiral an irregulars. These two arguments collide with the fact that in dense environments the encounter velocities are sometimes higher than 1,000 km s^{-1} which prevents the merging of the systems. This finally leads to the belief that mergers were important at earlier stages of the formation of clusters, when they were a collection of infalling poorer systems each with lower velocities for its members.

Several attempts have been made to constrain the role of galaxy-galaxy mergers in the evolution of galaxies in varying environments and epochs of the universe. In the low redshift regime, for instance, Duc et al. (2015) showed that $\sim$ 65 % of local ($z \lesssim 0{,}1$) field early-type galaxies observed a low surface brightness show features such as broad fans, ripples, shells, streams and tidal tails indicative of past, recent interactions, while in clusters, Adams et al. (2012) found that only $\sim$ 3 % of a large sample of early-type galaxies in local clusters ($0.04 < z \; 0.15$) show evidence of these features, although at shallower limiting magnitudes. Still at low redshift ($0.01 < z < 0.22$), De Propris et al. (2014) found a low merger rate of 1.5 per Gyr by studying the close pair fraction, which suggests that mergers are unimportant in galaxy growth, specially for mergers between galaxies of comparable masses (major mergers).

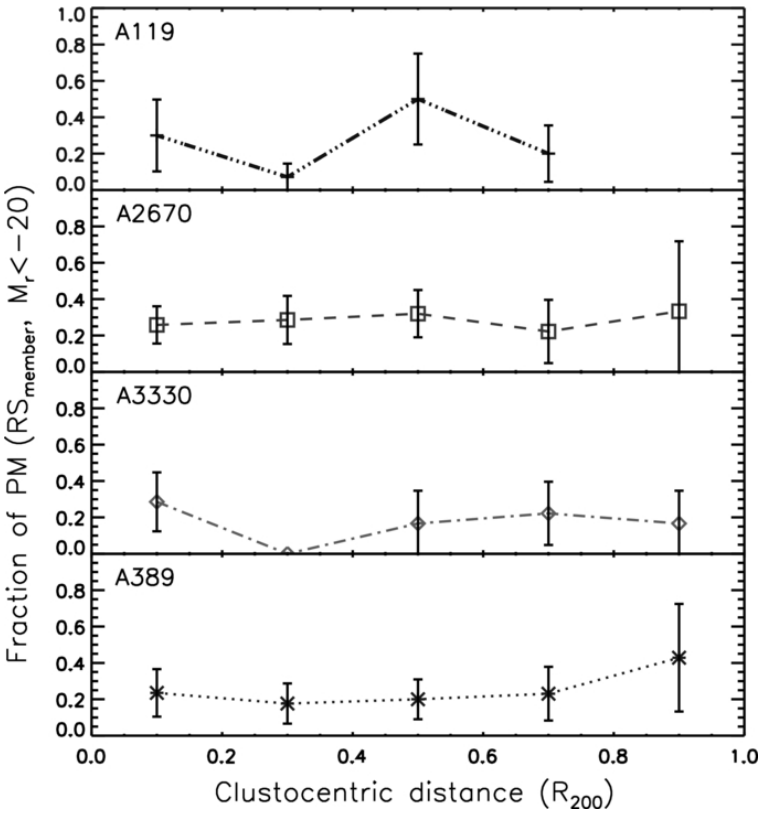

Figure 2.1 Fraction of post-merger galaxies along the projected distances from cluster centers found by Sheen et al. (2012) for 4 local rich clusters (A119, A2670, A3330, A389). The size of the distance bin is $0{,}2R_{200}$ in each galaxy cluster. Contrary to the general assumption, which would predict more frequent mergers at the outskirts of a cluster, the fraction of post-merger galaxies does not change much along the clustocentric distances.

This task becomes harder at intermediate and high redshift, where high spectroscopic and luminosity completeness are difficult to obtain. van Dokkum et al. (1999) found a high merger fraction of $L > L_*$ elliptical galaxies in the rich cluster MS 10454-03, at $z = 0{,}83$, by studying close pairs and their apparent morphology. This result was later confirmed Tran et al. (2005) with follow-up spectroscopy, finding that most of the pairs have radial velocity differences of less than 165 km s^{-1}, thus having a high change of coalesce. Lotz et al. (2013) found a high merger fraction, close to 60 % in a $z = 1{,}67$ protocluster, XMM-LSS J02182-05102, and compared this value with the merger fraction of field galaxies at the same redshift, finding that the cluster had a merger activity far more intense.

From the presented results, there seems to be enough evidence at high redshift to discard the picture of the formation of an elliptical galaxy in a single monolithic collapse and merging of massive galaxies appear to be much less common in the local universe, specially in high density environments, which can be considered to be the result of clusters reaching dynamical equilibrium and thus preventing mergers because of the high speed encounters.

Perhaps one of the most surprising results considering this picture is the one presented in Sheen et al. (2012) where Red sequence galaxies were identified via spectroscopic membership and red sequence fitting for 4 local massive rich clusters (Abell 119, 389, 2670, 3330). Using

Table 2.1. Fraction of Post-mergers, Interacting, Pair, and Faint Companion Galaxies among cluster's red sequence galaxies.

ID	PM	I	P	FC
A119	27 %(13/48)	0 %(0/48)	10 %(5/48)	10 %(5/48)
A2670	28 %(25/89)	8 %(7/89)	3 %(3/89)	6 %(5/89)
A3330	22 %(13/58)	5 %(3/58)	9 %(5/58)	3 %(2/58)
A389	22 %(17/78)	4 %(3/78)	8 %(6/78)	5 %(4/78)
Fractions for galaxies within 0.5 R_{200}				
A119	27 %(8/48)	0 %(0/48)	10 %(3/48)	10 %(5/48)
A2670	28 %(18/89)	8 %(6/89)	3 %(3/89)	6 %(5/89)
A3330	22 %(4/58)	5 %(1/58)	9 %(2/58)	3 %(0/58)
A389	22 %(10/78)	4 %(2/78)	8 %(5/78)	5 %(3/78)

very deep imaging, every galaxy was subjected to a visual inspection and two dimensional models of the light distribution were created in order to study the residuals left after model subtraction. A high fraction of post-merger galaxies was found on all clusters (around 25 %), and the fraction did not seem to decrease when the sample was restricted to within 0.5 R_{200} (See table 2). The post-merger fraction did not show any trend towards lower values even at small distances from the cluster center (Figure 2.1). They suggested that these faint features could be residuals of mergers that took place several Gyr ago, prior to the galaxies being accreted into the clusters themselves. Yi et al. (2013) performed hydrodynamical simulations of major merging galaxies indicating that post-merger features could remain detectable within the cluster for 3-4 Gyr, although they did not consider the infall of the merger remnant into a cluster, and only considered the case of isolated galaxies.

2.1. The Coma cluster: A description

The Coma cluster, also known as Abell 1656, is one of the nearest rich clusters and of the most studied structures of its kind. Biviano (1998) provides a comprehensive historical review of the knowledge and understanding of the properties and structure of the cluster, and how it has evolved over the years. Carter et al. (2008) also provides a detailed list of past imaging and spectroscopic surveys of the cluster. At a redshift of $z \sim 0{,}023$ it is the prototype of a massive relaxed local cluster, with more than 600 spectroscopic confirmed members and an estimated total population of around 2000 galaxies. This population includes a wide variety of different galaxies, including ultra-compact dwarf galaxies (UCDs), spiral, lenticular and ellipticals, although each one with very different relative fractions. Located at RA = 12h59m48.7s DEC = +27d58m50s, it is very close to the galactic pole making it very easy to distinguish from foreground stars. Its apparent size is of around half a degree on the sky, making it also of the largest structures on the sky. As expected for high density environments, it is dominated by early type galaxies and gas poor galaxies, which also tend to be distributed towards the central parts of the cluster. Two prominent central elliptical galaxies are located close to the center of the cluster: NCG 4874 and NGC 4889, which are two supermassive ellipticals concentrating a large fraction of the total stellar mass of the cluster. Some grand design spiral

galaxies are also linked to the cluster, but mostly located at the outskirts the most notable one being NCG 4911.

2.1.1. Dynamical properties and evolutionary state

The galaxy distribution of the cluster indicates a roughly spherical structure, which is confirmed by the x-ray emission of the cluster around the core, tightly correlated with the galaxy distribution. This spherical symmetry can be regarded as an indicator of the dynamic state of the cluster, having reached virial equilibrium. But this picture of a featureless structure is no longer observed in the outer parts of the cluster: several studies on the last 20 years, specially by means of x-ray temperature map studies have suggested that the cluster is not completely relaxed and the idea of a perfectly virialized system has been abandoned. The presence of substructure associated to the two bright central ellipticals in the cluster has been widely studied, considering the spatial distribution of galaxies, their velocity dispersion and the X-ray emission of the hot intracluster plasma. Bahcall (1973) was the first to observe an anisotropic distribution of galaxies observable in the E-W direction, matching the orientation of the two central supergiants and being supported by later studies of the mean velocity and velocity dispersion around NGC 4874 and NGC 4889 (Perea et al., 1986; Biviano et al., 1996; Colless & Dunn, 1996). Debate still exist regarding the origin of the substructure observed and whether the two subgroups associated to the central massive galaxies were the only ones giving birth to Coma or were accreted to a larger pre-existent structure. Another picture is the one presented by Colless & Dunn (1996) where NGC 4874 is the central dominant galaxy of the large pre-existent structure and the group associated to NGC 4889 was accreted.

In addition to the central structure, a relatively high over-density of galaxies is present in the SW region of the cluster, early detected in the twentieth century and later confirmed by analysis of the velocity space of the galaxies in that region (Perea et al., 1986). Briel (1997) has shown the presence of a homogeneous temperature distribution in the central area of the cluster which indeed reveals the relaxed state of the central core region, but this homogeneity is lost towards the south-west area were a bump in the gas temperature is measured. This increase is believed to be a result of an adiabatic compression generated by the infall of a group of galaxies associated with NGC 4839. On the south-east region, a lower temperature is measured close to a overdensity of galaxies around NGC 4911 and NGC 4921, indicating the presence of merging activity on this group.

While the assumption of spherical symmetry can be adopted in order to simplify numerous aspects such as the number density of galaxies and three dimensional extent of the cluster, there are of course numerous pieces of information which are unknown given the limitations in the observable properties such as the galaxy phase space. This uncertainty is the main impediment for creating an accurate representation of the current state of the cluster.

Chapter 3

Data description and the sample of Coma red sequence galaxies

In this chapter we describe the archive data we used on our study of the merger activity in the Coma cluster as well as the literature related. We also describe the methodology employed to select a spectroscopically complete sample of Red Sequence galaxies - which is the basis for our analysis

A key aspect of the work done over this project was to have the reliable set of data required to perform the intended analysis. High sampling and resolution are required since the structures we expect to observe often have dimensions of the order of arcseconds or even smaller. For example figure 3.1 shows the same galaxy observed using two different telescopes. left panel shows an image of IC 3973 obtained with the IRIM camera from the KPNO 2.1 meter telescope, at a pixel scale of 0.6 arcsec/pix, and a PSF FWHM of $\sim 1''$ while the right panel shows the galaxy observed through HST, in the F814W band, with a pixel scale of 0.05 arcsec/pix and a resolution in the F814W filter that varies from 0.1" to 1.4". Features observed at low resolution and pixel scale are barely observable, while a bar-like structure can be seen in the HST image, besides the multiple foreground and background objects which are undetectable in the low resolution version. Depth is also critical and crucial, since differences on the limiting surface brightness often lead to a completely different interpretation of the morphology observed on galaxies (Duc et al., 2015).

Duc et al. (2015) showed that a difference on 1-2 mag/arcsec^2 changed the perception of a galaxy, revealing in some cases the presence of faint structures previously unknown. This can be observed in figure 3.2, where the same field is compared, using regular imaging and an optimized flat fielding strategy where low surface brightness features rise and scattered light from bright sources disappears. The completeness of the sample in terms of photometry and radial velocity information is important as well, since it limits the mass or luminosity at which the samples can be studied without worrying about missing information. Finally, spatial coverage allows us to build a representative sample of the cluster population.

Given the high quality imaging needed to identify the detailed structure of Red Sequence galaxies, we use high resolution archive images, publicly available. In this section, a descrip-

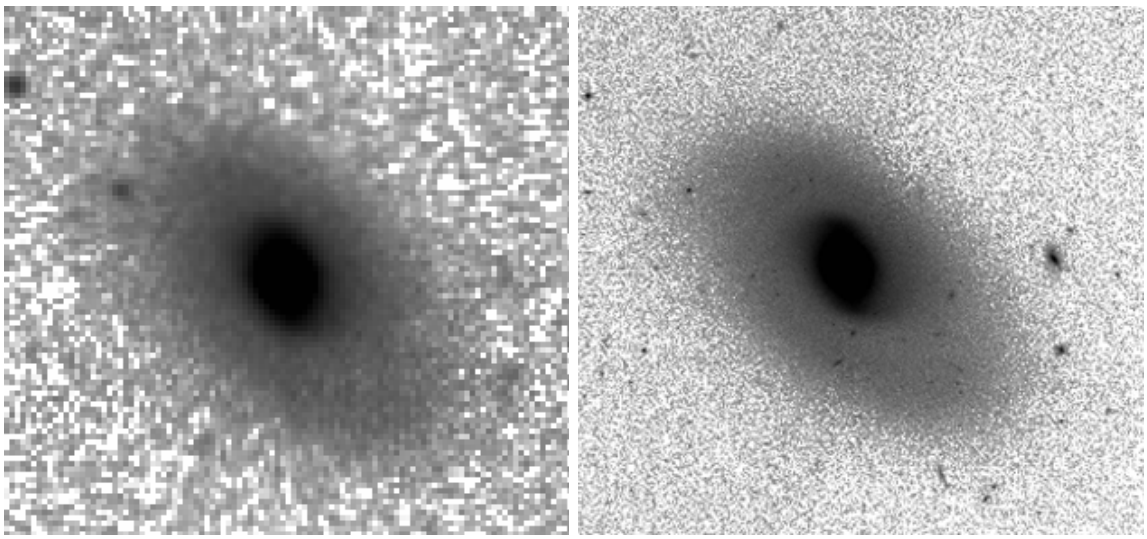

Figure 3.1 Comparison between different angular resolution imaging for the same galaxy. The image on the left shows IC3973 observed in the b band through the ground-based KPNO 2.1 meter telescope, using the IRIM camera, where little can be said regarding the internal structure and the faint objects that could be close to the galaxy. Image on the right shows the same galaxy observed with the HST band F814W. Small background and foreground objects can be seen clearly, as well as a faint structure that could be considered a bar in the central bulge of the galaxy.

tion of the data used for this work is given as well as the observational parameters relevant to our study. Since we are aiming at studying red, gas-poor galaxies, we focus on the cluster Red Sequence galaxies. The procedure adopted for the identification of Red Sequence galaxies is based on the available spectroscopic, astrometric and photometric information.

3.1. The Coma Treasury Survey: Carter et al. (2008)

The Hubble Space Telescope Coma Treasury Survey (Carter et al., 2008, From now on CTS,), is an optical survey originally intended to image approximately 740 square arcmin using the Advanced Camera for Surveys (ACS), using two bands: F814W, which is a broad I band filter; and F475W, which is basically a g SDSS band. Besides the imaging from the survey, two additional catalogs have been created as data products, one containing information for all extended and point sources down to $m_{\texttt{F814W}} = 25{,}8$ mag (AB), and a second one containing structural parameters for extended sources. The main goals of the survey were to characterize the Luminosity Function of the cluster including the presence of ultra compact dwarfs, estimate the impact of the cluster environment on morphological features of galaxies and to characterize the globular cluster population of Coma. Several papers from the CTS collaboration followed up, the most important ones for our study being Hammer et al. (2010), where SExtractor catalogues for galaxies are built, and Weinzirl et al. (2014), where a structural decomposition of a large number of galaxies are presented.

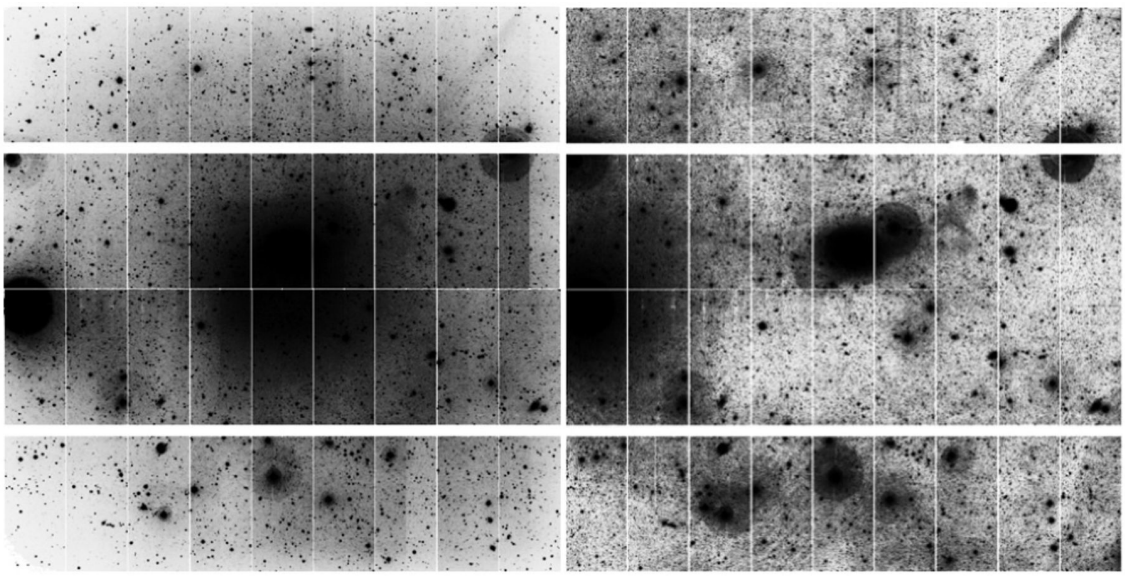

Figure 3.2 The dramatic gain of the low surface brightness optimized strategy used by Duc et al. (2014). Left panel shows one individual g-band exposure of NGC 5557 for which a bias and standard flat fielding correction has been applied. Scattered emission dominates at the chosen intensity contrast. On the right panel, the central scattered light has disappeared and the faint low-surface-brightness tidal features around the galaxy show up.

3.1.1. Spatial coverage

The survey aimed at imaging two main areas: The 'core', which was projected to cover a roughly square area of 18×21 arcminutes (roughly 5×6 Mpc) around cluster center, located at RA = 12h59m48.7s; DEC=27d58m50s ; and an infall south-west area where an over-density of x-ray emission has been observed, along with a large number of galaxies, believed to be in the process of being accreted into the cluster. This area was not intended to be imaged completely, but rather focusing on the location of the most massive cluster members. The ACS detector is divided into two regions, with a separation of about 3 arcseconds which was filled with a dittering of 3.011 arcseconds in the perpendicular direction. Each ACS pointing covers a roughly square area of 202×202 arcseconds, with a sampling of $2 \times 2048 \times 4096$ pixels. The pointings show noticeable overlapping, which must be considered in the catalog building stage in order to avoid duplicates in the entries.

Pointings were originally intended to be arranged in a 6×7 pattern for the core and 40 additional pointings were projected in the outskirts area, but the ACS failure in 2007 rendered the camera unusable while the survey was still being completed. This led to a partial completion of $\sim 28\,\%$ of the total data to be analysed. The total area imaged for the core region was about 170 square arcminutes, divided into 19 pointings, plus additional 60 square arcminutes in the south west outskirts divided in 6 pointings. The original intended distribution and the final covered area by the survey is presented in figure 3.3.

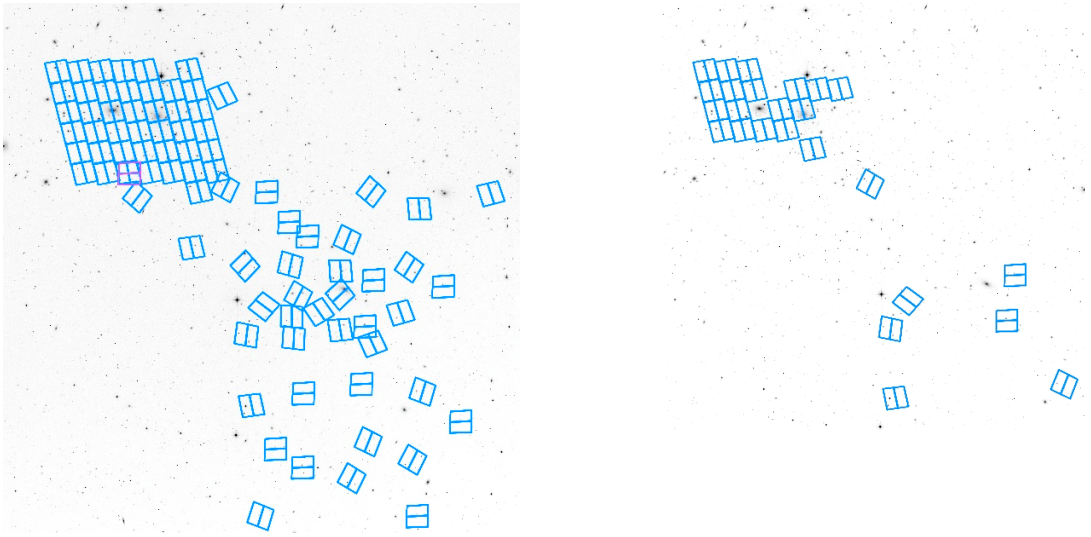

Figure 3.3 Left: Overlay on a DSS image of the ACS fields from the planned survey. Right: Overlay on a DSS image of the ACS fields observed before the ACS failure on the 27th of January, 2007. The HST survey had to stop with only a 28 % of the survey plan completed.

3.1.2. Pixel scale, resolution and limiting magnitudes

Given the pixel aperture and angular coverage, a pixel scale of 0.04931 arcsec/pixel is estimated, although the angular coverage is only approximate since the focal plane of the ACS is slightly distorted due to the optics of the telescope. This distortion, while treated by the reduction pipeline in order not to affect significantly the sampling and RA/DEC solution, does lead to small shifts on the obtained coordinates for the detected sources, specially close to the edges of the images. Compared to other large optical surveys, the HST offers a decent fine sampling and resolution: DECam pixel scale is only 0.263 arcsec/pixel and a resolution of at most 0.6" can be achieved, and the SDSS has a much larger pixel scale of 0.396 arcsec/pixel and lower resolution ($\sim$ 1,5"), compared to the 0.05 arcsec/pixel pixel scale and $\sim$ 0,1" resolution in the HST F814W band.

Surface bright limit at the 3-sigma level is estimated according to the following calculation

$$\Sigma = -2{,}5 \log\left(3\sigma\sqrt{N_{\mathtt{PIX}}}\right) + ZP$$

where σ, $N_{\mathtt{PIX}}$ and ZP are the standard deviation of counts in a 1 square arcsecond area of the image, number of pixels in the same area, and the photometric zeropoint for the corresponding filter, respectively. This calculation does not consider the possible effect of correlated noise that can arise from the dithering pattern of HST observations, but it works as an estimate that can be used to compare the depth of the imaging employed with similar surveys where the same calculation has been performed (Adams et al., 2012, and private communication with Scott Adams) In the F814W band, $ZP = 25.937$ mags and $N_{\mathtt{PIX}} = 400$, while the typical standard deviation on a 1 square second area found on the images is of $\sigma \sim 0{,}01$ counts in 1400 s exposures. This yields an approximate value for the 3-*sigma*

surface brightness limit of 26,5 mag/arcsec^2.

3.1.3. SExtractor photometric and structural parameter catalogues

Sources were automatically identified by the CTS team using SExtractor. The main source catalog lists nearly 73,000 unique extended and point sources from all 26 pointings, but since the parameters of SExtractor were optimized for detecting unresolved sources including the large globular cluster population, the list of extended sources is not exhaustive on the low surface brightness range. The catalogs provide magnitudes in both the F814W and F475W filter bands, as well as F475W-F814W color for all sources which allow us to build the red sequence of galaxies for Coma. Magnitudes were obtained using several fixed apertures (0.12,0.4,1,1.5,3,4.5,6,9,12") and source dependent elliptical apertures (Kron radius, Petrosian radius and Isophotal radius).

A second catalog was generated where structural parameter from single Sersic profile fits were ontained for approximately 8,500 galaxies, including effective radius $R_{\rm e}$, Sersic index n, ellipticity, position angle etc. While the parameters were obtained using GALFIT and GIM2D single Sersic profiles, the models and residuals are not public, so the residual inspection performed in section 4.4 is not possible at this stage, since the models do not consider the presence of multiple components for each galaxy. (See section 4.3.2) Still, the ellipticity, Petrosian radius and position angles for these galaxies are used when considering the first guesses in the GALFIT modelling process, and also are used when defining the area considered for the asymmetry calculations.

Both catalogs are matched so we end up with a custom galaxy catalog were magnitudes, colors and positions from the first catalog and structural parameters from the second catalog are presented exclusively for the objects detected in the second catalgo, thus reducing the initial source number of objects from ∼73,000 to ∼8,000.

3.2. Radial velocities

Radial velocities provide a fundamental piece of information regarding the dynamics of potential pairs, since a low velocity encounter is necessary for a merger to occur, and the radial velocity (that is, in the line of sigth) is the only one that can be measured. Line of sight velocities are obtained using the Nasa/IPAC Extragalactic Database[1] (NED), which is a *"comprehensive database of multiwavelength data for extragalactic objects (...)"*. In order to obtain the velocities, we perform a search based on the reported positions in the galactic catalog and register the radial velocities given in km s^{-1} in the case it is listed in NED. Most of the radial velocities found come from Biviano et al. (1995), which were obtained using the MOS-SIS spectrograph from the Canada-France-Hawaii telescope, and are listed as the main entry in NED. Some other sources include Smith et al. (2004) and den Brok et al. (2011).

[1] http://ipac.caltech.edu/

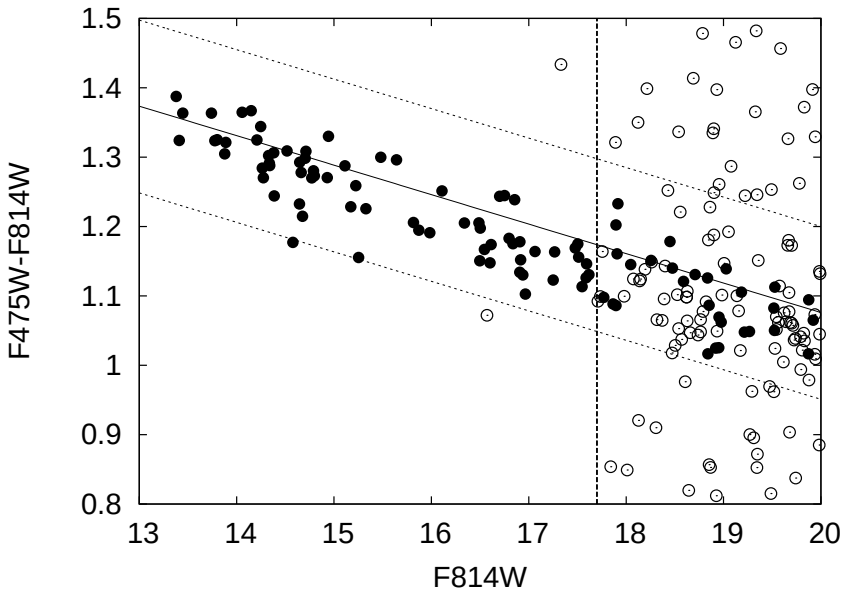

Figure 3.4 Color-magnitude diagram for objects brighter than F814W = 20. Red-sequence galaxies le within the 5σ region delimited by dotted lines, while the red-sequence relation is indicated by the solid line. Open circles show galaxies with unknown radial velocity, while filled black circles correspond to member galaxies with known radial velocities between 4000 and 10,000 km s^{-1}. Vertical line at F814W = 17.7 ($\sim 10^9 M_\odot$) marks the limit for a complete spectroscopic sample.

3.3. Red sequence galaxies

In order to build a spectroscopically complete sample of bright red sequence galaxies, several steps must be performed. First, we build a master catalog of galaxies from the CTS catalogs, removing duplicates that appear on the overlapping areas of pointings. In most of the cases, the existence of duplicates introduces uncertainty in the measured properties such as coordinates and magnitudes. Entries with similar magnitudes and positions on the original galaxy catalog are checked, and a list of possible duplicates is generated. A NED search for these possible duplicates reveals which of the entries are not found on the database. Since few cases occurred, images were examined in order to check if the positions indicated on the entries of the catalog correspond to duplicates of the same galaxy.

After duplicates are removed, we are left with a catalog of galaxies with their corresponding positions, magnitudes and colors, with which we build a color-magnitude diagram. This diagram allowed us to find the red sequence relation for the galaxies in the observed regions of the cluster. A preliminary cut in magnitude is done at F814W = 20, which is where a large number of background objects start to dominate on the photometric catalogs. A sigma-clipping rejection is made on galaxies, where a first linear red sequence relation in the form of $F475W - F814W = A + B \times F814W$ is fitted and galaxies deviating more than 2.5σ in color from the relation are rejected. In the next iteration a new red sequence relation is computed, and the rejection is made again, iterating until no galaxies are rejected. The values for the linear parameters found are $F475W - F814W = 1{,}916 - 0{,}0425 \times F814W$.

The final red sequence is defined by all the galaxies lying within a $\pm 2{,}5\sigma$ from the fitted red color-magnitude relation. This leaves a total of 176 preliminary red sequence galaxies, to F814W = 20, although this includes galaxies with very low/high radial velocities and galaxies with unknown spectroscopic information. This uncertainty is one of the main issues when building a spectroscopically complete sample, since it also affects cluster membership, and the cuts in radial velocity employed for this issue cannot leave them directly out of the sample. The final sample of bright red sequence galaxies is built according to the following two criteria:

- All galaxies must be spectroscopic confirmed members. For this, all galaxies with known radial velocities between 4,000 and 10,000 km/s are selected following the same membership criteria presented by Hammer et al. (2010).
- All galaxies brighter than the brightest red sequence galaxy with unknown radial velocity are selected, allowing us to build a spectroscopic complete sample of massive red sequence galaxies on the resultant luminosity range.

The resulting spectroscopic-complete sample of red sequence galaxies comprises 70 galaxies with luminosities ranging from $m_{\rm F814W}13{,}5$ to 17,7. Figure 3.5 shows the radial velocity distribution of the sample, clearly centered close to the nominal value for Coma (6925 km s^{-1}), and the spatial distribution with respect to the footprint of the CTS. The central 0.5 Mpc (0.2 R_{200}) region of the cluster is marked with a solid line circle for comparison.

3.4. Stellar masses

Stellar masses are useful for defining the nature of the possible merger that could occur in our sample, depending on the ratio of the masses inside a pair. We consider as possible major mergers to those with ratios higher than 1:10. The mass is also important since it defines the timescale in which a merger is expected to occur (See section 5.1). We calculated the stellas masses for the Red Sequence galaxies following the procedure described in Weinzirl et al. (2014), based on the HST F475W and F814W-band photometry. First, HST (AB) magnitudes are converted to the Cousins-Johnson (Vega) system according to the WFPC2 Photometry Cookbook[2]

$$I = F814W - 0{,}38$$

And from Price et al. (2009)

$$B - I = 1{,}287(F475W - F814W) + 0{,}538$$

Next, using the I-band mass to light ratio calibrations from Into & Portinari (2013), and a Kroupa IMF (Kroupa et al., 1993), it is obtained that

[2]http://www.stsci.edu/hst/wfpc2/analysis/wfpc2_cookbook.html

$$M_\star = (10^{-0,4(I-35-4,08)}) \times (10^{0,641(B-I)-0,997})$$

where 35 is the distance modulus to Coma and 4.08 is the solar absolute magnitude in the I band. The values obtained can have high uncertainties in large galaxies, such as NCG 4889, which is one of the cD galaxies of Coma, since a non negligible fraction of the low surface brightness envelope from these galaxies is not considered in the magnitudes obtained in Hammer et al. (2010).

The main properties of the sample of Coma Red Sequence are presented in table 3.1, where the names, positions and magnitudes come from Hammer et al. (2010), the radial velocity are the values found on the literature, and the stellar masses are the values obtained with the previously presented color relation.

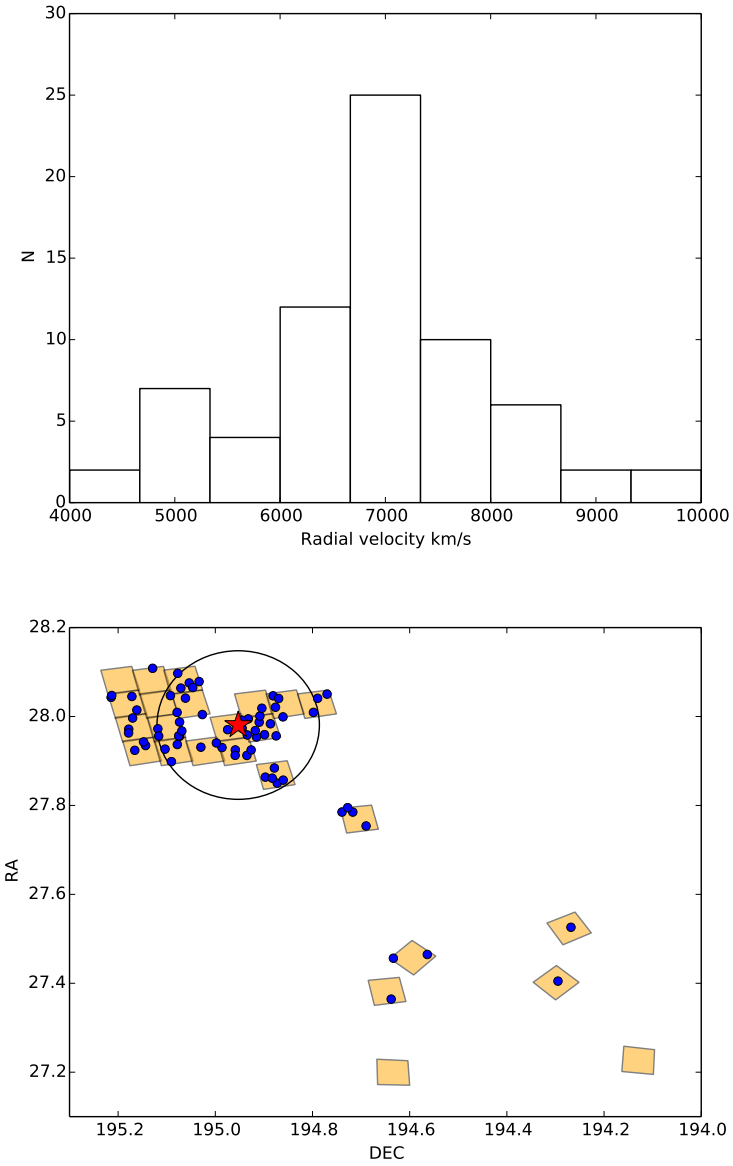

Figure 3.5 Top: Radial velocity distribution for galaxies in the spectroscopically complete sample sample of 70 red sequence galaxies within the CTS Coma survey. Bottom: Spatial distribution of red sequence galaxies in the CTS footprints. Cluster center is indicated by the red star marker, and the black circle marks the central 0.5 Mpc diameter.

Table 3.1. Main properties of the spectroscopic-complete sample of Coma red sequence galaxies

ID	RA [Deg]	DEC [Deg]	F814W [mag]	cz [km s^{-1}]	$M_\star/M_\odot$
COMAi125935.698p275733.36	194.8987435	27.9592686	13.3791	7176	7.69×10^{11}
COMAi13017.683p275718.93	195.0736831	27.9552587	13.4103	6903	7.06×10^{10}
COMAi13051.464p28234.86	195.2144359	28.0430186	13.4466	8793	7.48×10^{10}
COMAi13042.766p275817.38	195.1781939	27.9714955	13.7406	6392	5.73×10^{10}
COMAi125930.824p275303.05	194.8784349	27.8841822	13.7758	4775	5.02×10^{10}
COMAi13039.767p275526.19	195.1656963	27.9239429	13.8003	7521	5.02×10^{10}
COMAi125932.771p275901.04	194.8865496	27.9836239	13.8776	5789	4.49×10^{10}
COMAi125944.407p275444.84	194.9350307	27.9124574	13.8892	6678	4.62×10^{10}
COMAi125929.403p275100.46	194.8725164	27.8501304	14.0567	6865	4.26×10^{10}
COMAi125929.956p275723.26	194.8748175	27.9564621	14.1492	6729	3.92×10^{10}
COMAi125946.782p275825.99	194.944929	27.9738864	14.2079	9453	3.44×10^{10}
COMAi13008.003p28442.81	195.0333478	28.0785604	14.2464	7268	3.51×10^{10}
COMAi125852.097p274706.15	194.7170734	27.7850423	14.2631	5682	3.05×10^{10}
COMAi13022.170p28249.30	195.0923782	28.0470287	14.2751	8198	2.88×10^{10}
COMAi13040.838p275947.80	195.1701586	27.9966122	14.3279	7112	2.97×10^{10}
COMAi13014.746p28228.69	195.0614417	28.0413036	14.3364	5737	2.88×10^{10}
COMAi125931.453p28247.60	194.8810575	28.0465569	14.3398	6979	2.88×10^{10}
COMAi13018.093p275723.59	195.0753914	27.9565536	14.3809	6371	2.89×10^{10}
COMAi13038.761p28052.34	195.1615083	28.0145411	14.3858	7537	2.51×10^{10}
COMAi13042.832p275746.95	195.1784703	27.9630421	14.5179	8428	2.49×10^{10}
COMAi13016.534p275803.15	195.0688951	27.967542	14.5781	4634	1.84×10^{10}
COMAi125833.134p272151.73	194.63806	27.3643696	14.6455	6996	1.93×10^{10}
COMAi13028.370p275820.64	195.118212	27.9724	14.6478	7113	2.17×10^{10}
COMAi13012.868p28431.74	195.0536199	28.0754849	14.6629	7506	2.11×10^{10}
COMAi125710.760p272417.38	194.294836	27.40483	14.6763	6215	1.8×10^{10}
COMAi13027.966p275721.56	195.1165257	27.9559893	14.7045	6984	2.11×10^{10}
COMAi125943.721p275940.82	194.9321724	27.9946746	14.7111	6688	2.13×10^{10}
COMAi13006.395p28015.94	195.0266486	28.0044302	14.771	7268	1.87×10^{10}
COMAi125832.052p272722.87	194.6335524	27.4563528	14.789	7053	1.86×10^{10}
COMAi125956.697p275548.71	194.986241	27.9301996	14.7981	7735	1.82×10^{10}
COMAi125942.301p275529.15	194.9262556	27.924765	14.9303	6900	1.61×10^{10}
COMAi13017.014p28350.07	195.0708955	28.0639111	14.9425	6152	1.79×10^{10}
COMAi125928.721p28225.92	194.8696712	28.0405337	15.1121	5569	1.39×10^{10}
COMAi125944.208p275730.38	194.9342034	27.9584394	15.1726	6892	1.2×10^{10}
COMAi125939.659p275714.03	194.915246	27.9538998	15.224	8029	1.21×10^{10}
COMAi13018.772p275613.34	195.0782184	27.9370411	15.2529	5293	9.56×10^{9}
COMAi125938.321p275913.89	194.9096747	27.9871925	15.3277	6776	9.96×10^{9}
COMAi125940.270p275805.71	194.9177939	27.9682538	15.4806	7531	1.01×10^{10}
COMAi125950.105p275529.44	194.9587727	27.9248449	15.6423	9743	8.88×10^{9}
COMAi125704.337p273133.28	194.2680737	27.5259129	15.8162	8328	6.02×10^{9}
COMAi125857.437p274706.15	194.739322	27.7850432	15.871	6894	5.79×10^{9}
COMAi125935.286p275149.13	194.8970289	27.8636498	15.9832	6274	5.27×10^{9}
COMAi125909.468p28227.35	194.7894507	28.0409322	16.1087	7232	5.14×10^{9}
COMAi125904.797p28301.16	194.7699908	28.0503226	16.3385	5071	3.78×10^{9}
COMAi125926.564p275957.06	194.8606856	27.9991838	16.488	6684	3.26×10^{9}
COMAi125937.990p28003.52	194.9082917	28.0009788	16.4973	4924	2.97×10^{9}
COMAi125911.543p28033.32	194.7980988	28.0092582	16.5021	6942	3.26×10^{9}

Table 3.1 (cont'd)

ID	RA [Deg]	DEC [Deg]	F814W [mag]	cz [km s^{-1}]	$M_\star/M_\odot$
COMAi13011.143p28354.91	195.0464292	28.0652533	16.545	7387	2.83×10^9
COMAi13021.673p275354.81	195.0903082	27.8985594	16.6023	4890	2.71×10^9
COMAi13024.823p275535.94	195.1034295	27.9266523	16.6134	7955	2.73×10^9
COMAi13018.873p28033.38	195.0786388	28.0092725	16.7015	6202	2.98×10^9
COMAi125854.632p274742.16	194.727636	27.7950466	16.7509	6471	2.82×10^9
COMAi13018.545p28549.62	195.077272	28.0971187	16.7975	7825	2.25×10^9
COMAi125845.533p274513.75	194.6897239	27.7538197	16.8371	6665	2.21×10^9
COMAi13051.149p28249.90	195.213122	28.0471971	16.8551	6459	2.78×10^9
COMAi125931.893p275140.76	194.8828881	27.8613245	16.9071	4640	1.96×10^9
COMAi13041.193p28242.34	195.1716389	28.0450969	16.9085	8826	2.15×10^9
COMAi13034.430p275604.95	195.1434613	27.9347093	16.9166	8356	1.94×10^9
COMAi13034.430p275604.95	194.99782	27.9405637	16.9388	6439	1.94×10^9
COMAi13035.420p275634.06	195.1475863	27.942797	16.9655	6958	1.72×10^9
COMAi125950.183p275445.52	194.959098	27.9126465	17.0638	7250	1.81×10^9
COMAi125946.943p275930.90	194.9455974	27.9919171	17.2504	8360	1.40×10^9
COMAi13030.954p28630.22	195.1289774	28.1083964	17.2653	5203	1.46×10^9
COMAi125937.010p28106.95	194.904209	28.0185978	17.477	7293	1.23×10^9
COMAi125815.292p272753.05	194.5637167	27.4647363	17.5029	7625	1.2×10^9
COMAi125953.929p275813.75	194.974706	27.9704888	17.5125	6618	1.17×10^9
COMAi125926.458p275124.81	194.8602453	27.8568931	17.5475	5007	1.03×10^9
COMAi13007.123p275551.49	195.0296795	27.9309714	17.5889	7726	1.03×10^9
COMAi125930.270p28115.17	194.8761261	28.020883	17.5936	7166	1.05×10^9
COMAi13017.641p275915.27	195.0735082	27.9875773	17.6168	6136	9.97×10^8

Chapter 4

Pairs and post-mergers in the red sequence: Selection methods and results

This chapter describes the pair selection process, where Red Sequence galaxy pairs are identified based on astrometric information and radial velocities for the complete sample Red Sequence galaxies found on the 25 ACS images of the CTS. The pair selection process is described on the first section along with the selection criteria. An statistical estimation of the distribution of pairs given the structural parameters of Coma is presented afterwards. The measured pair numbers and the expected values are compared and discussed. Finally, the detailed structure of the galaxies in pairs is discussed by evaluating the morphology of the galaxies, inspecting the two dimensional light distribution.

4.1. Pair selection

The determination of the dynamics and spatial distribution of galaxies in a cluster poses a huge observational challenge, since little information can be inferred about relative positions of galaxies with respect to the observer and nothing can be said regarding the perpendicular motion of cluster members. Methods for estimating the distance to galaxies are also useless to disentangle the phase space of clusters, since they are either not sensitive enough to account for the small variations of distances in clusters, or are not well defined to take into consideration the particular physics of such a system. Hubble's law for instance, does not take into consideration peculiar motions of galaxies, and hence radial velocity is not indicative of relative distances between cluster members. A similar limitation exists when considering the velocity of galaxies. Only the line-of-sight component can be measured and the projection of the velocity vector in the plane of the sky is unknown. Even for Local Group galaxies such as M33 and M31, proper motions have only been measured very recently Sohn et al. (2012) so their vector velocities can be estimated, although subjected to high uncertainties. In the case of clusters, this information simply cannot be obtained which makes the identification of true galaxy pairs a difficult task. Only a few particular exceptions can be made, provided that unlikely projection events occur, such as an elliptical galaxy behind a dusty disk. In the

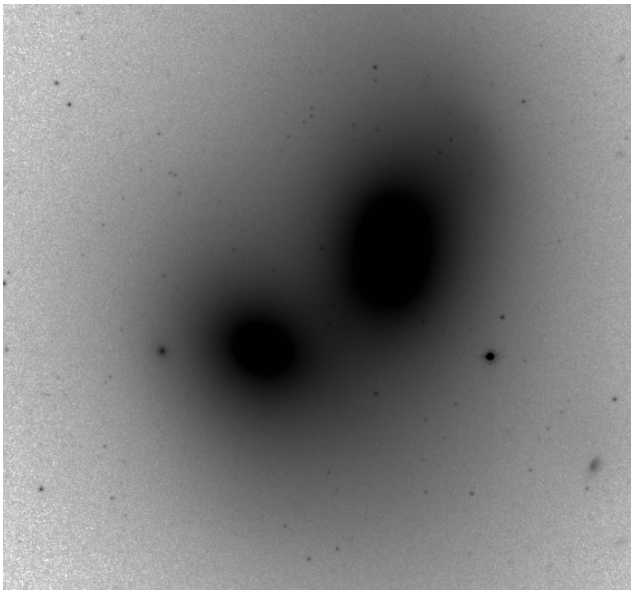

Figure 4.1 F814W image of projection pair NGC 4898 A & B. It can be seen that, regardless of the high overlapping between the two galaxies, they still appear as very smooth, elliptical objects, which is indicative of the pair being only a projection effect.

case of elliptical projection pairs, the identification of which galaxy is behind which can be a puzzle, and is usually difficult to obtain. Figure 4.1 shows the case of NGC 4898 A & B, both part of the red sequence of Coma. The two galaxies highly overlap making them difficult to characterize separately.

Given the limited information we have to identify true mergers, we have to track them by identifying properties that must be fulfilled in all cases:

- If galaxies are physically nearby they must appear close in the sky. Since we have no information about the line-of-sight relative position, projected distance is no indicative of actual closeness, but ensures that pairs are at least close in the the sky coordinates available.
- If galaxies are physically nearby but the velocity of the encounter is too large, a merger is unlikely to occur. Limiting the only component available is a first approximation to rule out high velocity encounters.

The aforementioned criteria replicates the approaches of van Dokkum et al. (1999), Tran et al. (2005) and Rudnick et al. (2012) in more distant clusters, where limits on radial velocity difference and projected distance are used to estimate pair fractions. We establish a limit on the projected separation of $30h^{-1}$ kpc and radial velocity difference of 300 km s^{-1}. The values selected here are common in the literature, and several examples can be seen in Patton et al. (2000); Lin et al. (2004); Tran et al. (2005); Casteels et al. (2013)

Projected distances between galaxies are estimated using the diameter angular distance D_A obtained for the redshift of Coma and the cosmological parameters adopted for this work: $\Omega_m = 0{,}3$, $\Omega_\Lambda = 0{,}7$ and $H_0 = 70$ km s^{-1} Mpc^{-1} and $z = 0{,}023$. An angular scale of 0,472

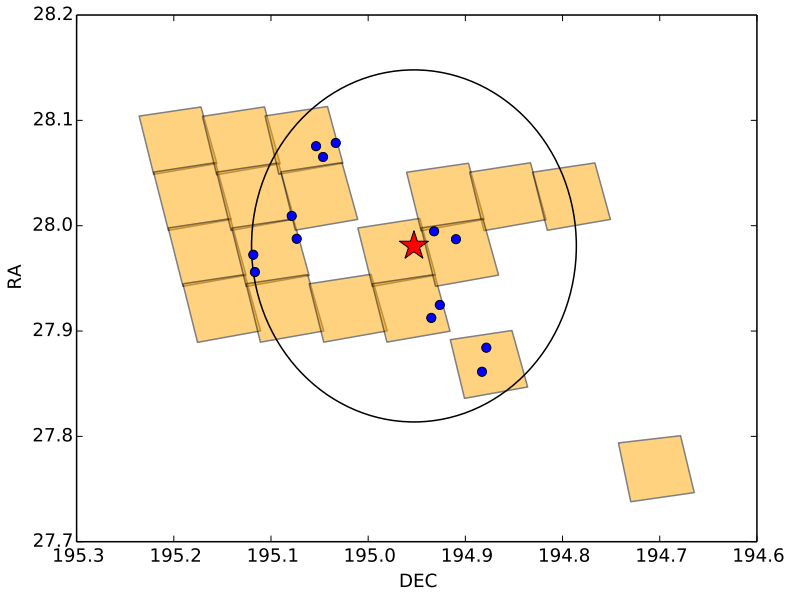

Figure 4.2 Distribution of the 13 galaxies selected as possible pairs. This is a close-up of the 19 HST/ACS fields from the core region of the CTS, where the red star indicates the center of the cluster and the solid line circle marks the central 0.5 Mpc.

kpc arcsec^{-1} and a projected distance limit of 42,85 kpc, is obtained, which translates into an angular separation of 90,799 arcseconds. Angular distances A between red sequence galaxies are then computed in terms of their equatorial coordinates (α, δ) as

$$\cos A = \sin\delta_1 \sin\delta_2 + \cos\delta_1 \cos\delta_2 \cos(\alpha_1 - \alpha_2)$$

By setting a projected distance limit of $r_s < 30h^{-1}$ kpc we find 54 of 70 galaxies lying in 50 individual pairs. However, if we add the difference in line-of-sight velocity criteria of $\Delta V \leq 300\,\mathrm{km\,s^{-1}}$ we are left a total of 13 galaxies, listed in Table 4.1, in five pairs and one triple system, all of them contained within the 19 ACS central pointings of the CTS. The distribution of the pairs is shown in figure 4.2, and their basic parameters are listed on table 4.1. It can be observed that the stellar mass ratios range from ∼1:1 to ∼1:3, that is, if they are physically related they could evolve into major mergers.

4.2. Pair likelihood

We investigated statistically the likelihood that these five observed close pairs and a close triple system are interacting and will merge in the future, or if instead they are simply chance alignments due to the high density of cluster galaxies in projected phase-space. If the pairs are simply caused by the alignment of foreground and background galaxies, then a similar number of pairs and triple systems should be obtained, on average, if we simulate randomized populations of Red Sequence galaxies with similar characteristics as those of our sample.

Table 4.1. Galaxies belonging to selected pairs/triplets by projection and velocity proximity

CTS ID[a]	Name	Stellar Mass ($M_\odot$)	F814W (mag)	r_s (kpc h^{-1})	ΔV (km s^{-1})
125930.824p275303.05	IC 3973	5.02×10^{10}	13.77	27.70	135
125931.893p275140.76	-	1.96×10^{9}	16.91		
125944.407p275444.84	NGC 4876	4.62×10^{10}	13.89	17.25	222
125942.301p275529.15	PGC 44649	1.61×10^{10}	14.93		
130028.370p275820.64	IC 4033	2.17×10^{10}	14.65	19.60	129
130027.966p275721.56	IC 4030	2.11×10^{10}	14.70		
125943.721p275940.82	PGC 44656	2.13×10^{10}	14.71	25.25	88
125938.321p275913.89	PGC 44636	9.96×10^{9}	15.32		
130018.873p280033.38	-	2.98×10^{9}	16.70	26.36	66
130017.641p275915.27	-	9.97×10^{8}	17.62		
130008.003p280442.81[1]	IC 4012	3.51×10^{10}	14.25	21.59	238[b]
130012.868p280431.74[2]	PGC 44723	2.11×10^{10}	14.66	14.32	119[c]
130011.143p280354.91[3]	-	2.83×10^{9}	16.55	20.96	119[d]
	Median values	$2{,}11\times10^{10}$		21,275	

[a]As defined in Hammer et al. (2010) using the prefix `COMAi`

[b]Difference between 1 and 2

[c]Difference between 2 and 3

[d]Difference between 1 and 3

Considering all known Coma cluster members within R_{200} (1.99 h^{-1} Mpc; Kubo et al., 2007), and having SDSS *ugriz* photometry, we built a sample of Red Sequence galaxies using an equivalent cut in i-band luminosity and $g-$i color, and a similar procedure to fit a Red Sequence relation and obtain galaxies in a $\pm 2.5\sigma$ region around the relation.

The position angles of these Red Sequence Coma galaxies are randomized with respect to the center of the X-ray emission from Coma (Neumann et al., 2003), but keeping the distance to center fixed in order to mimic the radial distribution of galaxies. To each sample of randomized angles a radial velocity is assigned based on the original sample of radial velocities of the cluster, which remained unchanged. This randomization process should model the expected galaxy density of the virialized population of galaxies in the Coma core, in which all resulting pairs are just chance projections along the line of sight. For each randomized population, we evaluated if they galaxies lie inside any of the 25 pointings of the CTS for which we defined the boundaries based on the reported positions of each pointing in Carter et al. (2008) and the shape of the ACS field. With this subsample of galaxies inside the CTS covering we ran the same criteria for the pair search. The expected number of galaxy pairs, with the adopted r_s and ΔV limits, that would be found within the 25 ACS images based on 10,000 randomized Coma Red Sequence populations is 7,0$\pm$2,2, including 1,3$\pm$1,1 triples (or more complex systems).

The predicted numbers are entirely consistent with the observed number of pairs/triplets, indicating that they all could be simply chance alignments. Nevertheless, this calculation does not rule out some of the observed pairs actually being physical ones. In order to test this, we search for evidence of recent or on-going interactions between galaxies belonging to the observed pairs/triplets.

4.3. Morphological inspection of Galaxies

A key aspect of this work is the fact that the aforementioned criteria by themselves are not enough to ensure that a pair of galaxies is actually bound. Therefore, a detailed examination of the morphology must be performed in order to identify, at least, early stages of gravitational perturbation. Visual identification of true mergers and their features proves to be a delicate issue for various reasons. Not all galaxies involved in a bound system show signs of perturbation from the beginning, and some structures that differ from smooth light distributions can be regarded as to be the result of internal processes such as bars, or star-burst events. Observational limitations are also strongly influential, and as mentioned in 1, surface brightness limit and resolution play a fundamental role. Finally, the procedures used to detect these structures and to identify them as remnants of mergers or internal structures is also crucial.

In order to identify which of the possible pairs found in the previous section could actually be bound systems, we analysed each galaxy of the possible pair sample looking for evidence of morphological perturbation as a result of gravitation interaction. We focused on asymmetrical structures such as ripples, tidal tails, star streams, halo discontinuities or rings (See section 1.2), which sometimes are hard to identify.

- We inspected each galaxy image looking for the mentioned features. This analysis was made by two members of our group, each one tagging the galaxy as perturbed or non-perturbed. In all cases, any particular feature observed was described and associated to either an external perturbation or internal process. The evaluation must take into consideration the fact that galaxies are being considered as part of a possible merger, so the presence of the companion galaxy must also be a factor in this evaluation.
- Two dimensional models of the galaxies light distribution were created using specific software. The models are subtracted from the original images in order to highlight very faint structures or deviations from symmetrical light distributions. Residuals were then evaluated by two members of our group, and the same categorization made on step one was made: galaxies were identified as perturbed or unperturbed depending on the observed features and its interaction with their companions

Galaxy models were build using two different software. In the first place, *IRAF* task *ELLIPSE* was used, but the results obtained were non satisfactory since resultant models were not smooth enough at high radius and the residuals were usually contaminated by the structure introduced by the models, which were difficult to differentiate from true galactic features. GALFIT was used then, given its stability, ease of use and improved physical relevance, given that the outputs of the models can be related directly and more easily with internal properties of galaxies.

Having selected GALFIT as the preferred method for modeling galaxies, we decided to inspect our entire sample of Red Sequence galaxies in order to look for signatures of recent past interactions. In this step, we considered also features that could not be considered as a result of an ongoing interaction, so the entire Red Sequence sample (70 galaxies) were inspected. Individual perturbed galaxies are identified as possible post-mergers as the fraction of post-merger galaxies is also indicative of the merger activity of the cluster, and the results obtained in this study were compared to similar results in the literature.

In the following section, the two modeling processes are discussed.

4.3.1. *ellipse* models

Since the complete sample of Red Sequence galaxies are classified as E/S0's, an elliptical isophote method was used to model galaxies. The method of isophotes fits elliptical regions around galaxy center with constant intensity, with several isophotes being fitted as a function of semi-major axis, then producing a two-dimensional model by interpolating the intensity between the isophotes. *IRAF* task *ellipse*, (Jedrzejewski, 1987) which is part of the *stsdas* package, reads two-dimensional image sections and produces as main output one table which contains a row for each elliptical isophote, and several columns indicating the structural parameters fitted for each isophote. Models using this technique were produced for the thirteen galaxies in the possible pair sample, along with the residual maps obtained.

The task takes the original galaxy image as input, as well as several initial values for the structural parameters of the corresponding isophotes to be fitted, such as X and Y center coordinates (given in pixels), ellipticity, position angle and semi-major axis length. For the

given parameters, the image is sampled according to an elliptical path given by the initial guesses, and the one dimensional intensity distribution as a function of position angle θ is analysed by least-squares fitting to the function:

$$I(\theta) = I_0 + A_1 \sin(\theta) + B_1 \cos(\theta) + A_2 \sin(2\theta) + B_2 \cos(2\theta)$$

Each of the harmonic amplitudes are related to a specific ellipse geometric component, and its deviation from the true value for that parameter. The steps of the iteration process shifts the most deviated considering the local gradient and computes a new set of parameters to be tested. After a convergence criteria is met or a certain number of iterations are made, the task increases the semi-major axis of the initial guess for the ellipse and re-runs the same procedure for a given interval of semi-major and at a given step for the increase of this value, until the user-defined range is completed. This fitting process allow all of the basic parameters for galaxies to be shifted, so that isophotes not necessarily share the same center, position angle or ellipticity. This behavior is usually observed in galaxies from our sample, where the outer parts of the halo appear sometimes to be rotated with respect to the central bulge.

Foreground and background sources, as well as unwanted artifacts from the images have to be flagged in order to be ignored during the fitting process. In this step, elliptical regions masking out pixels with sources that do not belong to the target galaxies were created, one for each galaxy. Task *ellipse* has as parameters a binary table with coordinates of pixels removed from the fitting region and a pre-defined threshold fraction of masked pixels at which the fitting procedure is allowed to run. If at a certain semi-major axis, a fraction of pixels larger than the threshold is masked, the iteration stops and the model is truncated to the last completed semi-major axis. In some cases, the threshold had to be relaxed in order to allow *ellipse* to run towards larger radii.

Having completed the isophote fitting stage, the task builds a two-dimensional map of the galaxy using as the isophote parameters obtained in the previous step trough the task *bmodel*. It interpolates the values for the intensities and creates a temporary high density map of isophotes which are then plotted.

In this paragraph we refer to the difficulties of the galaxy modelling using *ellipse*. Several problems were identified from the models and the residual maps. Since we dealt with high resolution images, temporary interpolated maps sometimes were not enough to cover the entire area covered by the galaxy, leaving gaps between successive isophotes. Also, the modeling task had difficulties generating smooth models, since the interpolation between isophotes did not appeared to be global, or to consider all isophotes to generate a smooth gradient. Figure 4.3 shows isophotal radial profiles obtained for modeled galaxies using *ellipse*, which in some cases are not perfectly smooth, making the evaluation of residuals a difficult task since models can produce artificial features. Also, given the sensitivity of isophotal fitting to localized intensity, models can reproduce these features partially removing them from residuals and making them hard to recognize. These issues made the identification of features a problematic task, since the residuals reflected the discontinuities from the models, which in some cases competed with the internal structure of the galaxy. For these reasons, we decided to abandon this method and use instead GALFIT, which provides smooth two-dimensional models, based on fewer but meaningful parameters such as the Sersic index and effective radius. Being these models smoother and well constrained, highlight efficiently the internal asymmetric structure of the galaxies.

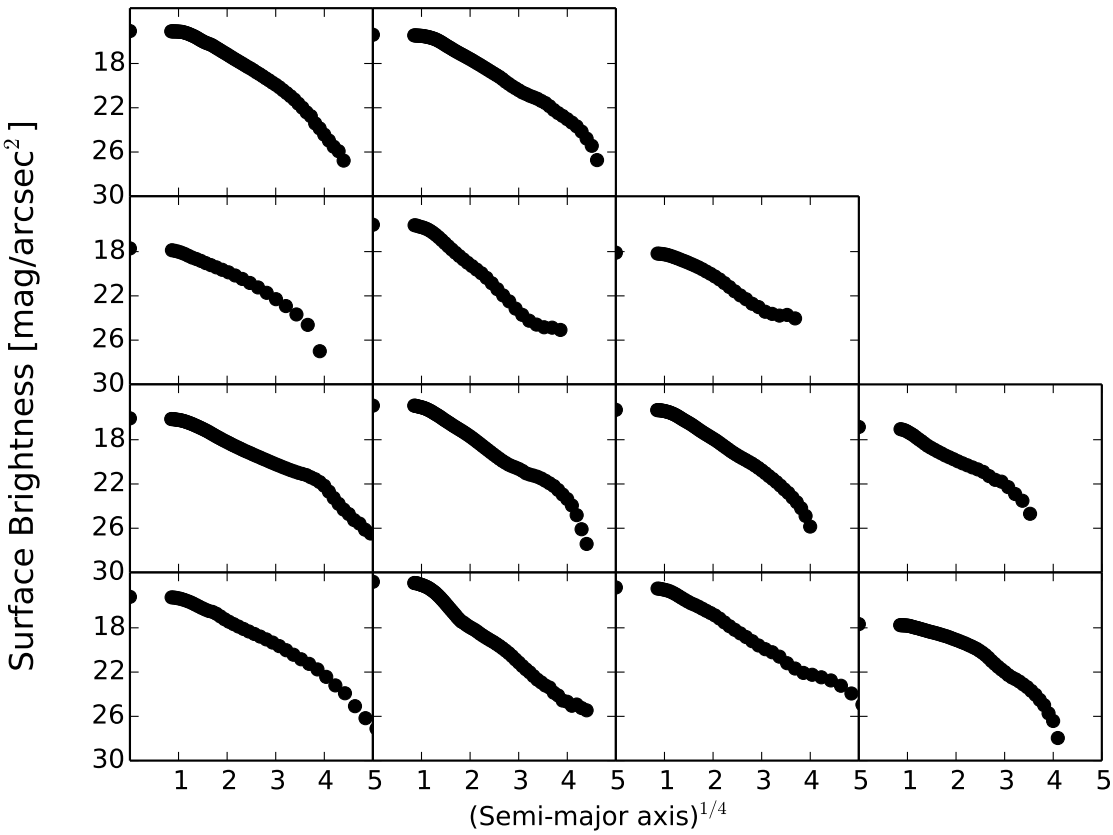

Figure 4.3 Radial isophotal profiles found for the 13 galaxies in the possible pair sample. Sampling at small semi-major axis is difficult given the small amount of pixels. It can be seen that models are not smooth in all cases, which can lead to misleading residual interpretation.

4.3.2. GALFIT models

GALFIT (Peng et al., 2010) is a fitting software based on the use of well established two-dimensional light distributions, which presents several advantages in comparison to *ellipse*. In the first place, it allows for component decomposition of galaxies by fitting multiple light distributions at once for a single galaxy, combining them in a single solution. This allows for a detailed examination of the morphology of each of the components of a galaxy (i.e.: bright cores, bulges, halos, bars) separately. The parameters for the light distributions can be easily related to astrophysical properties of the galaxies, and the number of parameters that can be tweaked or fine tuned is larger than for the *IRAF* task. Finally, GALFIT proved to be much more stable and easier to use, converging to reliable solutions with little information provided in the parameter files, not requiring extraordinary efforts in providing first guesses for the structural parameters.

The basic principle by which GALFIT works is to minimize the following function, using the Levenberg-Marquardt algorithm

$$\chi^2_\nu = \frac{1}{N_{\mathtt{dof}}} \sum_{x=1}^{nx} \sum_{y=1}^{ny} \frac{(\mathtt{flux}_{x,y} - \mathtt{model}_{x,y})^2}{\sigma^2_{x,y}}$$

where $\mathrm{flux}_{x,y}$, $\sigma_{x,y}$, nx and ny are the intensity at the pixel position x, y, flux uncertainty at the same position, x and y dimensions of the image, respectively. $\mathtt{model}_{x,y}$ is defined as

$$\mathtt{model}_{x,y} = \sum_{\nu=1}^{nf} f_{\nu,x,y}(\alpha_1 \ldots \alpha_n)$$

which is the sum of the different functions to be fitted, each of which correspond to a different two-dimensional light distribution described by the set of parameters $\alpha_1 \ldots \alpha_n$. This model is generated after convolution with the Point Spread Function of the images, which must be provided by the users and is fitted after rejecting user-defined masked areas.

Point Spread Functions

PSFs can be generated by multiple different processes. The simplest one is to assume a certain analytic distribution such as a Gaussian or Lorentzian radial profile, which facilitates the process but neglects almost completely the signature response of the telescope and the fact that, in the case of the HST, the focal plane is noticeable distorted. Indeed, this distortion makes the use of a single PSF for the entire image a non optimal solution. Another option is to generate an empirical PSF based on the stacking of multiple non-saturated point sources on the image. For the case of the images from the CTS, this is an issue given the small amount of stars on the field, which makes the building of the template a very difficult issue, considering that more than just one must be built, for the different areas of the detector. Fortunately, synthetic PSF can be built for the HST instruments using *Tinytim*[1] (Krist et al., 2011). It provides very accurate PSF for specific camera, filter and pixel position, so the specific template can be obtained on-demand for the requirements of a particular galaxy to be modeled.

[1] http://tinytim.stsci.edu/cgi-bin/tinytimweb.cgi

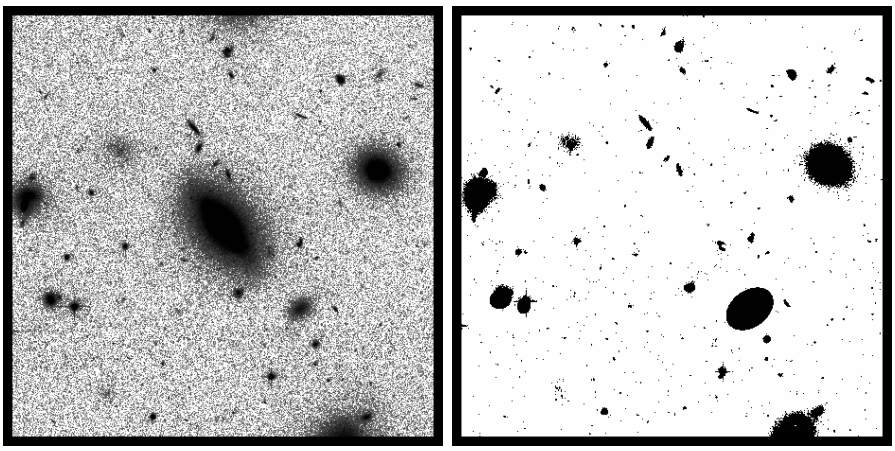

Figure 4.4 Left panel shows a sample of a crowded region on a F814W image of CTS with a Red Sequence galaxy to be modeled in the middle. Left panel shows a segment image produced by SExtractor with all background sources and artifacts identified and flagged in order to be ignored by the fitting task. In some cases, sources were not identified or only identified partially so they had to be masked manually.

Bad pixel masks and overlapping

In most of the cases, galaxies do not appear as isolated systems on the detector: Multiple foreground/background objects such as distant galaxies and stars, or image artifacts can affect the ability of GALFIT to provide a reliable model. In some cases, bright galaxies from the cluster can affect the modeling by being particularly close to the target galaxy. An example was already mentioned in section 4.1, where two bright galaxies overlap. In most of the cases, a bad pixel mask is enough to flag out pixels of unwanted light sources. This bad pixel mask is simply a binary image where each pixel is flagged by assigning it a non-zero count value if the corresponding pixel of the original image should not be considered when minimizing the residuals. In our case, we built the masks by using the segment image output of SExtractor, which identifies sources and assigns a value to each source pixel, corresponding to the index of the detected source. An example of mask image is given in figure 4.4, which shows the flag values assigned to different sources.

In more extreme cases, a simple strategy can be followed in order to improve the models when overlapping between galaxies exists, although the quality of the results in some cases are below average. The brightest galaxy of the pair is modeled by masking as much light as possible from the apparent companion. The modeled galaxy is then subtracted from the original image, and residuals are masked so that the second galaxy remains in the frame and can be modeled in the same way the first one was made. The model made for the second galaxy is then removed from the original image, and the first galaxy is then modeled again by masking out the residuals from the second galaxy. This procedure can iterate until no significant improvements on the models and residuals are observed. GALFIT also offers the possibility of performing a joint fit by establishing the parameters for the galaxy simultaneously, but the results usually led to an underestimation of the intensity on both galaxies, and it was difficult to obtain correct position angles for the galaxies. In such cases, we preferred to stay with the alternating fitting procedure in order to determine the initial guesses for the parameters of

the model in earlier iterations.

Modeling strategy

We fit galaxies using one, two or three Sersic profiles plus a nuclear point source when needed. The Sersic profile is given by

$$\Sigma(r) = \Sigma_{\rm e} \exp\left[-b_n\left(\left(\frac{r}{r_{\rm e}}\right)^{1/n} - 1\right)\right]$$

where $r_{\rm e}$ and n are the effective radius and Sersic index of the distribution, and are the main parameters fitted during the process. Other parameters fitted during the process included, but not limited to are the ellipticity, position angle, total integrated magnitude and center coordinates. Parameter b_n is a function of the Sersic index, and is defined so that

$$\Gamma(2n) = 2\gamma(2n, b_n)$$

where Γ and γ are the complete and incomplete gamma functions (reference). Below we present a brief outline of the modeling process based on the work by Weinzirl et al. (2014) from where the model strategy employed in the GALFIT models is adopted, including the number of Sersic profiles and the strategy for the guesses for the initial parameters:

- *Stage 1 (Single Sersic fit with nuclear point source if needed):* A single Sersic profile is fitted for the galaxy, using basic estimates for the ellipticity, position angle and center coordinates. Residuals are inspected and the model is adopted if no coherent structure is observed (e.g., inner/outer disks, bars, bulges or rings). If the the light profile downwards from the inward extrapolation of the Sersic profile (known as *Core Sersic profile* Trujillo et al., 2004) or shows any structure indicating the need of additional components, then we continue to stage 2. If a bright nuclear residual is observed in the center of tha galaxy, an additional component is added in the modeling, being a sampled PSF of the desired magnitude.
- *Stage 2 (Double Sersic model with nuclear point source if needed):* If the galaxy model of stage 1 is not sufficient to describe all the structure observed in the residuals, then a second Sersic component is added to the parameters given to GALFIT, plus a nuclear point source if it was required in the previous stage. The two component model is intended to represent the inner compact and outer extended structures observed.
- *Stage 3 (Triple Sersic model with nuclear point source if needed):* If the residuals from stage indicate the presence of a large scale bar on the galaxy, then we proceed to the third stage of adding a third sersic component. In this case, the Sersic indexes from the previous stages are fixed, while all other parameters such as integrated magnitudes and position information are allowed to vary freely. This allows the third added component to fit the missing bar more correctly.

Figure 4.5 shows an example of the modeling process, where a single component model is not enough to describe the observed light distribution. It is shown that employing additional Sersic components and nuclear point sources helps producing a better model of the galaxy with less residuals due to the galaxies not following an exact single Sersic profile.

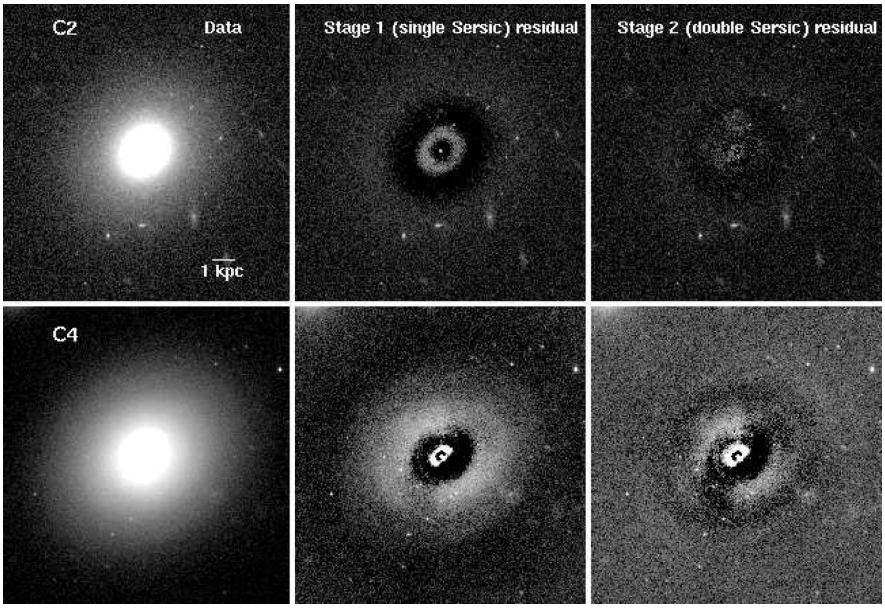

Figure 4.5 Top and bottom rows show how some of the galaxies (C2 = COMAi125935.286p275249.13 and C4=COMAi13014.746p28228.69) are poorly fitted by a singe Sersic model in stage 1, and how residuals improve the quality of the model after adding a second Sersic component. From left to right, the original data, the residual after subtraction of the 1-component model, and the residual after the 2-component model has been subtracted.

4.4. Morphological inspection of galaxies in the pair sample

In this section, a brief description of the galaxies on the pair sample is given, as well as any remarkable feature worth mentioning from the F814W images and the residuals. Each pair/system is described individually and the results from the visual inspection are presented Names presented in the subsections follow the codification given by Hammer et al. (2010). Common names for galaxies already catalogued are given in the description when available.

13 galaxies involved in 5 pairs and one triple system are inspected in detail, revealing that no galaxy presents features that could be regarded as a results of an ongoing interaction between the pair. In some cases, it can be seen that galaxies do show signs of internal structure such as bars or light distributions not following a perfect composition of Sersic profiles. For each pair/system, a figure is presented showing, from left to right, the direct F814W image, the model generated using GALFIT, and the residuals after model subtraction.

4.4.1. 125930.824p275303.05 & 125931.893p275140.76

125930.824p275303.05 has been catalogued as IC 3973 and it is the brightest galaxy selected as a member of a possible pair. The faint projected companion has no common name. IC 3973 shows a very peculiar morphology, showing a bright core with an angle of approxi-

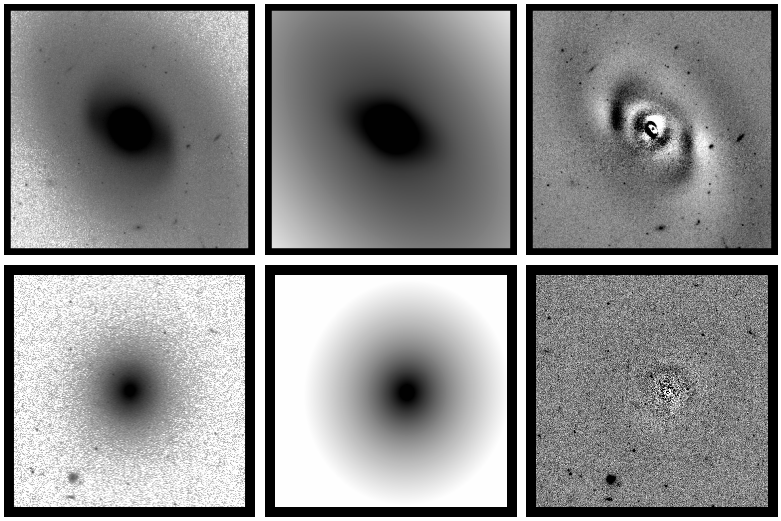

Figure 4.6 From left to right, direct images, GALFIT models and residual maps from GALFIT models for IC3973 and 125931.893p275140.76. We conclude that they are not gravitationally interacting (See text).

mately -30 degrees with respect to the horizontal image coordinate, and a fainter, extended halo which appears to be rotated with respect to the inner core, at an angle of about 45 degrees, as measured by GALFIT. The data image of the galaxy reveals what appears to be a small prominence in both sides of the core, which we interpret as a small bar system. These bars are fairly common in the Red Sequence galaxies of Coma. While in the inner core the galaxy appears highly symmetrical, at outer radius it can be seen a large prominence which resembles a spiral arm, coming out clockwise from the bottom right. This structure is not seen with equal intensity in the other side of the galaxy, and the residuals confirm the presence of this structure.

On the other hand, 125931.893p275140.76 appears as a very smooth object with no visible features. Residuals are almost non-existent and do not seem to reveal any additional structure. This faint companion does not appear to be responsible of the features observed in IC 3973, since it does not show any sign of perturbation, nor the feature observed in IC 3973 appears to point towards the companion. Further inspection of the entire image reveal that no nearby galaxy can be considered distorted, although no models for all galaxies were created.

From the direct images and the residuals (4.6) we conclude that these two galaxies do not show evidence of being interacting gravitationally, but we consider IC 3973 as a possible example of a post-merger galaxy, given the asymmetrical structure observed, at least at the surface brightness limit (26.5 mag/arcsec^2) achieved by the ACS imaging.

4.4.2. 125944.407p275444.84 & 125942.301p275529.15

Both galaxies have been previously catalogued as NCG 4876 and PGC 44649, respectively. NGC 4876 appears as a featureless elliptical in the F814W image, and the residuals do not show any evidence of perturbations towards the outer parts of the halo. Perhaps the most

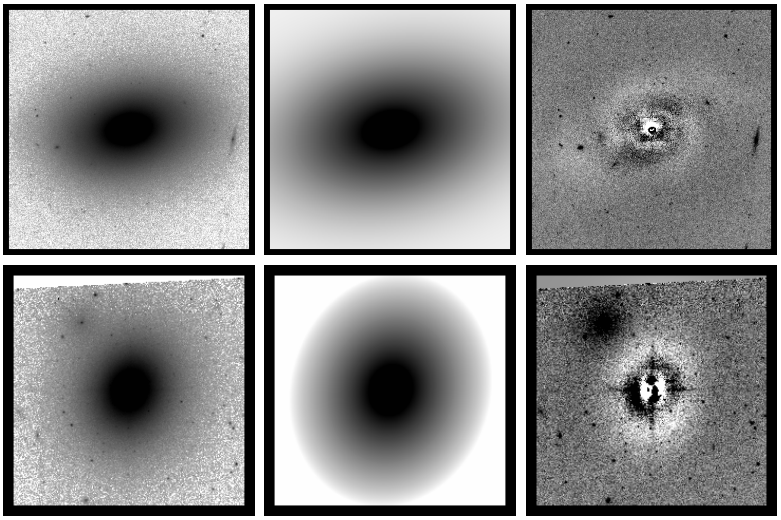

Figure 4.7 From left to right, direct images, GALFIT models and residual maps from GALFIT models for NGC 4876 and PGC 44649. We conclude that this is not a gravitationally interacting pair (See text).

interesting feature arises in the residuals in the inner region of the galaxy, where a faint but evident spiral structure can be observed. These structures appear in various examples on the pair sample and the entire Red Sequence sample galaxies.

PGC44649 has a very bright core, as revealed by the small artifacts that appear in both the direct image and the residuals, and despite its small apparent size. It also has a small projected companion easily recognizable in the residuals, which made the modeling process a bit more difficult. The residuals show a small overestimation of the intensity at intermediate radius, appearing as a bright ring around galaxy cluster (residuals are shown in negative), even using 3 Sersic components. Besides this feature, the galaxy looks very smooth and elliptical with no sign of perturbation (See figure 4.7).

We consider this pair a negative result, since no major asymmetries or signs of actual interaction can be observed, and the small structures of each galaxy clearly do not seem to be caused by the presence of the companion, since in the case of NGC 4876 the structure appears to be highly symmetrical, indicating an internal origin, and the ones in PGC44649 appear to be related to the bright core observed in that galaxy and does not show a preferential direction that matches with the position of NGC 4876.

4.4.3. 130028.370p275820.64 & 130027.966p275721.56

Both galaxies have been previously catalogued as IC 4030 and IC 4033 respectively and both are among the brightest members of the red sequence with very similar apparent magnitudes of F814W = 14.70 and 14.71.

Both galaxies present a noticeable inner structure: IC 4030 shows two prominent lobes aligned with the semi-major axis. Given the high apparent ellipticity of the galaxy, these lobes

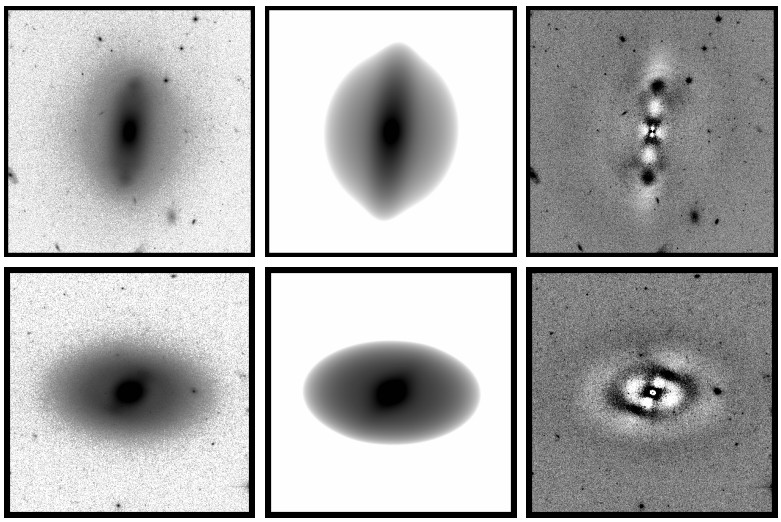

Figure 4.8 From left to right, direct images, GALFIT models and residual maps from GALFIT models for IC 4030 and IC 4033. This pair is not considered a physical one (See text).

could be actually the outer parts of a disk being observed almost edge-on. These lobes are also observed in the residuals after model subtraction. The model itself is of particularly interest, since it formed by three Sersic components, one having a large effective radius accounting for the outer halo of the galaxy, two inner components of high ellipticity which models what appears to be the inner disk ad a bar structure. Residuals show a characteristic shaped-mark, also visible in other examples, which appear as a result of the 'boxy' profile of the galaxy.

IC 4033 appears to have a bar structure orientated close to 45 degrees in figure 4.8. After model subtraction the residuals show a symmetrical system of concentric rings, probably as a result of the radial profile not matching exactly the true nature of the galaxy.

In both cases, residuals and observed features in the direct images do not reveal any noticeable asymmetry and we consider these two galaxies to be not related to each other.

4.4.4. 125943.721p275940.82 & 125938.321p275913.89

Both galaxies have been previously catalogued as PGC 44656 and PGC 44636 and in both cases the direct images show smooth light profiles with no noticeable features.

In the case of PGC 44656 the residuals show a symmetrical structure similar to those of IC 4033, although no bar-like structure is present here. Again, we do not interpret these features as resultant of an on-going interaction with PGC 44636.

PGC 44636 appears as round, smooth elliptical. On the upper part of the galaxy a small object can be seen, which does not appears to be part of a system with PGC 44636. The residuals show that the model does not follow the light profile perfectly, thus showing the characteristic concentric residuals. At larger radius the model leaves no residuals.

In both cases, residuals and direct images presented in figure 4.9 do not reveal any sign

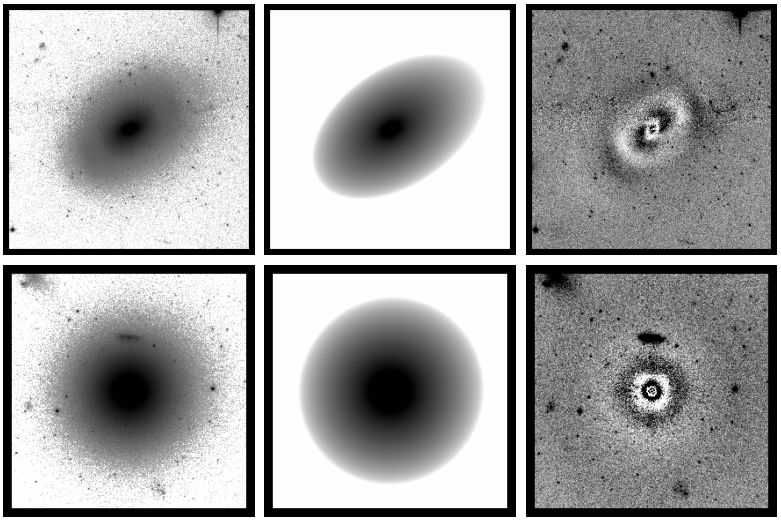

Figure 4.9 From left to right, direct images, GALFIT models and residual maps from GALFIT models for PGC 44656 and PGC 44636. This possible pair is not confirmed as a physical one (See text).

of perturbation caused by the presence of the companion.

4.4.5. 130018.873p280033.38 & 130017.641p275915.27

In this case, none of the galaxies have a catalog name previously assigned. Both galaxies lie inside two different frames of the CTS and both of them lie close to the edge of the detector. This is the possible pair with the smallest difference in radial velocity: $\Delta V = 66$ km s^{-1}. In both galaxies, models do a good job and follow very closely the light profiles of the galaxies. The residuals presented in figure 4.10 look a little bit strange in the central part of 130017.641p275915.27, and we believe this is similar to the case of PGC 44649, on which the bright core leaves strange residuals due to the PSF being slightly asymmetrical.

We consider this pair as a negative result.

4.4.6. 130012.868p280431.74, 130008.003p280442.81, & 130011.143p280354.91

This is the only system of possible related galaxies with more than 2 galaxies involved (a triple system), and it contains the pair with the smallest projected distance: 14.74 kpc between 130012.868p280431.74 (PGC 44723) and 130011.143p280354.91.

The brightest galaxy of the system is also known as IC 4012 and shows a structure similar to that of IC 4030, although the inner disk structure is less prominent, and the residuals after model subtraction do not reveal the lobes previously observed with the same intensity. The model does a good job at larger radius where no structure is observed. PGC 44723 lies close to

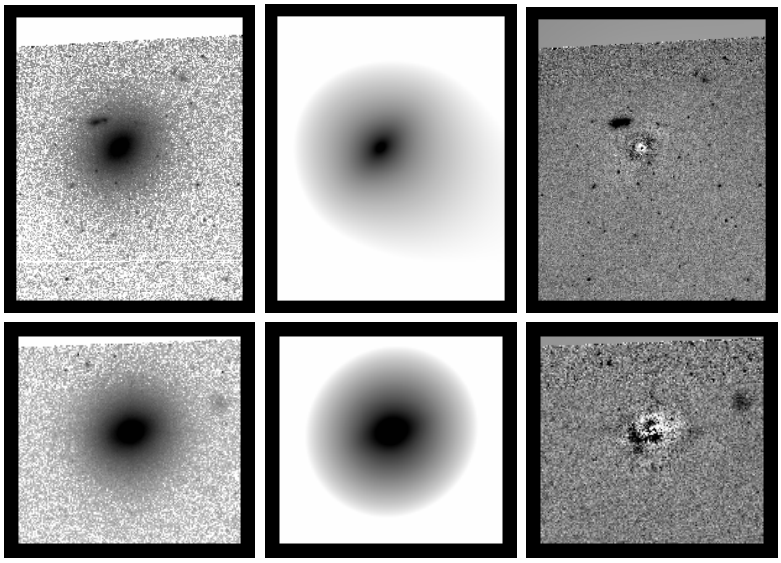

Figure 4.10 From left to right, direct images, GALFIT models and residual maps from GALFIT models for 130018.873p280033.38 and 130017.641p275915.27. We conclude that this apparent pair is not gravitationally interacting (See text).

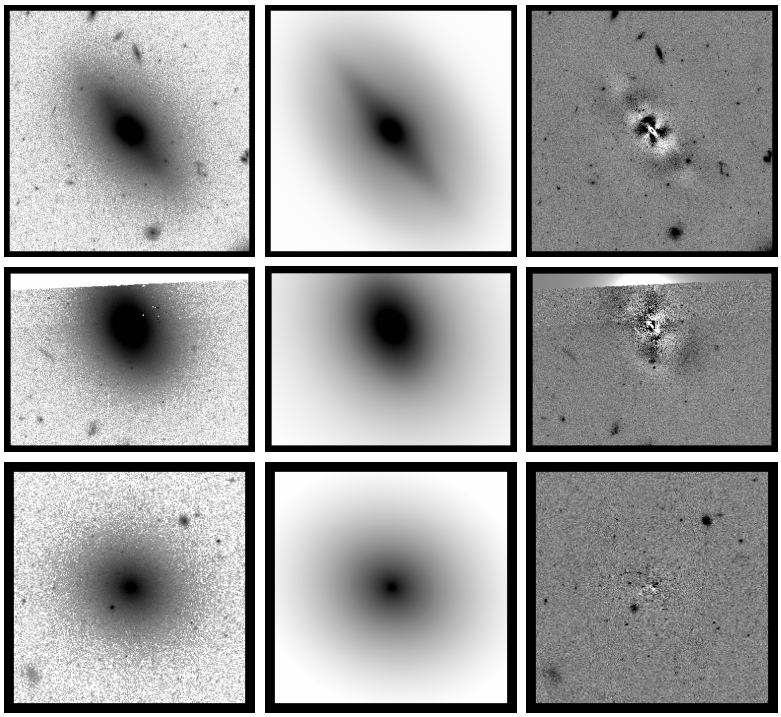

Figure 4.11 From left to right, direct images, GALFIT models and residual maps from GALFIT models for IC 4012, PGC 44723 and 130011.143p280354.91]. No signs of interaction is found in the galaxies of this candidate triple system.

the edge of the detector and it was difficult to model since a fraction of the light distribution is absent and the mask image had to consider that particular region. Regardless of these issues, the residuals look very clean and do not reveal any structure. The same happens with 130011.143p280354.91, which is a small elliptical perfectly fitted with two Sersic profiles. Almost no residuals can be observed.

None of these three galaxies show any evidence of perturbation after the evaluation of the direct images and residuals presented in figure 4.11 so we consider them as non-mergers.

4.5. Morphological inspection of galaxies in the Red Sequence

In this section, the galaxy decomposition after modeling is presented along with observations of any particularities in the direct images or residuals. From the complete sample of 70 Red Sequence galaxies, 3 galaxies have they centers lying outside the edge of the detector so the morphological inspection relies only on the visual inspection made over the direct images. The remaining galaxies were classified according to the number of components employed in the models, according to the modeling strategy presented in section 4.3.2. For each subsample a table is presented with the structural parameters for each Sersic component, with the 13 previously studied galaxies indicated with superscripts and a description of notable cases is given. The inspection is performed to look for evidence of post-merger features in the Red Sequence galaxies that could arise at the surface brightness limit of 26.5 mag/arcsec^2 achieved by the ACS imaging. Visual inspection of residuals and direct images were carried out by Tim Weinzirl (TW) from the University of Nottingham, and Juan P. Cordero (JPC), and the results of the inspection were compared in order to re-discuss those cases with discrepancies.

4.5.1. Single component models

Four galaxies of the complete sample were modeled by a single Sersic profile, being the most notable the cases of NGC 4874 (COMAi125935.698p275733.36) which is one of the two CD galaxies of the cluster, and and the projected pair NGC 4898 A & B.

In the first one, double or triple Sersic profiles only seemed to increase the value of χ^2_ν (Defined in section 4.3.2) with respect to the single profile which in any case does a good job specially at higher radius. Despite the large extent of the NGC 4874, a single Sersic profile seems to fit the galaxy quite well towards higher radius, where no features can be observed even in the proximities of other sources. The inspection of this galaxy is particularly difficult given the large number of background sources and cluster members which overlap with the galaxy, making the modeling of these companions also a difficult step. Also, a fraction of the outer halo of the galaxy lies outside of the CTS covering towards the south, where a small cluster member, NGC 4872 lies at a small projected distance. Since no imaging of that region is available nothing can be said regarding a possible interaction between NGC 4872 and NGC 4874, even while their reported velocity difference is of merely 17 km s^{-1}. Towards the center

Table 4.2. Structural decomposition parameters for galaxies fitted with a single Sersic component

Galaxy Name	C1 r_e [kpc]	C1 n
COMAi125935.698p275733.36	391.3	11.4
COMAi13017.683p275718.93	2.13	2.80
COMAi13018.093p275723.59	1.27	2.37
COMAi125909.468p28227.35	1.88	2.54

of the galaxy no features can be observed and the galaxy appears very smooth and elliptical.

In the case of the projected pair, adding multiple components to the fitting caused GALFIT to diverge or reaching a meaningless solutions so we decided to stay with only one component per galaxy and rely our inspection on the direct images mainly. While the galaxies appear very close on the sky, contrast settings reveal that their inner regions remain symmetrical and elliptical and the outer regions on the opposite directions to the other galaxy also show no evidence of perturbation. This is one of the most difficult cases in the Red Sequence sample but we opted to consider this as a non interacting system in the first place and each galaxy as a non post-merger. Both TW and JPC agreed on this picture.

The third galaxy has a prominent boxy shape but appears as a non perturbed galaxy as revealed by the residuals, which show a characteristic x-shaped pattern, typical of boxy and disky galaxies.

4.5.2. Double component models

The double Sersic sub-sample is composed of 37 galaxies, and in most cases they were catalogued by Weinzirl et al. (2014) as unbarred S0 with an outer elongated disk or an elliptical where a single Sersic profile had non satisfactory results such as an overestimation or underestimation of central luminosity. Given the results of the single component sample, and the fact that we only choose to model the galaxies using up to three Sersic components, it is expected that most of the galaxies modeled with two components appear as unperturbed, leaving the perturbed galaxies on the triple component sample.

In 33 cases both TW and JPC coincide in the conclusion that no features can be observed neither in the direct images and the residuals or only minor axisymmetric residuals can be observed in some cases mainly caused by disky or boxy light profiles.

The remaining 4 cases that deserve individual comments or had features not noticed TW and JPC simultaneously.

- **COMAi125815.292p272753.05** The direct imaging reveals a perfectly symmetric with no signs past or ongoing interaction, although at the very center of the residuals there seems to be a very small structure which is too small to be considered a post-merger feature. A small projected spiral companion of unknown radial velocity lies close to the galaxy and looks fairly distorted, but there seems to be no interaction between

Table 4.3. Structural decomposition parameters for galaxies fitted with two Sersic components.

Galaxy Name	C1 r_e [kpc]	C1 n	C2 r_e [kpc]	C2 n
COMAi13051.464p28234.86	3.90	2.01	0.61	2.21
COMAi125929.403p275100.46	2.37	1.86	0.28	2.19
COMAi13008.003p28442.81[a]	0.99	3.00	1.66	0.57
COMAi125852.097p274706.15	2.12	6.95	1.74	1.41
COMAi13040.838p275947.80	3.16	2.34	0.34	1.83
COMAi13014.746p28228.69	0.90	3.68	2.26	0.47
COMAi125931.453p28247.60	1.61	3.51	2.36	0.86
COMAi13016.534p275803.15	3.26	6.16	3.59	0.48
COMAi125943.721p275940.82[a]	0.76	3.20	1.83	0.72
COMAi13006.395p28015.94	1.60	6.78	2.08	0.84
COMAi125832.052p272722.87	0.35	1.82	2.54	1.83
COMAi125942.301p275529.15[a]	0.08	1.53	0.98	1.48
COMAi125944.208p275730.38	5.43	5.82	1.95	0.56
COMAi125939.659p275714.03	0.32	1.91	1.97	1.08
COMAi125938.321p275913.89[a]	0.71	2.06	3.27	0.89
COMAi125704.337p273133.28	0.46	1.21	2.69	0.89
COMAi125935.286p275149.13	1.37	2.08	0.70	0.31
COMAi125911.543p28033.32	0.54	0.95	1.55	1.21
COMAi13011.143p28354.91[a]	0.66	2.64	1.48	1.40
COMAi13021.673p275354.81	0.40	1.14	1.71	0.56
COMAi13024.823p275535.94	0.58	1.36	3.06	1.20
COMAi13018.545p28549.62	0.76	0.97	2.83	0.86
COMAi125845.533p274513.75	2.98	2.09	1.52	1.71
COMAi13051.149p28249.90	0.96	1.57	5.98	1.35
COMAi125931.893p275140.76[a]	1.04	2.09	0.62	0.65
COMAi13041.193p28242.34	0.41	1.08	1.11	0.84
COMAi13034.430p275604.95	1.15	1.8	2.83	1.00
COMAi125959.476p275626.02	1.07	1.67	2.67	0.72
COMAi13035.420p275634.06	0.73	1.05	2.51	0.76
COMAi125946.943p275930.90	0.31	0.98	1.47	1.01
COMAi125937.010p28106.95	0.79	2.13	0.35	0.51
COMAi125815.292p272753.05	1.53	2.51	0.65	1.08
COMAi125953.929p275813.75	0.79	2.13	0.35	0.51
COMAi125926.458p275124.81	1.05	1.72	0.42	0.85
COMAi13007.123p275551.49	0.63	1.94	0.32	5.88
COMAi125930.270p28115.17	1.13	1.83	0.62	0.70
COMAi13017.641p275915.27[a]	0.50	1.60	1.23	1.76

the two.

- **COMAi125942.301p275529.15** This case was already mentioned, as it is one of the 13 galaxies of the projected pair sample. It has a very bright nucleus and there seems to be a slight asymmetry close to the center of the galaxy, probably caused by the PSF on the center of the galaxy or an unmasked source. Still, the global morphology of the galaxy looks perfectly symmetrical with no evidence of recent past interactions.
- **COMAi13006.395p28015.94** The galaxy lies close to the limit of the detector, and an elongated structure passes close to the center. It is difficult to determine the nature of this structure, which is best seen in the residuals, but it appears extremely sharp and straight, possibly being a foreground disk or arc. The rest of the image and residuals look very smooth with no signs of recent merger activity.
- **COMAi13008.003p28442.81** Being close to the edge of the detector, it is impossible to say whether the small bright patched on the residuals are actually asymmetric or not, but at least at the radius of the distance to the edge, the residuals look symmetrical and the outer regions of the visible part show no structure nor in the direct image or the residuals.

4.5.3. Triple component models

A total of 26 galaxies were modeled by three Sersic components following or modeling strategy, most of them being classified as barred S0 where the third component having a large ellipticity and sometimes large effective radius and small Sersic index. The residuals of barred lenticular usually leave a distinctive pattern in the residuals and thus are considered to be caused by internal processes rather than caused recent past interactions.

Only 5 cases of the triple component sample show interesting features not identified by both observers.

- **COMAi125833.134p272151.73**

  What appears to be a background source is clearly visible in the direct image and the residuals. The structure appears as a couple of bright point sources embedded in a fainter envelope similar to the many other background galaxies observed in the field. The Red Sequence galaxy shows two prominent lobes also visible in other galaxies of the sample, which are aligned with the direction of the bar. At larger radius, the galaxy remains very smooth with no signs of perturbation.
- **COMAi125929.956p275723.26**

  While the residuals show no evidence of perturbation or traces of post-merger features, the residuals show a structure similar to those left by the subtraction of a bar structure.
- **COMAi125930.824p275303.05**

  IC 3973. The galaxy was already mentioned in the projected pair sample, where a long arc coming out clock-wise from the bottom part of the galaxy is barely seen in the direct image at the surface brightness limit achieved by the ACS but very prominent in the residuals. Also, the galaxy has a bright nucleus in comparison with the outer halo which also seems to be rotated and shifted with respect to the inner structure.

Table 4.4. Structural decomposition parameters for galaxies fitted with three Sersic components.

Galaxy Name	C1 r_e [kpc]	C1 n	C2 r_e [kpc]	C2 n	C3 r_e [kpc]	C3 n
COMAi13042.766p275817.38	1.27	2.99	6.23	0.35	1.42	0.17
COMAi125930.824p275303.05[a]	0.54	1.89	6.41	0.66	1.79	0.46
COMAi13039.767p275526.19	1.28	3.05	3.59	1.42	0.89	0.28
COMAi125932.771p275901.04	2.21	6.05	3.01	0.83	0.50	0.54
COMAi125944.407p275444.84[a]	0.75	2.59	2.92	1.09	1.38	0.23
COMAi125929.956p275723.26	0.45	1.75	5.59	0.33	3.15	1.02
COMAi125946.782p275825.99	0.31	1.75	3.44	0.67	1.23	0.72
COMAi13022.170p28249.30	0.31	1.35	3.49	1.24	1.31	0.48
COMAi13038.761p28052.34	0.46	1.68	3.81	0.85	2.86	0.61
COMAi13042.832p275746.95	0.75	3.01	3.81	0.47	1.51	0.39
COMAi125833.134p272151.73	0.30	1.12	4.61	0.55	2.84	0.57
COMAi13028.370p275820.64[a]	0.85	2.53	5.02	0.38	3.61	0.59
COMAi13012.868p28431.74[a]	0.77	2.42	5.07	0.41	3.00	0.53
COMAi125710.760p272417.38	0.31	2.32	3.54	1.04	1.83	0.67
COMAi13027.966p275721.56	0.42	2.67	3.32	0.32	1.01	0.98
COMAi125956.697p275548.71	1.89	4.33	3.57	0.25	2.48	0.41
COMAi13017.014p28350.07	0.70	4.67	3.57	0.58	0.80	0.64
COMAi125928.721p28225.92	0.40	1.65	3.28	0.57	1.54	1.05
COMAi13018.772p275613.34	0.49	0.98	2.87	0.69	1.64	0.60
COMAi125940.270p275805.71	0.31	3.39	1.82	0.86	0.48	0.14
COMAi125950.105p275529.44	0.80	2.37	1.99	1.66	0.51	0.28
COMAi125904.797p28301.16	0.21	1.22	2.72	1.12	0.83	0.85
COMAi125937.990p28003.52	0.37	2.38	1.40	0.50	0.67	0.33
COMAi13018.873p28033.38[a]	0.18	2.95	0.86	1.04	0.51	0.56
COMAi125950.183p275445.52	0.19	0.76	1.68	0.91	0.88	0.42
COMAi13030.954p28630.22	0.14	1.11	1.87	1.20	0.61	0.85

The same structure is much less prominent in the upper part. While this galaxy has a projected pair with a similar radial velocity, the two do not seem to be related as the small companion does not show evidence of perturbation. We classified this galaxy as a possible post-merger given the asymmetry observed both in the direct F814W image and the residuals.

- **COMAi125944.407p275444.84**

  While the direct image of the galaxy reveals no apparent structure or signs of perturbation, the residuals reveal a faint symmetric spiral structure close to the center of the galaxy.

- **COMAi13018.873p28033.38**

  One of the smallest galaxy of the entire sample, the single and double Sersic models of the galaxy always left an annular symmetric residual which only vanished after adding a third component. This behaviour is possible because of brute force rather than a structural decomposition of the galaxy. A small off-center structure at small radius is visible in the residuals, which could explain the difficulty in modeling the galaxy since it was not masked by SExtractor. At higher radius the galaxy looks perfectly fitted by the model and with no signs of perturbation

4.6. Asymmetry of galaxies in the pair sample

Visual inspection of direct images and residuals can sometimes lead to very a subjective interpretation of the information contained in images. The inspection of each galaxy made in section 4.3 was carried out by two members of the project and then compared. While in most cases the classification for each galaxy agreed, in only 9 out of 70 cases the identification did not match completely there where cases where the identification of features was not only dependent on the ability of the observer to spot certain features, but also on the interpretation of whether a feature observed in a galaxy is due to actual interactions caused by recent merger activities, or simply due to internal processes. This is why an objective measurement is extremely useful in order to support the inspection process, since it provides an estimator which is independent of the different appreciations and interpretations of data.

Several morphology estimators are present in the literature, based on the two-dimensional light distribution. Among them, Gini coefficient (Lotz et al., 2004), Sersic index (Sérsic, 1963), Concentration, Asymmetry and Clumpiness (Conselice, 2003) and Residual Flux Fraction (Hoyos et al., 2011) are the most popular. The nature of the features we are looking for should reveal past or ongoing interaction where highly asymmetrical structure appear, given that a merger is a process with a predominant direction. For this reason we choose to measure the asymmetry parameter for each galaxy in order to provide an unbiased estimator that supports the visual inspection previously performed.

The asymmetry parameter A is defined as

$$A = \frac{\sum_{\mathrm{i},j} |I_{\mathrm{i},j} - I^{\phi}_{\mathrm{i},j}|}{\sum_{\mathrm{i},j} I_{\mathrm{i},j}}$$

where $I_{\mathrm{i},j}$ is the intensity at a the pixel i, j and $I^{\phi}_{\mathrm{i},j}$ is the intensity measured at the pixel i, j of a 180° rotated image of the galaxy. This definition assumes that the background is completely noiseless, and gives a value of $A = 0$ for a completely symmetric distribution, and $A = 1$ for a completely asymmetric one. Since in reality the images have an uneven background level, the intrinsic asymmetry of this background must me accounted for. A corrected formula for the intrinsic background asymmetry takes the following form

$$A = \frac{\sum_{\mathrm{i},j} |I_{\mathrm{i},j} - I^{\phi}_{\mathrm{i},j}|}{\sum_{\mathrm{i},j} I_{\mathrm{i},j}} - \frac{\sum_{\mathrm{i},j} |B_{\mathrm{i},j} - B^{\phi}_{\mathrm{i},j}|}{\sum_{\mathrm{i},j} I_{\mathrm{i},j}}$$

where $B_{\mathrm{i},j}$ and $B^{\phi}_{\mathrm{i},j}$ are the intensity at a background area of the same size as the galaxy, and a 180° rotated image of the same background.

The asymmetry calculation is implemented using a modified version of the CAS system devised by (reference), implemented in python, whose functioning is explained below.

Center of rotation

Asymmetry value is highly dependent on the center of rotation. It is then defined as the coordinates which yields a minimum for the asymmetry parameter. In order to search for

this minimum, an initial value for the asymmetry is calculated at a guess rotation center and 8 neighboring positions, which can deviate a fraction of a pixel from the central position. Rotation of the image is done using bi-linear interpolation, allowing to rotate the galaxy with respect to fractional values of a pixel. 9 asymmetry values are calculated, and the routine iterates beginning from the center which returned the minimum value for A in the previous iteration. When no lower value is found on the 8 neighbouring positions the routine returns the value found for that central position. This proceeding has the caveat of not being able to recognize local minimums over global values and not being able to initially look at intermediate points between the central center of rotation and its 8 neighbouring points. In order to account for this, the code runs on a grid of 9 pixels centered in the brightest pixel of the galaxy and the distance to the 8 close positions is gradually lowered, starting from center which yield the minimum value for A in the 9 pixel grid.

Galaxy area and image masking

The area considered for the asymmetry calculation has also a considerable impact on the final value. If the area to be considered is too large, the asymmetry tends to be underestimated. In this work, we define an elliptical area of semi-major axis equal to 1.5 times the Petrosian radius, with the same ellipticity found using SExtractor which are the same specifications used in Conselice (2003) and in the training sample described below.

Background and foreground sources as well as detector artifacts must be flagged so the code does not consider contaminated pixels when calculating the asymmetry parameter. All sources and the rotated pixels with respect to the brightest pixel of the galaxy are removed from the sums involved in the calculation, so the asymmetry parameter does not consider them. Masks used for this procedure are the same employed in section 4.3.2.

Background asymmetry calculation

Since the background itself contains an asymmetric component given the pixel to pixel comparison made, it must be accounted for and removed from the preliminary asymmetry value obtained for the original image. It must be noted that the difference in the value of inverted pixels for the background is compared to the total intensity of the galaxy, $\sum_{\mathrm{i},j} I_{\mathrm{i},j}$ and not to the sum of the background values $\sum_{\mathrm{i},j} B_{\mathrm{i},j}$, since in average, the sum of the pixels in the background is zero. Several approaches exist to tackle this issue.

- Find an empty area on the image of the same dimensions as the galaxy and obtain the asymmetry of the background on that area following the same procedure for the galaxy asymmetry calculation. This is particularly difficult for crowded fields, specially for large effective radius galaxies, and also assumes an even distribution of the background over the detector, which is not true when very extended galaxies are in the field, or when artifacts such as ghosts in certain areas of the image appear, which is the case of ACS data.
- Similarly to the previous alternative, the asymmetry of a portion of the background is

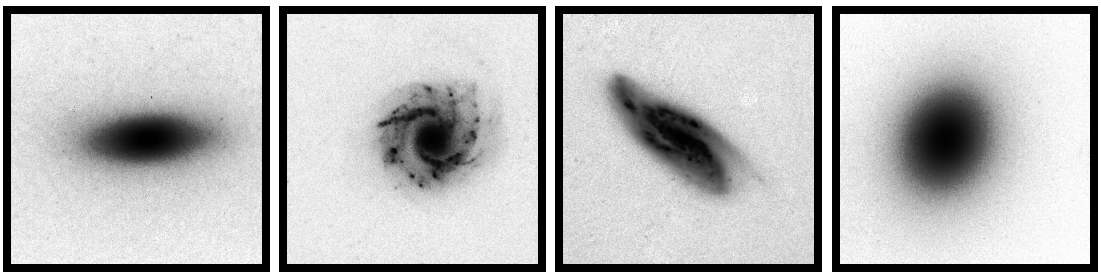

Figure 4.12 From left to right: images of NGC 2768, 3631, 4088, and 4472, extracted from Frei et al. (1996). All 4 galaxies where observed using the Lowell 1.1 meter telescope, using band R. Galaxies were selected in order to test the code over different morphology types.

Table 4.5. Asymmetries for the training set galaxies extracted from the Frei catalog.

Name	Morphology	A_{C03}	A_{abs}
NGC 2768	S0	0.02 ± 0.01	0.01
NGC 3631	SAc	0.13 ± 0.02	0.09
NGC 4088	SABbc	0.37 ± 0.01	0.33
NGC 4472	E2	0.01 ± 0.01	0.02

obtained but on a smaller area of the image. The sum obtained is then scaled to an area of the same size as the galaxy and then the asymmetry parameter is calculated exactly the same way as before.

- The final option, is to generate a synthetic noise image of the same characteristics as the local background, close to the galaxy of the original image. This synthetic image can be arbitrarily large, which avoid having to look in the image for large empty areas.

We decided to employ the later strategy, since it does not require a search for empty areas in the image of the same size and resulted to be much more straightforward than scaling the values obtained to the total areas of the galaxies.

Training set

The code was tested prior to it being applied on the set of Coma Red Sequence galaxies in order to search for inconsistencies on the values obtained for the asymmetry. A test sample of galaxies with known asymmetries was obtained from the Frei catalog[2] (Frei et al., 1996), from where we selected images of 4 galaxies of varying morphologies observed using the Lowell 1.1 telescope (See figure 4.12). Using an adapted Python version of the Asymmetry code we calculated the asymmetries for these galaxies, testing for different approaches on the background asymmetry calculation and rotation center selection. Values obtained for the asymmetry using our code are presented also in table 4.5 along with the reported values from Conselice (2003) and the morphological type for each galaxy.

In the case of highly symmetrical galaxies such as gas poor S0 and elliptical systems, the relative variation in the asymmetry parameter is large, but always on the range of values

[2]http://www.zsolt-frei.net/catalog.htm

Table 4.6. Asymmetries 13 galaxies in the projected pair sample.

Name	Morphology	$A_{\mathtt{abs}}$
125930.824p275303.05	S0/a	0.0417
125931.893p275140.76	E	0.0332
125944.407p275444.84	S0	0.0287
125942.301p275529.15	S0	0.0590
130028.370p275820.64	S0	0.0248
130027.966p275721.56	S0	0.0270
125943.721p275940.82	S0	0.0241
125938.321p275913.89	S0/a	0.0384
130018.873p280033.38	S0	0.0277
130017.641p275915.27	S0	0.0191
130008.003p280442.81	S0	0.0447
130012.868p280431.74	S0	0.0397
130011.143p280354.91	S0	0.0405

expected for such systems. The asymmetry is indeed larger for irregulars and disk galaxies, and their calculation is subject to the determination of the correct center of rotation, which is much more difficult to find here. In the case of smooth light distributions, the rotation center is easily found by providing an initial guess close to the highest intensity pixel. The code probed to be an appropriate tool for measuring the asymmetries, so it was applied to the sample of galaxies selected as possible pair members.

Results

The asymmetries for the 13 galaxies involved in projection pairs were computed using the same procedure for the training set given the limitations on the estimation of the background. Synthetic background images of the same dispersion as the ones from the original images were created and the code run on the same area defined for the galaxies of our sample.

Values obtained for the $A_{\mathtt{abs}}$ are listed in table 4.6 range from 0.0191 to 0.059, which are typical for non perturbed elliptical galaxies. Expected values for perturbed and starburst galaxies are in the range of 0.2 to 1.0 in extreme cases Conselice (2003) and Hoyos et al. (2012), although some peculiar cases can exist such as rings and shells (See chapter 1.2) where regardless of a recent merger event, symmetric structures form. The asymmetry parameters found are consistent with results obtained in section 4.4 the only exception being the case of IC 3973 which despite having a prominent asymmetric structure extending from one side, has a small value for the asymmetry parameter. We believe that given the high contrast between the outer halo and the central bulge of the galaxy, the total intensity of the galaxy diminishes the effect of the outer faint asymmetry calculated. The highest asymmetry found was for 125942.301p275529.15 (PGC 44649) with a value of 0.059. The galaxy looks completely unperturbed, and unlike IC 3973, direct images do not reveal an low surface brightness feature. After model subtraction, a small asymmetric patch can be seen very close to the center of the galaxy in figure 4.7 which could be causing the asymmetry value to rise slightly.

Chapter 5

Dry merger rate and post-merger fraction

In order to quantify the merger activity in the Coma cluster and compare it to theoretical and observational results, two main measurements can be done from the sample we have built after selecting pairs by projected distance and radial velocity difference, and after the Red Sequence sample of galaxies within the ACS imaging, with a surface brightness limit of 26.5 mag/arcsec^2, has been visually inspected. The measurement of the merger fraction and the statistical upper values found is presented in the first part along with a detailed description of the merger time-scale. Then, the post-merger fraction is described for our sample of Red Sequence galaxies. Obtained values are then compared with recent literature and discrepancies are explored in detail.

The results obtained here along with a summarized description of the procedures employed in this work are presented in (Cordero et al., 2016). A small discussion regarding the comparison of our work with the recent literature is also given.

5.1. Pair fraction and merger rate

Having defined what is considered to be a pair, the *pair fraction* is defined as the fraction of galaxies of the complete sample which fulfil the criteria of belonging to one of these pairs. In our case, we have defined a pair as two (or more, so a more accurate word would be *system*, instead of pair) galaxies lying close on the sky, with a projected separation of no more than $30h^{-1}$ kpc and a radial velocity distance of less than 300 km s^{-1}. While we have considered these two criteria as necessary for a true merger to occur, they are not sufficient to consider a pair as a gravitationally bound system, since the projected distance does not consider projection effects, and the radial velocity cut employed here is not indicative of line-of-sight distance and does not consider the perpendicular component of the relative velocity between galaxies, but is necessary for possible mergers to actually merge after a collision. Hence, merger fraction and pair fraction are considered two completely different concepts,

the later accounting for the fraction of actually bound systems.

Given the definition for the pair fraction presented in section 1.3.1, we find that 13 out of 70 red sequence galaxies are involved in possible pairs, as far as the selection criteria dictates, giving a pair fraction of $F \approx 18{,}5\,\%$. This value seems to be in fair agreement with similar studies at higher redshift where no confirmation about the true nature of these mergers can be done using morphology examination. van Dokkum et al. (1999) found that $\sim 17\,\%$ of galaxies in cluster MS 1054-03 at z=0,83 are selected as possible pair members, but no morphological inspection is done. In a follow-up paper, Tran et al. (2005) confirmed that radial velocities differences in all pairs are indeed small, but no morphology analysis is given. Lotz et al. (2013) finds even a larger fraction $F \sim 49\,\%$ in a proto-cluster at $z = 1,62$, but again, this fraction comes from close pairs found on the sample. These authors mention that these high-z clusters either have sub-structure or that merging occurs in the periphery, consistent with dynamically young systems. Although in both cases a statistic study of chance alignment was made and results seem to indicate that the expected pair count is lower than the actual number of pairs found, these results could change if a detailed morphological evaluation of the galaxies was made, ruling out some of the systems identified as pairs, making it a necessary step to perform in Coma, although it is expected that these fractions are indeed larger at high redshift given the dynamical state of clusters. For instance, van Dokkum et al. (2001) reports a fraction of $\sim 10\,\%$ of galaxies in the $z \sim 1.27$ cluster RX J0484+4453, involved in recent or ongoing interaction events which is supported by direct observations and morphology evaluation of likely cluster members. Furthermore, the second brightest member of the cluster appears to be in fact the merger of three red galaxies and a considerable fraction of the luminous end of the population in that cluster reveals signs of interaction.

In order to estimate the true merger fraction, and rate, of galaxies in Coma, the fraction involved in mergers and the typical time-scale for these events to occur must be estimated. We defined true future mergers as those that have signs of on-going interaction, and in sections 4.3 and 4.6 we performed visual inspection and asymmetry calculations over the sample of possible pairs in order to determine which fraction of the total sample is currently undergoing merger activity.

The merger rate is defined in several ways in the literature, but in all cases the idea is to quantify the number of merger events per unit time, thus requiring a time-scale for these events to be defined. In our case we measure the merger rate as the fraction of galaxies involved in merger events per Gyr. It can be easily obtained as

$$\mathcal{R} = \frac{\mathcal{F}}{\langle T_{\mathtt{merge}} \rangle}$$

where $\langle T_{merge} \rangle$ is the characteristic time for the event to occur. Definitions for this time-scale varies: in some cases is it defined as the time it takes to the system to achieve certain dynamical state, while in some other cases it considers the time the characteristic features of the merger remain visible. In this study, we assume the empirical estimation for the merger timescale obtained by Kitzbichler & White (2008) on which the merging times of a virtual galaxy catalog from the millenium simulation are used. A relation for $\langle T_{\mathtt{merge}} \rangle$ in terms of the pair separation r_s, $M_\star$ and z is calibrated by obtaining the ratio of the abundance of pairs

at a certain redshift to the merger rate measured.

$$\langle T_{\mathtt{merge}} \rangle = 3{,}2 \text{ Gyr} \frac{r_s}{50 \text{ kpc}} \left(\frac{M_\star}{4 \times 10^{10} M_\odot} \right)^{-0{,}3} \left(1 + \frac{z}{20} \right)$$

If tentatively, it is assumed that the 13 galaxies from the possible pair sample are actually in interacting systems, then using the median stellar mass ($M_\star$) and separation r_s from table 4.1 and the above formula, a merger timescale of 1.65 Gyr is obtained that would lead to a nominal dry merger rate of 11.2 % per Gyr in the Coma core.

However, the visual inspection and asymmetry determination conducted for these 13 galaxies do not provide evidence that they are interacting systems. This null result, nevertheless, requires an estimation of the dry merger rate by using binomial statistics. We follow the procedure by Burgasser et al. (2003) where the $\pm 1\sigma$ range of acceptable values for the pair fractions are defined as a function of the sample size N and measured pair fraction F. The binomial distribution determines the probability of finding n binaries as

$$B(n; N, F) = \frac{N!}{n!(N-n)!} F^n (1-F)^{N-n}$$

From which the probability of a certain fraction F given the observed quantities N and n can be obtained. The upper uncertainty equivalent to a 1σ limit for a Gaussian distribution can be computed numerically by solving

$$\sum_{\mathrm{i}=0}^{n} \frac{(N+1)!}{\mathrm{i}!(N+1-\mathrm{i})!} x^{\mathrm{i}} (1-x)^{N+1-\mathrm{i}} = 0,16$$

For our sample, where $n = 0$ and $N = 70$, we obtain an upper limit for the merger fraction of

$$F^U - \sqrt[71]{0{,}16} \approx 0,0255$$

Considering the merger timescale of 1.65 Gyr estimated above, from our null result we obtain a 1σ upper limit for the major dry merger rate of $\sim 1{,}5\,\%$ per Gyr within the core of Coma.

5.2. Post-merger fraction

The complete sample of red sequence galaxies was inspected to estimate the fraction that shows signatures of the coalescence of two or more galaxies, such as ripples, tidal structures, halo discontinuities, shells, and other structures unrelated to the presence of a companion. Using the high resolution images and the models generated for each galaxy, only one of the 70 red sequence galaxies is classified as a post-merger from the inspection of HST images at a surface brightness limit of 26.5 mag/arcsec^2. The only post-merger candidate found is

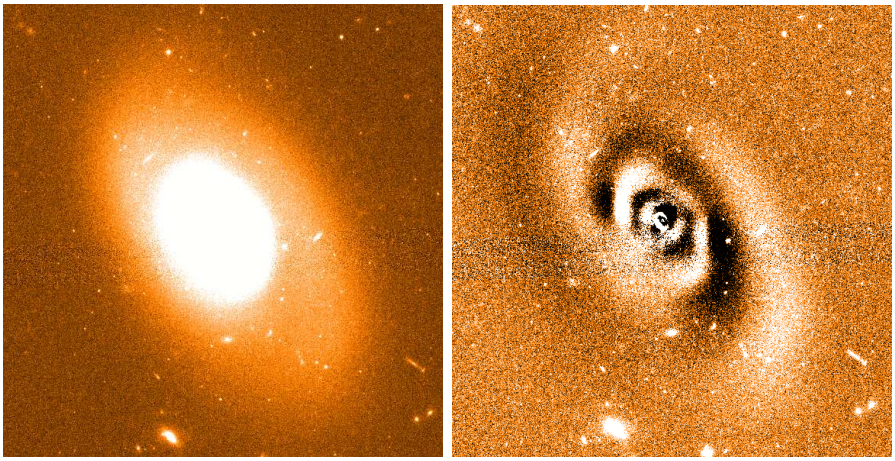

Figure 5.1 Left: F814W image of IC 3973 showing the apparent shift between the central nucleus and the faint outer halo. Right: Residual map after a triple component Sersic model has been subtracted, showing a large arc coming out of the galaxy clockwise.

IC 3973, which was previously identified as a member of one of the five pairs and one triple system found in section 4.1. This galaxy is not identified as a member of an ongoing merger since the observed features do not appear to be related to the presence of the projected partner, and the parter itself does not show any evidence of perturbation.

The asymmetry parameter for this galaxy is 0.0419, a value still small for a perturbed galaxy; we believe that this parameter does not actually reflect the merger remnant character detected visually due to the very low surface brightness of its external halo compared with the galaxy nucleus. In direct F814W image of this galaxy (See figure 5.1) the outer halo of the galaxy appears to be rotated with respect to the inner bright core, while in the residual image, a curved extension is apparently coming out clockwise from the lower right corner of the galaxy halo.

Finding only one candidate post-merger galaxy implies a post-merger fraction in the Coma cluster core of $\sim 1{,}4\,\%$.

Adams et al. (2012) found a similar value for the post-merger fraction at the same surface brightness limit, studying a larger sample of elliptical cluster galaxies. Interestingly, they found no evidence for a relationship between local density and the incidence of tidal features, but they do find a deficit of tidally disturbed galaxies with decreasing clustocentric distance. This finding seems to be in concordance with the picture of higher post-merger fractions towards the outskirts of clusters, where the accretion of galaxy groups perturbes the equilibrium of the system, but at the same time the authors argue about the possibility that the lifetime of tidal features as a function of clustocentric radius play a significant role in their detection. Since we only find evidence of a single galaxy with such features, no comparison can be made regarding the distribution of post-merger fraction as a function of radius, although the limits employed in Adams et al. (2012) and the sample size would allow us to compare their results once we have extended our study to a larger sample, including more clusters.

However, the values we obtain for Coma and the ones reported by Adams et al. (2012) seem to strongly contradict the high $\sim 24\,\%$ mean fraction determined by Sheen et al. (2012) even within $\sim 0{,}2R_{200}$ in four $z \lesssim 0{,}1$ Abell clusters (See figure 2.1). The apparent large discrepancy may be due to the conjugation of several effects: the evolutionary stage of the clusters, error bars in the fraction of post-mergers, projection effects, radial extent, and depth of the survey.

Clusters at redshifts ~ 0.1 to 0.2, such as those in Sheen et al. (2012), could be actively accreting field and group galaxies (which are tidally distorted due to their ongoing or past mergers) while clusters at lower $z \sim 0{,}025$ (a few Gyrs later) such as Coma, could experience a reduced accretion of field and group galaxies (e.g.; Heiderman et al., 2009). Furthermore, any distorted galaxies that Coma accreted earlier at $z \sim 0{,}2$ would have lost their tidal features by $z \sim 0{,}025$ since these features disappear on a dynamical timescale which is close to 1 Gyr at moderately large radii in a galaxy. From this evolutionary perspective, the absolute value of the fraction of distorted galaxies, would be much lower in Coma than in the Abell clusters of Sheen et al. (2012). This is the trend we see and expect. Nonetheless, the absolute values of the post-merger fractions in Sheen et al. (2012) do seem higher than expected. This could be due to depth and normalization of the fraction determined by Sheen et al. (2012).

Projection effects can cause infalling galaxies to appear at all regions of the phase-space of a cluster. If we consider the population of a cluster in terms of the accretion state of their members, we can distinguish between galaxies in the infall regions yet to pass within the core of the cluster for the first time, recently accreted but still to pass for the pericenter of their orbits, back-splash galaxies which have passed through their pericenter and are not coming back for the next 3-4 Gyr and finally the older viriralized population which resides mainly in the inner $0.2R_{200}$. The back-splash population is expected to populate the entire caustic diagrams of clusters, matching the observed post-merger fraction in Sheen et al. (2012) since these galaxies are the ones with higher chance of having undergone a recent merger and still show a perturbed morphology. What remains a puzzle is the fact that Sheen et al. (2012) finds no evidence of a trend of the post merger fraction towards the very small clustocentric distances where the old virialized population dominates (See figure 2.1).

We also considered the radial extent of the ACS Coma imaging with respect to cluster center as a possible source of discrepancy, since we have focused on the central region ($R < 0{,}5R_{200}$) where the population is expected to be virialized. While this is concordant with the expected rise in merger activity towards the outskirts of the cluster, it still contradicts the findings of Sheen et al. (2012) regarding the high fraction of post-mergers towards the core of the studied clusters.

Finally, surface brightness limits arise as another possible explanation for the different results obtained. The surface brightness limit of the imaging we use reaches 26.5 mag/arcsecond^2 Duc et al. (2015) mentions that the observed morphology of galaxies can be perceived completely different if deep imaging is available. The main question that appears then is if the features observed at low surface brightness were caused by recent interactions or are relics of very ancient events. Sheen et al. (2012) speculates about the possibility of these features being caused by a merger event prior to the accretion of the galaxy into the cluster. In a follow up study by Yi et al. (2013), N-body simulation of major mergers suggest that merger

features such as shells or ripples could be detected at ~ 28 mag arcsec^{-2} up to 4 Gyr after the first perigee. But again, this study does not consider the nocive effect of intracluster medium in such features, and thus the puzzle of the high post-merger fraction at small clustocentric distance, where this effect is expected to be higher, remains. Two of the cluster studied by Sheen et al. (2012), A119 and A2670, are also part of the sample of clusters studied by Adams et al. (2012) and the results found are very different for the same limits in clustocentric distances. While Sheen et al. (2012) finds a combined post-merger fraction of 26 % in their Red Sequence sample ,Adams et al. (2012) only found that around 7 % of elliptical galaxies have identifiable tidal features. Among many method dependent differences, the difference in limiting surface magnitude can be responsible of the observed discrepancy. We have considered as a future exercise to test this last possibility by artificially degrading the imaging of deeper surveys using FERENGI (Barden et al., 2008), which would allow us to compare the appearance of a known sample of post-merger galaxies under similar conditions to the ones presented in our work.

Conclusions

By combining the identification of close pairs with the requirement of galaxy assymmetries, we find no evidence for major ongoing mergers in a spectroscopically complete sample of 70 Red Sequence galaxies within $\sim 0.5\ R_{200}$ from the center of Coma and derive an upper limit to the dry merger rate of $\sim$1.5 % per Gyr at the 1σ level. This rate is not sufficient for dry mergers to account for the Red Sequence evolution inside clusters.

Also, we find that from the 70 galaxies in our sample only one shows evidence of low surface brightness features identifiable as the remnants of a past merger or interaction, yielding a post-merger fraction of 1.4 % within a projected distance of $\sim$0.5 R_{200} from the Coma center. Although the Coma brightest member (NGC 4889) is not in our sample, it actually is an Red Sequence galaxy sitting in the cluster center, and, interestingly, it has been found to contain a system of shells identifiable to a minor ($\sim$1/100) merger (Gu et al., 2013). If NGC 4889 would have been part of our sample, presumably, it would have been counted as a galaxy with tidal signatures, implying a larger post-merger fraction of $\sim$ 2.8 %. There is, however a relevant caveat that derives from the work of Gu et al. (2013) on NGC 4889, i.e., that an observation alone of tidal signatures in a galaxy may sometimes be the consequence of a very minor merger.

The small post-merger fraction we observe is consistent with similar results, such as the one by Adams et al. (2012) where $\sim$3 % of a large sample of early-type galaxies in clusters ($0.04 < z < 00{,}15$) show evidence of tidal features found in imaging with surface brightness limit comparable to those of the HST imaging employed by us in this study. However, it is puzzling that the post-merger fraction we observe is a factor of 10 lower than the one measured by Sheen et al. (2012) in four $z \lesssim 0.1$ clusters. This discrepancy merits further investigation with consideration of the differences in survey limits and cluster evolutionary stage.

Appendix A : Summary

The where and when of the evolution of red massive galaxies is still an uncertain topic, as well as the relative importance of the different processes involved. Mergers between gas poor spheroids offer a feasible explanation for the low scatter seen in the Fundamental Plane, since they are believed to not induce significant star formation and thus the metal abundances remain fairly constant. While mergers are believed to be one of the most important processes in the picture of mass evolution and strong evidence exist about the occurrence of these events, they are not expected to be important today as they were at early ages of the Universe. Clusters of galaxies, where most of the gas poor early type and lenticular galaxies reside, have evolved to relaxed dynamical states where collisions between galaxies are not believed to lead to a merger given the large impact velocities. But recent observations carried out at intermediate (Duc et al., 2015) and high (Sheen et al., 2012) density environments in the local Universe seem to support the idea that recent coalescence between red sequence progenitors is still possible.

Estimations of merger fractions per unit volume have been done mainly using pair statistics and a definite set of assumptions regarding the true nature of projection pairs such a fixed estimated percentage of pairs that will merge. The Coma cluster of galaxies is the perfect laboratory to test and compare merger fractions with theoretical expectations and recent results. Given its closeness and rich nature, high resolution and high spectroscopic completeness is achievable with present day facilities.

In the following we highlight the main aspects and results of this work.

1. **Coma Red Sequence** A sample of massive red sequence galaxies was built using photometric information from the Coma Treasury Survey catalog. The sample was built so it contains only the brightest galaxies with known radial velocity information. The red sequence was obtained after a linear fitting of relation observed in the color magnitude diagram and galaxies lying in a 5-σ region around the obtained relation were considered. The sample contains luminous ($L > L_*$) galaxies with masses larger than $10^9 M_\odot$ and the possible pairs obtained are likely to evolve into major mergers.
2. **Pair selection** A sample of "possible pairs" was constructed by looking for pairs of galaxies with projected distances smaller than $30h^{-1}$ kpc and radial velocity differences no larger than 300 km s^{-1}. These pairs are not necessarily gravitationally bounded but consider the minimum criteria for being considered as a true merger. 13 galaxies in 5 pairs and one triple system are found using the above criteria. These galaxies and the residuals after model subtractions are inspected in order to confirm or discard any possible ongoing true interaction. None of the galaxies appears to be undergoing an actual process of merging.
3. **Asymmetry calculation** The asymmetry for the sample of possible pairs found above was obtained in order to support the observations made in the morphology evaluation. Asymmetry values found are in the range of 0.01 - 0.04, which is expected for non-perturbed elliptical galaxies, confirming the negative results obtained after visual inspection.
4. **Morphology inspection of Red Sequence galaxies** The complete sample of Red

Sequence galaxies was visually inspected for evidence of asymmetric features that could be regarded as result of an ongoing or recent past interaction. For this matter, two-dimensional models using Sersic profiles for the components of the galaxies were obtained using GALFIT, and the residuals after model subtraction were inspected. While no galaxy of the pair sample presents features that could be considered as results of an ongoing interaction or due to the presence of the companion, one of the galaxies of the red sequence was found to have a slightly distorted morphology, possibly caused by the coalescence of two progenitor galaxies.

5. **Merger rate and post-merger fraction** Upper values for the merger rate and merger fraction were obtained using pair statistics. The rate, in particular, required a estimation of the mean merger time-scale, which was obtained from the mean separation and stellar masses of the possible pair sample. An upper limit of $\sim 2\,\%$ Gyr is found for the merger rate. These results can be compared to similar studies performed at low and intermediate redshift: while there seems to be a tight concordance with the results from Adams et al. (2012) carried out under similar observational conditions, it contradicts the results of Sheen et al. (2012) who finds a much larger post-merger fraction in 4 massive local clusters. Possible explanations for this discrepancy are discussed.

The global picture we observe for the core of Coma is that of a relaxed system where high velocity dispersion suppresses merger activity. Despite of the substructure reported in the literature, specially towards the south-west region of the cluster covered by the CTS, where a noticeable galaxy overdensity suggest the infalling of a galaxy group, no signs of enhanced merger activity are observed as the post-merger fractions suggests after visual inspection of the complete Red Sequence sample. This is, of course, not a new statement since Coma has been largely considered over the years the prototype of a local relaxed massive cluster (Biviano et al., 1995). The non detection of ongoing mergers and the low fraction of post-merger galaxies seems to confirm the expectation for a rich massive cluster such as Coma, and to some point contradicts the findings of Sheen et al. (2012), where a high post-merger fraction is found in Red Sequence galaxies selected with similar methods to the ones we used.

One possible explanation for this discrepancy is the difference in limiting surface brightness. While we only reach 26.5 mag arcsec^{-2}, Sheen et al. (2012) states a value of 30 mag arcsec^{-2} for their models using *ellipse*, which suggest that their imaging reach similar limits, and thus features at extremely low surface brightness can be observed. This, however, has to be taken cautiously since at the same time, deeper observations could reveal features caused by interactions occurred at a much earlier epochs. This is indeed discussed in Yi et al. (2013), where the persistence of faint structures is studied using N-body simulations, revealing that these can remain visible at cited limiting magnitudes for 3-4 Gyr, enough to have occurred prior to the galaxy being accreted to the cluster.

Distribution of galaxies with respect to clustocentric distances can also be in part responsible of the observed post-merger differences. Galaxies in Sheen et al. (2012) are located up to 1.0 R_{200} from cluster center, while our sample consist of galaxies located mainly in the central $0.5R_{200}$ (See figure 5.2), where merger activity is expected to be unlikely and features are expected to survive for much shorter periods due to the dense hot intra-cluster medium. The observational impact of surface brightness limit and redshift in our measurements has to be considered also, for which we have considered the use of FERENGI (Barden et al., 2008),

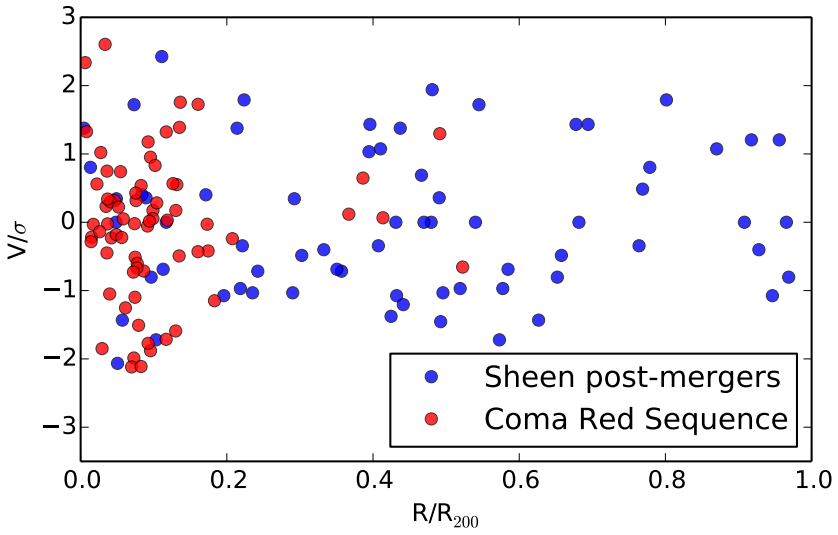

Figure 5.2 Caustic diagram for galaxies in the red sequence of the Coma cluster and post-mergers found by Sheen et al. (2012). Galaxies in the Coma cluster are contained mainly in the inner region of the cluster core ($0.5R_{200} \sim 1$ Mpc), while post-mergers extend evenly up to $1.0R_{200}$.

which allows us to artificially "redshift" observed local galaxy to simulate the observational conditions of identified post-merger galaxies at shallower brightness limits.

Appendix B : Future work: The Shapley Supercluster

In order to study the global effect of environment, a larger number of clusters representative of different galaxy densities must be inspected by obtaining merger rates and post-merger fraction using similar techniques.

We started a similar study using deep, high resolution g-band images of the core of the Shapley super cluster where a sample of massive elliptical and lenticular Red Sequence galaxies were modelled using GALFIT. The cluster is the largest structure in the local Universe ($z \sim 0{,}043$) and shows a very unrelaxed morphology where multiple sub-clusters can be identified (Merluzzi et al., 2015, See also figure 5.3) With a similar procedure to the one applied in Coma, we have searched for galaxies with signs of on-going or recent interaction by inspecting the direct images and residuals after model subtraction.

A catalogue of 198 confirmed Red Sequence galaxies from Smith et al. (2007) was used as reference with known radial velocities obtained using the AAOmega facility at the Anglo-Australian Telescope and near-infrared magnitudes measured by WISE which accounts for old star populations and can be used as a proxy for stellar masses. For the models, a deep g-band DECam exposure of the central region of the supercluster covering 5 sub-clusters (See table 5.1) is used.

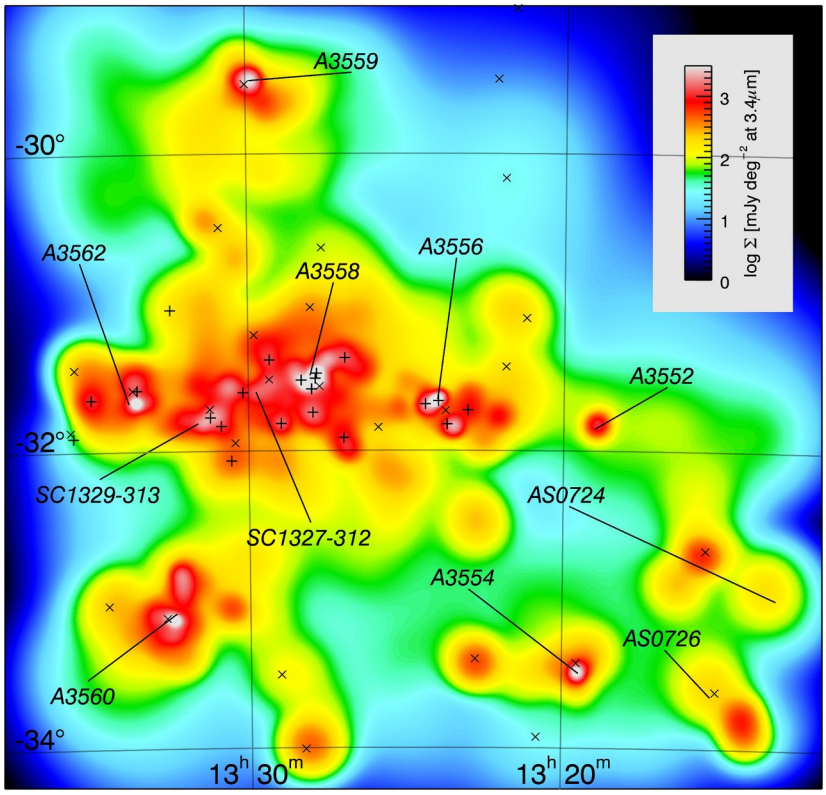

Figure 5.3 Shapley Supercluster Survey (Merluzzi et al., 2015) density map in units of mJy deg^{-2} at 3.4 μm. Abell clusters and groups are labelled with labels indicating the centers of local X-ray emission. The DECam field used in the modeling and visual inspection covers most of the high density region around Abell 3558 and SC 1327-312

Table 5.1. Sub-clusters in the central region of the Shapley supercluster

Name	R_{200} [kpc]	σ_v [km s^{-1}]	v_H [km s^{-1}]	Observed members	Center on image
A3558	2267	921	14481	18	Yes
SC 1329-313	867	348	13414	3	Yes
A3562	1769	714	14820	3	Yes
A3556	1347	535	17794	1	Yes
A3560	1425	586	14369	1	No
SC 1327-312	1908	774	14778	6	No

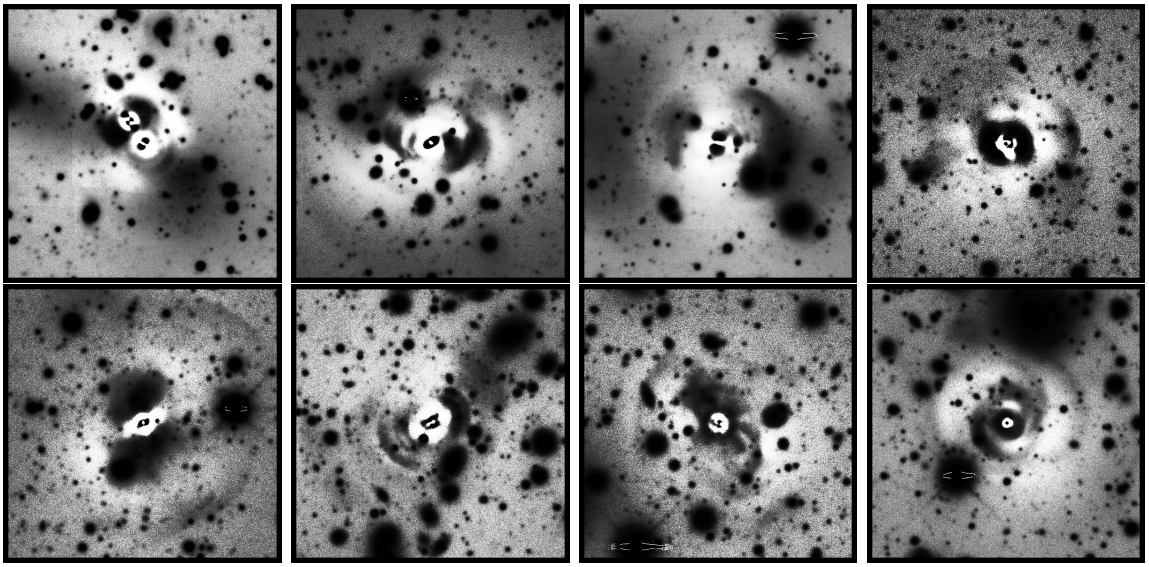

Figure 5.4 Residuals of post-merger galaxies after direct images and residuals of model subtraction. Is most cases large shells can be seen around galaxy center, which are easily visible in the residuals.

We selected all galaxies with radial velocities between 10800 and 18000 km s^{-1} for cluster membership and near-infrared magnitude $W < -12$ mag ($\sim 10^{11} M_{\odot}$) in order to test our method on a small sample of the most massive galaxies of the sample. 32 galaxies were selected by this criteria and their membership to the sub-clusters is defined by the projected distances to the centers.

Models for the 32 galaxies in the sample are created following the same methodology presented in section 4.3.2 and a single PSF was built for the entire image using a sample of isolated stars on the field. The residuals after model subtraction were then inspected and revealed that 8 galaxies of the sample could be classified as possibly perturbed due to ongoing or recent interactions. (See figure 5.4)

A key aspect of the study is to determine the role of the dynamical state of the cluster in the merger activity and how does it change as a function of the distance to the center of the clusters. It is expected that the fraction of galaxies involved in mergers or with signs of post-merger features rises as a function of clustocentric distance, since it is on the outskirts where the recent accretion of galaxy groups has had less time to relax, contrary to what is happening in the center of clusters where the galaxy population is expected to be virialized. We studied

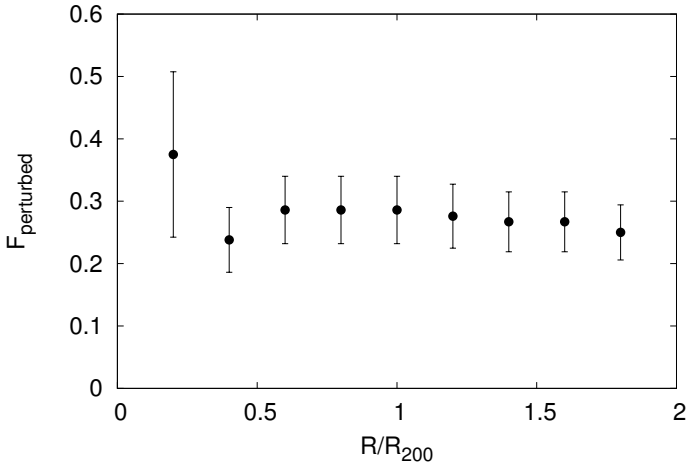

Figure 5.5 Fraction of galaxies in Shapley identified as on-going mergers or post-mergers, as a function of R/R_{200}. No clear trend can be seen for the post-merger fraction, contrary to the expected increment in post-merger galaxies towards larger clustocentric distances were the accretion of galaxy groups occurs.

the fraction of perturbed galaxies as a function of clustocentric distance considering those clusters whose centers lie inside the DECam field, and found that the fraction does not decrease significantly towards higher values of R/R_{200} (See figure 5.5).

While this is still an unfinished investigation, the following step is to consider a larger spectroscopically complete sample of Red Sequence galaxies and perform a similar search for pairs of galaxies considering projected distance and radial velocity difference, which could allow us to identify the origin of the features observed in the massive Red Sequence sample from Shapley.

In order to compare the results obtained in Coma and Shapley to different environments under similar observational conditions we have considered other local clusters such as Antlia and Fornax, which have lower densities compared to the already studied systems. For the first one, deep, high resolution imaging is needed for which we have applied in the past. Spectroscopic information of the cluster is already available for most of the galaxies in the core in public databases such as NED. For Fornax, DECam images of the core of the cluster have been made publicly available recently and radial velocities for a vast majority of the bright galaxy population in the core can be found on Drinkwater et al. (2000). With these data in hand we plan to build a larger sample of measurement in order to draw more solid conclusions about the role of environment in the massive galaxy mass evolution

Appendix C: Cordero et al. (2016)

The Astrophysical Journal Letters, 817:L6 (7pp), 2016 January 20 doi:10.3847/2041-8205/817/1/L6

DRY MERGER RATE AND POST-MERGER FRACTION IN THE COMA CLUSTER CORE

Juan P. Cordero[1], Luis E. Campusano[1], Roberto De Propris[2], Christopher P. Haines[1], Tim Weinzirl[3], and Shardha Jogee[4]
[1] Departamento de Astronomía, Universidad de Chile, Casilla 36-D, Santiago, Chile; jcordero@das.uchile.cl
[2] Finnish Centre for Astronomy with ESO, University of Turku, Vaisalantie 20, Piikkio, FI-21500, Finland
[3] School of Physics and Astronomy, The University of Nottingham, University Park, Nottingham NG7 2RD, UK
[4] Department of Astronomy, The University of Texas at Austin, Austin, TX 78712-1205, USA
Received 2015 August 27; accepted 2015 December 21; published 2016 January 19

ABSTRACT

We evaluate the dry merger activity in the Coma cluster, using a spectroscopically complete sample of 70 red-sequence (RS) galaxies, most of which (∼75%) are located within $0.2R_{200}$ (∼0.5 Mpc) from the cluster center, with data from the Coma Treasury Survey obtained with the *Hubble Space Telescope*. The fraction of close galaxy pairs in the sample is the proxy employed for the estimation of the merger activity. We identify 5 pairs and 1 triplet, enclosing a total of 13 galaxies, based on limits on projected separation and line-of-sight velocity difference. Of these systems, none show signs of ongoing interaction, and therefore we do not find any true mergers in our sample. This negative result sets a 1σ upper limit of 1.5% per Gyr for the major dry merger rate, consistent with the low rates expected in present-day clusters. Detailed examination of the images of all the RS galaxies in the sample reveals only one with low surface brightness features identifiable as the remnant of a past merger or interaction, implying a post-merger fraction below 2%.

Key words: galaxies: clusters: individual (Abell 1656) – galaxies: elliptical and lenticular, cD – galaxies: evolution – galaxies: interactions

1. INTRODUCTION

Mounting observational and theoretical evidence suggests that galaxy growth proceeds through a combination of major mergers, (e.g., Springel et al. 2005; Khochfar & Silk 2009), minor mergers (e.g., Jogee et al. 2009; Weinzirl et al. 2011), cold-mode gas accretion (e.g., Brooks et al. 2009; Dekel et al. 2009), and secular processes (e.g., Kormendy & Kennicutt 2004; Jogee et al. 2005). Mergers are particularly important, contributing to the stellar mass growth of galaxies, triggering star formation, inducing nuclear activity, and leading to morphological transformation.

If major mergers are actually common, it is difficult to explain the very low scatter seen in the fundamental plane scaling relations, even at redshifts approaching 1 and beyond (e.g., Fernández Lorenzo et al. 2011; van de Sande et al. 2014). Major dry mergers (between two gas-poor quiescent galaxies) may offer an escape from this apparent contradiction, as they are believed not to affect the scaling relations (e.g., Boylan-Kolchin et al. 2005; Skelton et al. 2012).

Major mergers in present-day clusters are not expected to be frequent, as the encounter velocities between cluster galaxies are much higher than the internal velocity dispersions of the galaxies, preventing their coalescence (Aarseth & Fall 1980). Therefore, the evolution in the mass function of cluster galaxies should closely follow that seen in the wider field and group populations that are continually accreted into the clusters over time (Haines et al. 2015). In fact, the cluster galaxy mass function appears not to have evolved significantly since $z \sim 1.5$ or even earlier (e.g., De Propris et al. 2007; Muzzin et al. 2008).

Some recent results are shedding new light on the merger activity in the local universe. Very deep imaging studies of local ($z \lesssim 0.1$) field early-type galaxies have reported that features such as broad fans, ripples, shells, streams, and tidal tails are found in 50%–70% of them, pointing to recent mass assembly through dry mergers (van Dokkum 2005; Duc et al. 2015). In a similar deep optical survey of four rich clusters at $z \lesssim 0.1$ (A119, A389, A2670, A3330), Sheen et al. (2012) also identified such features in ∼25% of red-sequence (RS) cluster galaxies, a result particularly surprising for such environments. Sheen et al. (2012) suggested that these faint features could be residuals of mergers that took place several Gyr ago, prior to the galaxies being accreted into the clusters themselves. Yi et al. (2013) performed hydrodynamical simulations of major merging galaxies indicating that post-merger signatures could remain detectable for 3–4 Gyr.

In this Letter, we consider the use of close pair fractions and image inspection to estimate the dry merger rate of galaxies in the Coma cluster ($z = 0.0231$) and the fraction of post-merger, or merger remnant, galaxies in the RS, using the extensive available spectroscopic information and deep *Hubble Space Telescope* (*HST*) imaging obtained with the Advanced Camera for Surveys (ACS) for the Coma Treasury Survey (CTS). These measurements are not only useful for comparison with similar investigations of low-z clusters, but also constitute a suitable counterpart to previous studies of distant clusters ($z \sim 0.8$–1.6) where high merger fractions have been claimed to exist based on galaxy pair counts (e.g., van Dokkum et al. 1999; Tran et al. 2005). The much better data quality available for local systems allows us to identify signs of ongoing interactions and explore systematic effects on the determination of the merger rate.

This analysis is based on a complete spectroscopic sample of RS galaxies consisting of gas-poor elliptical and lenticular galaxies. The dry merger rate is derived from the number of close pairs that show signs of galaxy–galaxy interactions in the model-subtracted images of the component galaxies. We also estimate the post-merger fraction in Coma from the number of galaxies in the complete RS sample that show remnant features from a past coalescence, for comparison with the results of

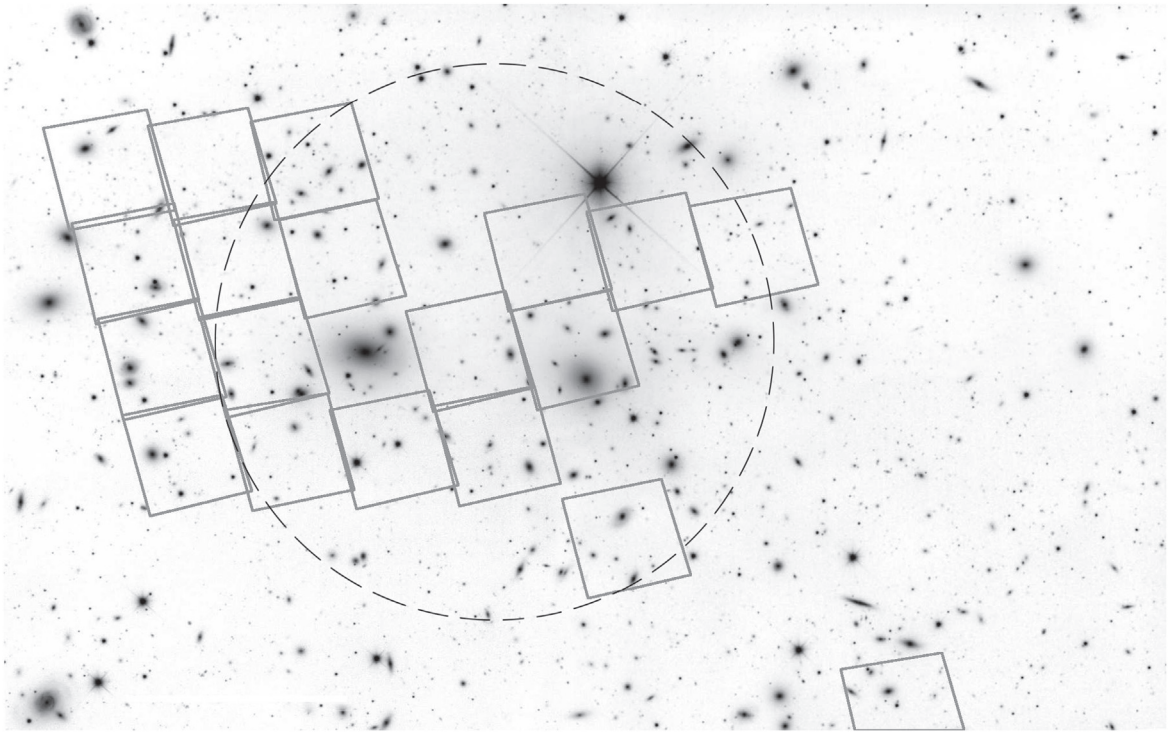

Figure 1. Core region of Coma and the footprints of 19 *HST*/ACS frames, of a total of 25, distributed mainly over a 0.7 × 0.5 Mpc region (the circle, 0.5 Mpc in diameter, marks the cluster center). Note that the brightest galaxy, NGC 4889, is not within the *HST* imaging.

Sheen et al. (2012). A cosmology with $\Omega_m = 0.3$, $\Omega_\Lambda = 0.7$, and $H_0 = 70\,\mathrm{km\,s^{-1}\,Mpc^{-1}}$ is adopted.

2. DATA AND SAMPLE SELECTION

We select Coma galaxies within the footprint (Figure 1) of the CTS (Carter et al. 2008). The angular scale for Coma is $0.472\,\mathrm{kpc\,arcsec^{-1}}$. The CTS provides high-quality ($0.05\,\mathrm{arcsec\,pixel^{-1}}$) imaging in both F475W (g) and F814W (I) *HST* filters, and only the galaxies contained therein are covered by our analysis. The surface brightness limit (SBL) is estimated to be $\Sigma_{\mathrm{F814W}} \sim 26.5\,\mathrm{mag\,arcsec^{-2}}$ at the 3σ level. Nineteen pointings, out of 25, cover roughly 20% of the projected area within 0.5 Mpc from the Coma center. The other six pointings are between 0.9 and 1.75 Mpc southwest of the cluster center. We use the available photometry from the CTS (Hammer et al. 2010) to construct the color–magnitude diagram and determine the RS (Figure 2). Radial velocities are compiled from NED. One hundred and seventy-six galaxies, ranging from F814W ∼ 13.5 to ∼20 mag and lying within 5σ (dotted lines) of the mean relation, are considered to be RS. Out of these, 70 are brighter than F814W = 17.7 mag, the limit to which the redshift information is 100% complete, and have radial velocities between 4000 and $10{,}000\,\mathrm{km\,s^{-1}}$, the redshift limits for membership of the Coma cluster. Using the stellar mass estimates from Weinzirl et al. (2014), this limit equates to a threshold of $\sim 10^9\,M_\odot$.

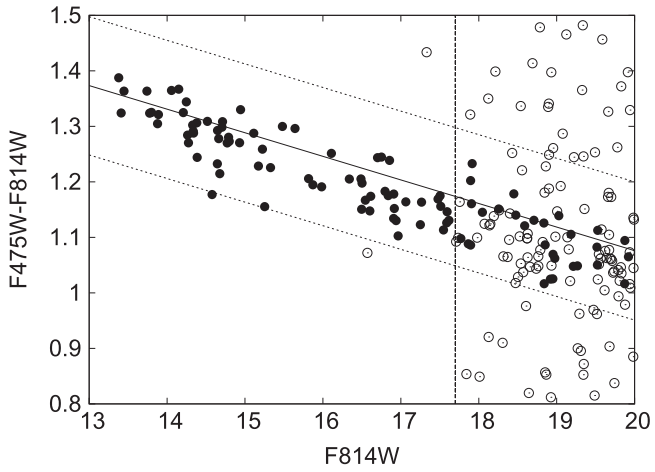

Figure 2. Color–magnitude diagram for objects brighter than F814W = 20. Red-sequence galaxies lie within the 5σ region delimited by dotted lines, while the red-sequence relation is indicated by the solid line and is given by F475–F814W = −0.0425 × F814W + 1.916. Open circles show galaxies with unknown radial velocity, while filled black circles correspond to member galaxies with known radial velocities between 4000 and $10{,}000\,\mathrm{km\,s^{-1}}$. Vertical line at F814W = 17.7 ($\sim 10^9 M_\odot$) marks the limit for a complete spectroscopic sample.

3. PAIRS

3.1. Pair Selection

The complete sample is searched for close pairs/triplets, which are considered pre-mergers if they show signatures of interaction on the *HST* images. This replicates the approaches of van Dokkum et al. (1999), Tran et al. (2008), and Rudnick et al. (2012) in more distant clusters, but adds progressively more information to test systematic effects on the determination of merger rates in distant clusters. Additionally, asymmetry parameters are measured for these galaxies.

By setting a projected distance limit of $r_s < 30\,\mathrm{h^{-1}\,kpc}$, we find 54 of 70 galaxies lying in 50 individual pairs. However, if we add the difference in line-of-sight velocity criteria of $\Delta V \leqslant 300\,\mathrm{km\,s^{-1}}$, we find a total of 13 galaxies (listed in

Table 1
Galaxies Belonging to Selected Pairs/Triplets by Projection and Velocity Proximity (See the Text)

CTS ID[a]	Name	Stellar Mass ($M_\odot$)	F814W (mag)	Projected r_s (kpc h^{-1})	ΔV (km s^{-1})	A_{abs}	Sersic Index	Morphology
125930.824p275303.05	IC 3973	5.02×10^{10}	13.77			0.0419	3.77	S0/a
				27.70	135			
125931.893p275140.76	…	1.96×10^{9}	16.91			0.0332	1.88	E
125944.407p275444.84	NGC 4876	4.62×10^{10}	13.89			0.0287	2.96	S0
				17.25	222			
125942.301p275529.15	PGC 44649	1.61×10^{10}	14.93			0.0590	7.49	S0
130028.370p275820.64	IC 4033	2.17×10^{10}	14.65			0.0248	4.04	S0
				19.60	129			
130027.966p275721.56	IC 4030	2.11×10^{10}	14.70			0.0270	4.68	S0
125943.721p275940.82	PGC 44656	2.13×10^{10}	14.71			0.0241	3.81	S0
				25.25	88			
125938.321p275913.89	PGC 44636	9.96×10^{9}	15.32			0.0384	3.50	S0/a
130018.873p280033.38	…	2.98×10^{9}	16.70			0.0277	3.29	S0
				26.36	66			
130017.641p275915.27	…	9.97×10^{8}	17.62			0.0191	3.30	S0
130008.003p280442.81[1]	IC 4012	3.51×10^{10}	14.25	21.59	238[b]	0.0447	2.59	S0
130012.868p280431.74[2]	PGC 44723	2.11×10^{10}	14.66	14.32	119[c]	0.0397	3.21	S0
130011.143p280354.91[3]	…	2.83×10^{9}	16.55	20.96	119[d]	0.0405	2.12	S0

Notes.
[a] As defined in Hammer et al. (2010) using the prefix COMAi.
[b] Difference between 1 and 2.
[c] Difference between 2 and 3.
[d] Difference between 1 and 3.

Table 1) in 5 pairs and 1 triple system, all of them contained within the 19 ACS central pointings. These cuts on r_s and ΔV are similar to those used in the literature for pair-count-based merger rate estimations (Patton et al. 2000; Lin et al. 2004; Tran et al. 2005; Casteels et al. 2013). Stellar mass ratios for the selected pairs range from ∼1:1 to ∼1:3, that is, if they are actually physically related they could evolve into major mergers.

3.2. Pair Likelihood in Coma

We investigate statistically the likelihood that these five observed close pairs and a close triple system are interacting and will merge in the future, or if instead they are simply chance alignments due to the high density of cluster galaxies in the projected phase space. For this calculation, we adopt spherical symmetry. Considering all known Coma cluster members within R_{200} ($1.99\,h^{-1}$ Mpc; Kubo et al. 2007) and having SDSS *ugriz* photometry, equivalent $g - i$ color, and *i*-band magnitude cuts to that used to identify our RS population in the ACS F814W and F475W imaging are applied. The position angles of these RS Coma galaxies are randomized with respect to the center of the X-ray emission from Coma (Neumann et al. 2003), and their velocities are randomized by repeatedly swapping the redshifts of cluster members. This randomization process should model the expected galaxy density of the virialized population of galaxies in the Coma core, in which all resulting pairs are just chance projections along the line of sight. The expected number of galaxy pairs, with the adopted r_s and ΔV limits, that would be found within the 19 ACS images based on 10,000 randomized Coma RS populations is 7.0 ± 2.2, including 1.3 ± 1.1 triples (or more complex systems).

The predicted numbers are entirely consistent with the observed number of pairs/triplets, indicating that they all could be simply chance alignments. Nevertheless, this calculation does not rule out some of the observed pairs actually being physical ones. In order to test this, we search for evidence of recent or ongoing interactions between galaxies belonging to the observed pairs/triplets.

3.3. Morphological Inspection of Galaxies

The search for evidence of recent galaxy–galaxy interactions in the 5 pairs and 1 triplet identified in Section 3.1 requires the generation of model-subtracted images for the 13 member galaxies. In most cases, it is on these residual images only that tidally induced low surface brightness features can be discerned.

The adopted galaxy models come from Weinzirl et al. (2014). They were obtained using GALFIT (Peng et al. 2010), considering up to three Sersic sub-components. Single-Sersic profile models were separated into photometric ellipticals and disks, while multi-component models were classified as S0 and E depending on the index of their main component. The morphological classification and Sersic index for each galaxy is given in Table 1. Features generated by recent galaxy–galaxy interactions generally tend to be highly asymmetric, such as tails, arcs, shells, ripples, bridges, and asymmetric spiral arms. In contrast, most internal features generated through internal instabilities tend to be symmetric with respect to the galaxy center or with respect to some reflection axis. These internal perturbations are easily distinguishable in the GALFIT residuals from the highly asymmetric interaction-driven features. Tidal interactions and minor mergers may also induce "bar-like" elongated structures, which tend to display asymmetries (e.g., in length, axial ratio, and shapes of dust lanes) not seen in internally induced bars. Unperturbed galaxies should show smooth gradients toward the outer parts of the galaxy and no noticeable asymmetric structures on the residuals, leaving

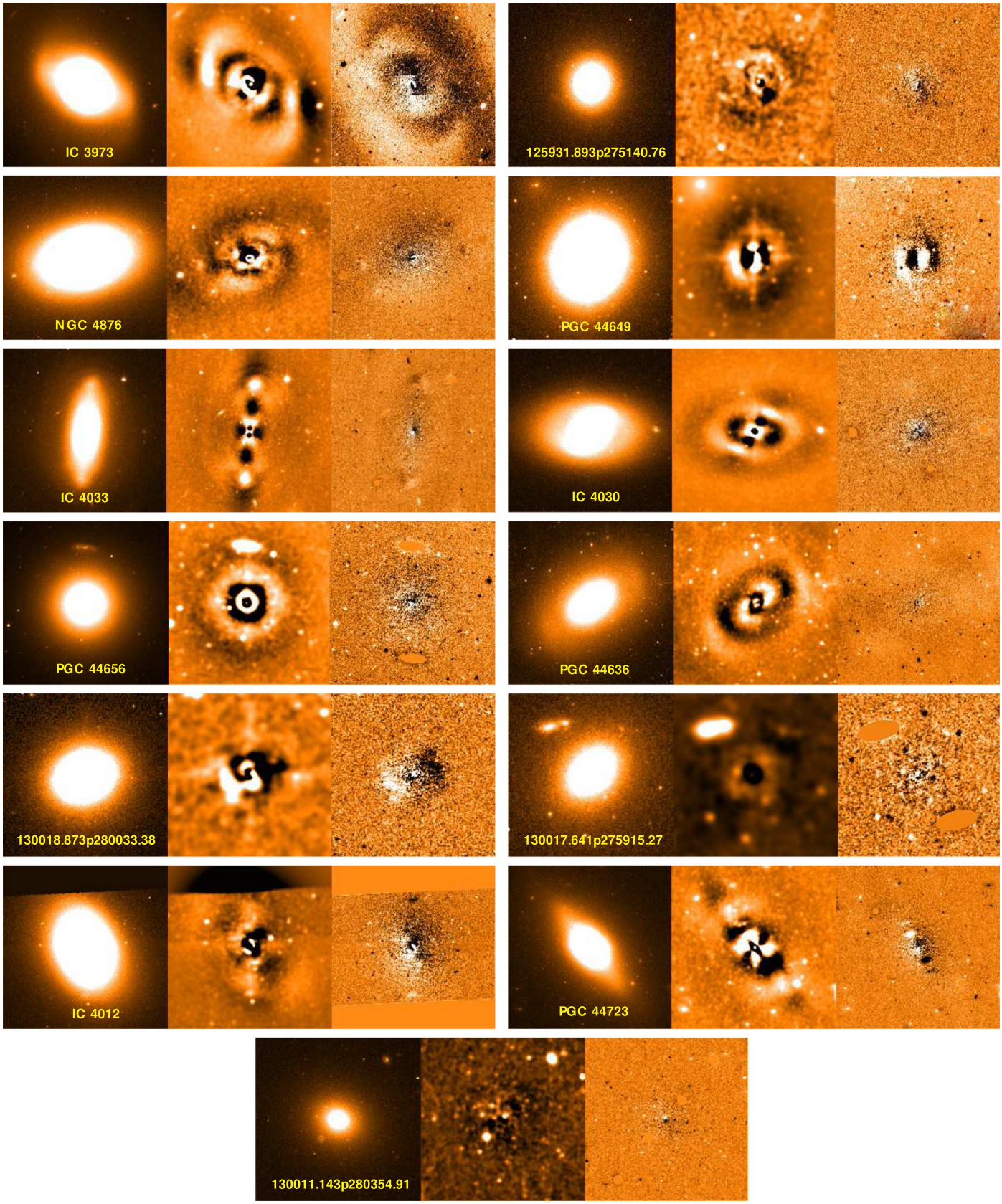

Figure 3. F814W images, models, and rotation residuals for the 13 galaxies in pairs/triplet are presented from left to right on each column. The first five rows correspond to the pairs. The last three images on the bottom correspond to the galaxies in the triple system.

only minor residuals, such as those arising from the boxy or disky profiles present in some ellipticals or from the presence of bars.

Figure 3 displays F814W images for the 13 galaxies in the selected pairs/triplet, the model-subtracted image, and residuals after subtraction of the galaxy after rotation by 180°. Model residuals are smoothed to highlight medium and large structures. To facilitate the diagnoses from the residual images after galaxy rotation, the foreground and background bright sources are masked. After model subtraction, the presence of structures such as bars and disk or boxy light profiles can be observed in some of the residual images. These are all symmetric with respect to the galaxy center, and are thus likely to be a result of internal processes (e.g., bars). Examples of residuals caused by bars can be seen for IC 4030 and PGC 44636. The boxy profile of IC 4033 is revealed on the corresponding residual image. In all cases, the structures observed in the residuals appear to be symmetrical with respect to the galaxy center, consistent with the expectations for inner galaxy structures. We have also examined a pair that did not qualify to be included in Table 1, NGC 4898A/B, but that is of particular interest because of the small projected separation of 2.59 h^{-1} kpc and comparable F814W magnitudes (13.42 and 14.38) of the two galaxies. Although the difference in their radial velocities is 532 km s^{-1}, higher than the cut employed here, it is lower than the average difference between the pairs selected by projected distance ($\sim$1100 km s^{-1}). Still, it is large enough to make coalescence unlikely. A visual inspection of the images of this projected pair reveals high overlapping, while the residuals of the GALFIT models reveal asymmetric structures on both galaxies. Nevertheless, these features cannot unmistakably be regarded as result of an ongoing interaction since the correct modeling becomes more difficult to achieve when the two galaxies overlap.

In conclusion, for the candidate bound pairs/triplet we do not find indications of low surface brightness features attributable to recent galaxy–galaxy interactions.

3.4. Asymmetry of Galaxies in Pairs

The asymmetry parameter $A_{\rm abs}$ is measured for the 13 galaxies in the pairs/triplet following the procedure by Conselice (2003) where the intensity of the galaxy and a 180° rotated image of itself is compared pixel to pixel. Values for $A_{\rm abs}$ range from 0 for a completely symmetric light distribution to 1 for one that is completely asymmetric. A correction for uncorrelated noise from the background is applied computing the asymmetry parameter for a synthetic area of the same size and rms noise measured close to the galaxy. Sky level subtraction and masking of fore/background sources is applied in order to minimize the effect of non-galactic sources. Typical values for unperturbed early-type galaxies range from 0.01 to 0.1, while irregular and starburst galaxies have been found to have values of 0.2–1.0 (Conselice 2003; Hoyos et al. 2012).

The asymmetry parameters determined for these 13 galaxies are listed in Table 1. Their parameters lie in the 0.02–0.06 range, corresponding to unperturbed galaxies, a result consistent with the conclusions of Section 3.3.

4. DRY MERGER RATE

The merger timescale for a given number of physical pairs can be estimated using the formula by Kitzbichler & White (2008), which considers typical stellar masses and distances between pair members. The merger timescale is given by

$$\langle T_{\rm merge}\rangle = 3.2\ {\rm Gyr}\frac{r_s}{50\ {\rm kpc}}\left(\frac{M_*}{4\times10^{10}M_\odot}\right)^{-0.3}\left(1+\frac{z}{20}\right).$$

In Section 3.1, we selected 13 galaxies (18.5% of the complete sample) complying with the adopted r_s and ΔV limits, whose median mass and projected separation are $2.11\times10^{10}M_\odot$ and 21.275 h^{-1} kpc, respectively. If, tentatively, it is assumed that these 13 galaxies are actually in interacting systems, then using the above formula, a merger timescale of 1.65 Gyr is obtained that would lead to a nominal dry merger rate of 11.2% per Gyr in the Coma core.

However, the visual inspection and asymmetry determination conducted for these 13 galaxies do not provide evidence that they are in interacting systems. This null result, nevertheless, allows an estimation of the dry merger rate by using binomial statistics. We follow the procedure by Burgasser et al. (2003), where the $\pm1\sigma$ range of acceptable values for the pair fractions are defined as a function of the sample size and pair fraction. From our finding of the number of pairs ($n = 0$) for a sample size of 70 galaxies ($N = 70$), we find an upper limit for the merger fraction of $\sim$2.5%. Considering the merger timescale of 1.65 Gyr estimated above, we obtain a 1σ upper limit for the major dry merger rate of $\sim$1.5% per Gyr within the Coma cluster core. This is not sufficient for dry mergers to account for the red-sequence evolution inside clusters (Skelton et al. 2012), consistent only with growth rates of $<$10% since $z = 1.5$ as derived by several previous studies (De Propris et al. 2007; Muzzin et al. 2008).

5. POST-MERGER FRACTION

The complete sample of RS galaxies is inspected to estimate the fraction that shows signatures of the coalescence of two galaxies, such as ripples, tidal structures, halo discontinuities, shells, and other structures unrelated to the presence of a companion. Using images to an SBL of $\sim$26.5 mag $arcsec^{-2}$, only 1 out of the 70 RS galaxies is classified as a post-merger. The only remnant candidate found is IC 3973, which was previously identified as a member of one of the five pairs and the triple system in Section 3.3. This galaxy is not identified as a member of an ongoing merger since the observed feature does not appear to be related to the presence of the projected partner, and the partner itself does not show any evidence of perturbation. The asymmetry parameter determined for this galaxy is 0.0419, a value still small for a perturbed galaxy; we believe that this parameter does not actually reflect the merger remnant character detected visually due to the low surface brightness of its external halo compared with the galaxy nucleus. In the direct F814W image of this galaxy (Figure 4, upper panel), the outer halo of the galaxy appears to be rotated and shifted with respect to the inner bright core, while in the residual image (lower panel), a curved extension is apparent coming out clockwise from the lower right corner of the galaxy halo.

Finding only one candidate merger remnant galaxy implies a post-merger fraction in the Coma cluster core of $\sim$1.4%. This

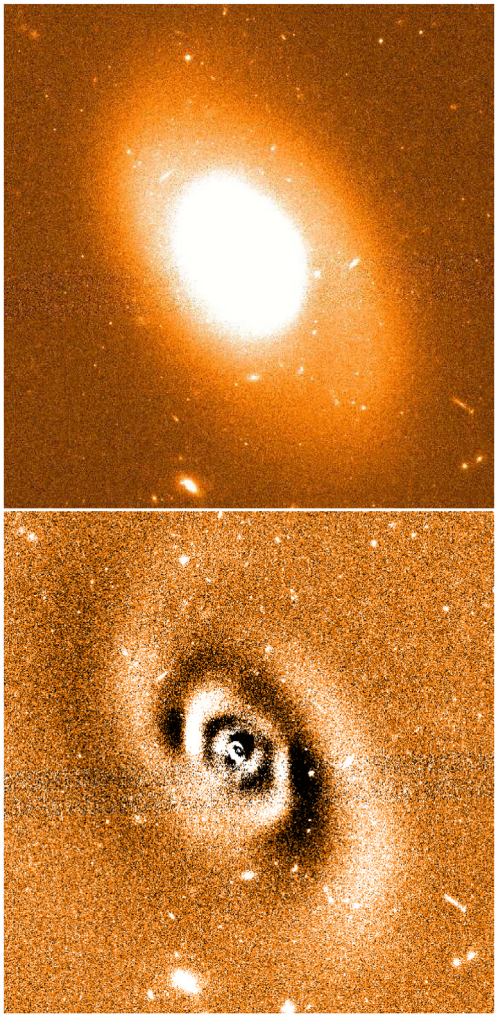

Figure 4. In the top panel is the F814W image of the only candidate post-merger galaxy IC 3973. The lower panel shows the residuals after subtraction of the model. A long, clockwise arm can be observed coming from the southwest.

result is in agreement with the estimate (3%) of Adams et al. (2012) for similar SBLs. However, our value is much smaller than the ∼25% mean fraction determined by Sheen et al. (2012), even within ∼0.2 R_{200} (their Figure 14), in four $z \lesssim 0.1$ Abell clusters using images with an SBL of $\Sigma_r \sim 30$ mag arcsec^{-2}.

6. CONCLUSIONS

On the one hand, by combining the identification of close pairs with the requirement of galaxy asymmetries, we find no evidence for major ongoing mergers in a spectroscopically complete sample of 70 RS galaxies within ∼0.5 R_{200} from the center of Coma and derive an upper limit to the dry merger rate of ∼1.5% per Gyr at the 1σ sigma level. This rate is not sufficient for dry mergers to account for the RS evolution inside clusters.

On the other hand, we find that from the 70 galaxies in our sample only one shows evidence of low surface brightness features identifiable as the remnants of a past merger or interaction, yielding a post-merger fraction of 1.4% within a projected distance of ∼0.5 R_{200} from the Coma center. Although the Coma brightest member (NGC 4889) is not in our sample, it actually is an RS galaxy sitting in the cluster center, and, interestingly, it has been found to contain a system of shells identifiable to a minor (∼1/100) merger (Gu et al. 2013). If NGC 4889 would have been part of our sample, presumably, it would have been counted as a galaxy with tidal signatures, implying a larger post-merger fraction of ∼2.8%. There is, however, a relevant caveat that derives from the work of Gu et al. (2013) on NGC 4889, i.e., that an observation alone of tidal signatures in a galaxy may sometimes be the consequence of a very minor merger.

The small post-merger fraction we observe is consistent with similar results, such as the one by Adams et al. (2012) where ∼3% of a large sample of early-type galaxies in clusters ($0.04 < z < 0.15$) show evidence of tidal features found in imaging with SBLs comparable to those of the *HST* imaging employed by us in this study. However, it is puzzling that the post-merger fraction we observe is a factor of 10 lower than the one measured by Sheen et al. (2012) in four $z \lesssim 0.1$ clusters. This discrepancy merits further investigation with consideration of differences in survey limits and cluster evolutionary stage.

L.E.C. and J.P.C. received partial support from the CONICYT Anillo project ACT-1122. L.E.C. is grateful for support from the Center of Excellence in Astrophysics and Associated Technologies (PFB06). J.P.C. acknowledges CONICYT/PCHA/MagisterNacional/2014—folio 22141888. C.P.H. was funded by CONICYT Anillo project ACT-1122. S.J. acknowledges support from NSF grant AST-1413652 and the NASA/JPL SURP program. This research made use of the NASA/IPAC Extragalactic Database (NED), which is operated by the Jet Propulsion Laboratory, California Institute of Technology, under contract with the National Aeronautics and Space Administration. We thank the referee for suggestions that contributed to the improvement of the paper.

REFERENCES

Aarseth, S. J., & Fall, S. M. 1980, ApJ, 236, 43
Adams, S. M., Zaritsky, D., Sand, D. J., et al. 2012, AJ, 144, 128
Boylan-Kolchin, M., Ma, C.-P., & Quataert, E. 2005, MNRAS, 362, 184
Brooks, A. M., Governato, F., Quinn, T., Brook, C. B., & Wadsley, J. 2009, ApJ, 694, 396
Burgasser, A. J., Kirkpatrick, J. D., Reid, I. N., et al. 2003, ApJ, 586, 512
Carter, D., Goudfrooij, P., Mobasher, B., et al. 2008, ApJS, 176, 424
Casteels, K. R. V., Bamford, S. P., Skibba, R. A., et al. 2013, MNRAS, 429, 1051
Conselice, C. J. 2003, ApJS, 147, 1
Dekel, A., Sari, R., & Ceverino, D. 2009, ApJ, 703, 785
Duc, P.-A., Cuillandre, J.-C., Karabal, E., et al. 2015, MNRAS, 446, 120
De Propris, R., Stanford, S. A., Eisenhardt, P. R., Holden, B. P., & Rosati, P. 2007, AJ, 133, 2209
Fernández Lorenzo, M., Cepa, J., Bongiovanni, A., et al. 2011, A&A, 526, A72
Gu, M., Ho, L. C., Peng, C. Y., & Huang, S. 2013, ApJ, 773, 34
Haines, C. P., Pereira, M. J., Smith, G. P., et al. 2015, ApJ, 806, 101
Hammer, D., Verdoes Kleijn, G., Hoyos, C., et al. 2010, ApJS, 191, 143
Hoyos, C., Aragón-Salamanca, A., Gray, M. E., et al. 2012, MNRAS, 419, 2703
Jogee, S., Scoville, N., & Kenney, J. D. P. 2005, ApJ, 630, 837
Jogee, S., Miller, S. H., Penner, K., et al. 2009, ApJ, 697, 1971
Khochfar, S., & Silk, J. 2009, MNRAS, 397, 506
Kitzbichler, M. G., & White, S. D. M. 2008, MNRAS, 391, 1489
Kormendy, J., & Kennicutt, R. C., Jr. 2004, ARA&A, 42, 603
Kubo, J. M., Stebbins, A., Annis, J., et al. 2007, ApJ, 671, 1466
Lin, L., Koo, D. C., Willmer, C. N. A., et al. 2004, ApJL, 617, L9
Muzzin, A., Wilson, G., Lacy, M., Yee, H. K. C., & Stanford, S. A. 2008, ApJ, 686, 966
Neumann, D. M., Lumb, D. H., Pratt, G. W., & Briel, U. G. 2003, A&A, 400, 811
Patton, D. R., Carlberg, R. G., Marzke, R. O., et al. 2000, ApJ, 536, 153

Peng, C. Y., Ho, L. C., Impey, C. D., & Rix, H.-W. 2010, AJ, 139, 2097
Rudnick, G. H., Tran, K.-V., Papovich, C., Momcheva, I., & Willmer, C. 2012, ApJ, 755, 14
Sheen, Y.-K., Yi, S. K., Ree, C. H., & Lee, J. 2012, ApJS, 202, 8
Skelton, R. E., Bell, E. F., & Somerville, R. S. 2012, ApJ, 753, 44
Springel, V., White, S. D. M., Jenkins, A., et al. 2005, Natur, 435, 629
Tran, K.-V. H., Moustakas, J., Gonzalez, A. H., et al. 2008, ApJL, 683, L17
Tran, K.-V. H., van Dokkum, P., Franx, M., et al. 2005, ApJL, 627, L25
van de Sande, J., Kriek, M., Franx, M., Bezanson, R., & van Dokkum, P. G. 2014, ApJL, 793, L31
van Dokkum, P. G. 2005, AJ, 130, 2647
van Dokkum, P. G., Franx, M., Fabricant, M., Kelson, D. D., & Illingworth, G. D. 1999, ApJL, 520, L95
Weinzirl, T., Jogee, S., Conselice, C. J., et al. 2011, ApJ, 743, 87
Weinzirl, T., Jogee, S., Neistein, E., et al. 2014, MNRAS, 441, 3083
Yi, S. K., Lee, J., Jung, I., Ji, I., & Sheen, Y.-K. 2013, A&A, 554, A122

Bibliography

Aarseth, S. J., & Fall, S. M. 1980, ApJ, 236, 43

Adams, S. M., Zaritsky, D., Sand, D. J., et al. 2012, AJ, 144, 128

Aguilar, L. A., & White, S. D. M. 1985, ApJ, 295, 374

Bahcall, N. A. 1973, ApJ, 183, 783

Barden, M., Jahnke, K., Haumlußler, B. 2008, ApJS, 175, 105-115

Barnes, J. E. 1988, ApJ, 331, 699

Barnes, J. E. 1992, ApJ, 393, 484

Biviano, A., Durret, F., Gerbal, D., et al. 1995, A&A, 111, 265

Biviano, A., Durret, F., Gerbal, D., et al. 1996, AA, 311, 95

Biviano, A. 1998, Untangling Coma Berenices: A New Vision of an Old Cluster,

Binney, J., & Tremaine, S. 1987, Princeton, NJ, Princeton University Press, 1987, 747 p.,

Bournaud, F., Duc, P.-A., & Emsellem, E. 2008, MNRAS, 389, L8

Briel, U. G. 1997, Astrophysical Letters and Communications, 36, 181

Brooks, A. M., Governato, F., Quinn, T., Brook, C. B., & Wadsley, J. 2009, ApJ, 694, 396

Burgasser A. J., Kirkpatrick J. D., Reid I. N., Brown M. W., Miskey C. L., Gizis J. E. 2003, ApJ, 586, 512

Carter, D., Goudfrooij, P., Mobasher, B., et al. 2008, ApJS, 176, 424

Casteels, K. R. V., Bamford, S. P., Skibba, R. A., et al. 2013, MNRAS, 429, 1051

Colless, M., & Dunn, A. M. 1996, ApJ, 458, 435

Conselice, C. J. 2003, ApJS, 147, 1

Condon, J. J., Helou, G., Sanders, D. B., & Soifer, B. T. 1993, AA, 105, 1730

Cooper, A. P., Martínez-Delgado, D., Helly, J., et al. 2011, ApJL, 743, L21

Cordero, J. P., Campusano, L. E., De Propris, R., et al. 2016, ApJL, 817, L6

De Propris, R., Stanford, S. A., Eisenhardt, P. R., Holden, B. P., & Rosati, P. 2007, AJ, 133, 2209

De Propris, R., Baldry, I. K., Bland-Hawthorn, J., et al. 2014, MNRAS, 444, 2200

Dekel, A., Sari, R., & Ceverino, D. 2009, ApJ, 703, 785

den Brok, M., Peletier, R. F., Valentijn, E. A., et al. 2011, MNRAS, 414, 3052

Dressler, A. 1980, ApJ, 236, 351

Drinkwater, M. J., Phillipps, S., Jones, J. B., et al. 2000, A&A, 355, 900

Duc, P.-A., Cuillandre, J.-C., Karabal, E., et al. 2015, MNRAS, 446, 120

Faucher-Giguère, C.-A., Kereš, D., & Ma, C.-P. 2011, MNRAS, 417, 2982

Fernández Lorenzo, M., Cepa, J., Bongiovanni, A., et al. 2011, A& A, 526, A72

Frei, Z., Guhathakurta, P., Gunn, J. E., & Tyson, J. A. 1996, AJ, 111, 174

Gu, M., Ho, L. C., Peng, C. Y., & Huang, S. 2013, ApJ, 773, 34

Haines, C. P., Pereira, M. J., Smith, G. P., et al. 2015, ApJ, 806, 101

Hammer, D., Verdoes Kleijn, G., Hoyos, C., et al. 2010, ApJS, 191, 143

Hammer, D., Hornschemeier, A. E., Mobasher, B., et al. 2010, ApJS, 190, 43

Heiderman, A., Jogee, S., Marinova, I., et al. 2009, ApJ, 705, 1433

Hernquist, L., & Quinn, P. J. 1988, ApJ, 331, 682

Hoyos, C., den Brok, M., Verdoes Kleijn, G., et al. 2011, MNRAS, 411, 2439

Hoyos, C., Aragón-Salamanca, A., Gray, M. E., et al. 2012, MNRAS, 419, 2703

Into, T., & Portinari, L. 2013, MNRAS, 430, 2715

Jedrzejewski, R. I. 1987, MNRAS, 226, 747

Jogee, S., Scoville, N., & Kenney, J. D. P. 2005, ApJ, 630, 837

Kitzbichler M. G. & White S. D. M. 2008, MNRAS, 391, 1489

Khochfar, S., & Silk, J. 2009, MNRAS, 397, 506

Kormendy, J., & Kennicutt, R. C., Jr. 2004, ARA&A, 42, 603

Krist, J. E., Hook, R. N., & Stoehr, F. 2011, PSPIE, 8127, 81270J

Kroupa, P., Tout, C. A., & Gilmore, G. 1993, MNRAS, 262, 545

Kubo, J. M., Stebbins, A., Annis, J., et al. 2007, ApJ, 671, 1466

Lin, L., Koo, D. C., Willmer, C. N. A., et al. 2004, ApJL, 617, L9

Lotz, J. M., Primack, J., & Madau, P. 2004, AJ, 128, 163

Lotz, J. M., Papovich, C., Faber, S. M., et al. 2013, ApJ, 773, 154

Merluzzi, P., Busarello, G., Haines, C. P., et al. 2015, MNRAS, 446, 803

Muzzin, A., Wilson, G., Lacy, M., Yee, H. K. C., & Stanford, S. A. 2008, ApJ, 686, 966

Neumann, D. M., Lumb, D. H., Pratt, G. W., & Briel, U. G. 2003, A& A, 400, 811

Patton, D. R., Carlberg, R. G., Marzke, R. O., et al. 2000, ApJ, 536, 153

Peng, C. Y., Ho, L. C., Impey, C. D., & Rix, H.-W. 2010, AJ, 139, 2097

Perea, J., del Olmo, A., & Moles, M. 1986, MNRAS, 219, 511

Price, J., Phillipps, S., Huxor, A., et al. 2009, MNRAS, 397, 1816

Quinn, P. J. 1984, ApJ, 279, 596

Rudnick, G. H., Tran, K.-V., Papovich, C., Momcheva, I., & Willmer, C. 2012, ApJ, 755, 14

Schweizer, F. 1982, ApJ, 252, 455

Schweizer, F. 1996, AJ, 111, 109

Sérsic, J. L. 1963, Boletin de la Asociacion Argentina de Astronomia La Plata Argentina, 6, 41

Sheen, Y.-K., Yi, S. K., Ree, C. H., & Lee, J. 2012, ApJS, 202, 8

Smith, R. J., Hudson, M. J., Nelan, J. E., et al. 2004, aj, 128, 1558

Smith, R. J., Lucey, J. R., & Hudson, M. J. 2007, MNRAS, 381, 1035

Sohn, S. T., Anderson, J., & van der Marel, R. P. 2012, ApJ, 753, 7

Springel, V., White, S. D. M., Jenkins, A., et al. 2005, Nature, 435, 629

Tran, K.-V. H., van Dokkum, P., Franx, M., et al. 2005, ApJL, 627, L25

Toomre, A., & Toomre, J. 1972, ApJ, 178, 623

Toomre, A. 1977, in The Evolution of Galaxies and Stellar Populations, ed. B. Tinsley & R. Larson (New Haven: Yale Univ. Obs)

Trujillo, I., Erwin, P., Asensio Ramos, A., & Graham, A. W. 2004, AJ, 127, 1917

van de Sande, J., Kriek, M., Franx, M., Bezanson, R., & van Dokkum, P. G. 2014, ApJL, 793, L31

van de Voort, F., Schaye, J., Booth, C. M., Haas, M. R., & Dalla Vecchia, C. 2011, MNRAS, 414, 2458

van Dokkum P. G., Franx M., Fabricant M., Kelson D. D., Illingworth G. D. 1999, ApJ, 520, L95

van Dokkum P. G., Stanford S. A., Holden B. P., Eisenhardt P. R., Dickinson M., Elston R. 2001,ApJ, 552, L101

Weinzirl, T., Jogee, S., Neistein, E., et al. 2014, MNRAS, 441, 3083

Yamada T., Koyama Y., Nakata F., Kajisawa M., Tanaka I., Kodama T., Okamura S., De Propris R. 2002, ApJ, 577, L89

Yi, S. K., Lee, J., Jung, I., Ji, I., & Sheen, Y.-K. 2013, A&A, 554, A122